TAL TECH

DOCTORAL THESIS

Mathematical Modeling and Numerical Analysis of Structural Dynamics with Applications to Damage Detection

Marmar Mehrparvar

TALLINNA TEHNIKAÜLIKOOL
TALLINN UNIVERSITY OF TECHNOLOGY
TALLINN 2025

TALLINN UNIVERSITY OF TECHNOLOGY
DOCTORAL THESIS
3/2026

Mathematical Modeling and Numerical Analysis of Structural Dynamics with Applications to Damage Detection

MARMAR MEHRPARVAR

TAL TECH PRESS

TALLINN UNIVERSITY OF TECHNOLOGY
School of Engineering
Department of Mechanical and Industrial Engineering
This dissertation was accepted for the defence of the degree 11/12/2025

Supervisor: Prof. Jüri Majak
School of Engineering
Tallinn University of Technology
Tallinn, Estonia

Co-supervisor: Prof. Kristo Karjust
School of Engineering
Tallinn University of Technology
Tallinn, Estonia

Opponents: Prof. Helle Hein
Faculty of Science and Technology
University of Tartu
Tartu, Estonia

Prof. Imran Aziz
Department of Mathematics
University of Peshawar
Peshawar, Pakistan

Defence of the thesis: 12/01/2026, Tallinn

Declaration:
Hereby I declare that this doctoral thesis, my original investigation and achievement, submitted for the doctoral degree at Tallinn University of Technology has not been submitted for doctoral or equivalent academic degree.

Marmar Mehrparvar

---
signature

European Union
European Regional
Development Fund

Investing
in your future

ISSN 2585-6898 (publication)
ISBN 978-9916-80-441-4 (publication)
ISSN 2585-6901 (PDF)
ISBN 978-9916-80-442-1 (PDF)
DOI https://doi.org/10.23658/taltech.3/2026
Printed by EVG Print

Mehrparvar, M. (2025). *Mathematical Modeling and Numerical Analysis of Structural Dynamics with Applications to Damage Detection* [TalTech Press]. https://doi.org/10.23658/taltech.3/2026

TALLINNA TEHNIKAÜLIKOOL
DOKTORITÖÖ
3/2026

Konstruktsioonide dünaamika matemaatiline modelleerimine ja numbriline analüüs kahjustuste tuvastamise rakendusnäidetega

MARMAR MEHRPARVAR

TAL TECH
KIRJASTUS

Contents

List of Publications

The PhD thesis is based on the following publications:

I M. Mehrparvar, J. Majak, K. Karjust, and M. Arda, “Free vibration analysis of tapered Timoshenko beam with higher order Haar wavelet method,” *Proceedings of the Estonian Academy of Sciences*, vol. 71, no. 1, p. 77, 2022, doi: https://doi.org/10.3176/proc.2022.1.07.

II M. Mehrparvar, J. Majak, and K. Karjust, “Free vibration analysis of Timoshenko beam by higher-order Haar wavelet method,” *AIP Conference Proceedings*, vol. 2849, no. 1, p. 250007, 2023, doi: https://doi.org/10.1063/5.0162269.

III M. Arda, J. Majak, and M. Mehrparvar, “Longitudinal Wave Propagation in Axially Graded Raylegh–Bishop Nanorods,” *Mechanics of Composite Materials*, vol. 59, no. 6, pp. 1109–1128, Jan. 2024, doi: https://doi.org/10.1007/s11029-023-10160-4.

IV L. Kivistik, M. Mehrparvar, M. Eerme, and J. Majak, “Dynamics of flight of the fragments with higher order Haar wavelet method,” *Proceedings of the Estonian Academy of Sciences*, vol. 73, no. 2, pp. 108–115, Mar. 2024, doi: https://doi.org/10.3176/proc.2024.2.02.

V M. Mehrparvar, L. Kivistik, M. Eerme, and K. Karjust, “Haar wavelet based analysis of dynamics of flight of the fragments,” *AIP conference proceedings*, vol. 3315, no. 1, pp. 240001–240001, Jan. 2025, doi: https://doi.org/10.1063/5.0287481.

VI M. Mehrparvar, J. Majak, and K. Karjust, “Enhanced Crack Detection in Composite Plates: Integrating Haar Wavelet Transform with Convolutional Neural Networks,” *E3S Web of Conferences*, vol. 631, p. 01008, 2025, doi: https://doi.org/10.1051/e3sconf/202563101008.

Author's Contribution to the Publications

Contribution to the papers in this thesis are:

I First and corresponding author. Wrote the simulation program, analysed the results, prepared the Figures and wrote the manuscript.

II First and corresponding author. Wrote the simulation program, analysed the results, prepared the Figures and wrote the manuscript.

III Co-author. Assisted with methodology, writing the manuscript and proofreading.

IV Co-author. Wrote the simulation program, analysed the results and assisted with writing the manuscript.

V First and corresponding author. Wrote the simulation program, analysed the results, prepared the Figures and wrote the manuscript.

VI First and corresponding author. Wrote the simulation program, analysed the results, prepared the Figures and wrote the manuscript.

Abbreviations

HWM	Haar Wavelet Method
HOHWM	Higher Order Haar Wavelet Method
SHM	Structural Health Monitoring
CNN	Convolutional Neural Networks
CFRP	Carbon Fiber Reinforced Polymer
FRF	Frequency Response Functions

1 Introduction

In this thesis, wavelet-based computational tools have been developed and used for the purpose of analyzing structural dynamics and diagnostic applications in mechanical structures. This section initially discusses the foundational background and motivation behind the research, followed by an exploration of the inherent challenges in modeling and analyzing structural dynamics. Subsequently, a comprehensive literature review is presented to investigate relevant prior studies and identify existing research gaps. Finally, the research objectives, scope and novel contributions are outlined.

1.1 Background and Motivation

Structural dynamics offers a fundamental basis for comprehending the behavior of engineering structures when subjected to both transient and periodic loads. Precise dynamic analysis facilitates prediction of vibrational characteristics, fatigue life and potential failure mechanisms within components exposed to operational or environmental excitations. Modern industries, such as aerospace, automotive, mechanical, marine and civil engineering, increasingly depend on dynamic simulations for design optimization and safety assurance. Nevertheless, as structures have become lighter, thinner and incorporate advanced materials, the complexity of these systems' behavior has significantly increased.

For instance, composite and functionally graded materials exhibit spatially variable stiffness, density and damping characteristics, leading to highly coupled and nonlinear dynamic responses. Similarly, micro and nanoscale structures demonstrate nonlocal effects that classical continuum theory cannot adequately capture. Analytical solutions for such complex systems are either limited or unattainable, thus highlighting the necessity for efficient and accurate numerical formulations capable of explaining multiscale dynamic behavior.

Simultaneously with advancements in computational mechanics, structural health monitoring has emerged as a crucial domain for ensuring the integrity of infrastructure and high performance systems. SHM methodologies increasingly leverage vibration-based data, such as frequency response functions (FRFs), modal parameters and acceleration signals, to identify, locate and quantify structural damage. Accurate numerical modeling supports these endeavors by providing baseline dynamic characteristics for comparison with experimental or in-service measurements. However, the dual challenge of precisely modeling dynamic behavior and interpreting measured responses within uncertainty persists as an unresolved research problem.

In this respect, wavelet theory has proved to be a particularly flexible mathematical tool because of its ability to express localized features in both the time and frequency domains and because it provides an efficient description of discontinuities and transients. The Haar wavelet, for instance, provides an orthogonal and simple basis to discretize differential equations efficiently on the one hand, while being a powerful tool of signal analysis on the other. Exploiting this dual nature, wavelets are considered first as a basis for numerical approximation, then applied as a data preprocessing operator to improve the structural dynamic model and vibration-based damage detection.

Recently, the introduced HOHWM has outperformed HWM as reference method. However, higher order Haar wavelet methods considered here are few studied and need further evaluation and adaptation, especially in the case of complex engineering problems.

1.2 Challenges in Modeling and Analysis of Structural Dynamics

Although computational mechanics and sensing technologies have progressed significantly, several challenges persist in structural dynamics and SHM. These challenges can be broadly categorized into three groups: numerical, physical, and diagnostic [1], [2], [3].

From a numerical standpoint, the governing equations for structural dynamics are inherently nonlinear, coupled and time-dependent. Accurately solving these equations necessitates fine discretization, which, in turn, escalates computational expenses [4]. Conventional finite element methods frequently encounter difficulties with localized discontinuities, intricate boundary conditions, and multiscale characteristics [5]. Consequently, even moderately sized nonlinear dynamic problems may demand thousands of elements and iterative time integration, potentially leading to slow convergence rates and numerical instabilities [6].

From a physical modeling perspective, the emergence of advanced materials such as functionally graded composites and nanostructures introduces further complexity. Their mechanical behavior is contingent upon localized variations in material composition and effects that are dependent on size. Accurately capturing these behaviors necessitates the use of higher order or nonlocal formulations, which in turn escalate mathematical and computational demands [7]. Traditional analytical methodologies are often inadequate for accurately characterizing size-dependent phenomena, while conventional numerical approaches frequently incur prohibitive computational costs. Furthermore, the precise assessment of localized discontinuities within such intricate material systems often necessitates integrated analytical and data-driven strategies, exemplified by those employing Haar wavelet assisted learning [8]. From a diagnostic standpoint, vibration-based damage detection entails the interpretation of noisy and frequently incomplete data. Fluctuations in temperature, humidity or boundary conditions can obscure or simulate damage signatures [9]. Furthermore, as structures increase in size and intricacy, acquiring full-field measurements becomes unfeasible. Damage indicators derived from modal parameters or frequency shifts often lack sensitivity to localized degradation. Consequently, researchers have increasingly adopted signal processing and machine learning techniques to extract more salient features from dynamic data [10].

The convergence of these challenges underscores the necessity for a computational framework capable of efficiently resolving multiscale, nonlinear dynamic problems and enhancing data-driven damage detection by emphasizing physically interpretable features. The Haar wavelet method and its higher order extension offer a promising foundation for achieving both of these objectives.

1.3 Literature Review

This literature review outlines the evolution of wavelet-based methods in structural dynamics and structural health monitoring, highlighting key advancements and existing gaps.

The application of wavelet theory has become widespread in engineering due to its efficacy in representing localized phenomena with a minimal set of basis functions [11]. In the context of numerical analysis, wavelet-based methodologies were introduced as alternatives to traditional discretization techniques, offering a synergistic balance between global spectral precision and the localized adaptability characteristic of finite element methods. Among these early formulations, the Haar Wavelet Method utilizes step function bases, which facilitate piecewise approximation of derivatives and integrals

[12]. Its inherent orthogonality simplifies matrix assembly, while its hierarchical structure enables multiresolution refinement without the need for remeshing. Research indicates that HWM demonstrates particular effectiveness in problems characterized by discontinuities or sharp gradients, where polynomial basis methods may struggle to achieve efficient convergence [13]. Furthermore, the Haar wavelet's capacity for singularity detection, coupled with its ability to handle noisy data, makes it particularly suitable for vibration-based damage detection applications [14]. However, challenges remain in optimizing wavelet scale selection for damage identification, particularly in plate like structures with sparse response data [15].

Subsequently, the Higher-Order Haar Wavelet Method was developed to enhance accuracy and broaden the applicability of Haar-based formulations. By repeatedly integrating Haar functions, HOHWM creates higher order continuous approximations while retaining compact support [16], [17]. This extension substantially improves the order of convergence, facilitating precise solutions for both smooth and intricate systems. HOHWM has been successfully deployed in the bending and vibration analyses of beams and plates, as well as in nonlinear boundary value problems [18], [19]. Nevertheless, its application in transient structural dynamics or problems involving nonlocal material behavior remains largely unexplored. However, its fundamental advantages for handling discontinuities and its capacity for high order accuracy suggest significant potential for these complex scenarios, warranting further investigation into its adaptivity and computational efficiency.

Meanwhile, wavelet transforms have found extensive application in signal processing and damage detection. Both discrete and stationary wavelet transforms are employed to decompose vibration signals into distinct frequency bands, thereby isolating localized energy variations indicative of stiffness degradation or crack formation [20], [21], [22], [23]. These extracted features have proven effective in detecting and pinpointing damage in composite beams, plates, and shells [24], [25], [26]. Despite the fact that wavelet transform is a powerful tool for achieving good localization properties in both, time and frequency domain (which can be instrumental in analyzing damage related data), it introduces additional complexity to CPU calculations, which is why among many mother wavelets, Haar has become very appealing for SHM due to its computational ease as well as accurate time localization [27]. Nevertheless, most of these applications rely on empirical signal decomposition, lacking a direct connection to the physical models governing dynamic behavior.

More recently, machine learning and deep learning, particularly convolutional neural networks, have gained prominence in structural health monitoring [28], [29], [30], [31], [32]. These advanced techniques, when coupled with wavelet analysis, have shown promising results in processing the complex, multidimensional data generated from structural responses, offering enhanced capabilities for autonomous damage detection and localization [21], [33].

While CNNs are highly effective in pattern recognition, they necessitate well-structured input data [34], [35], [36]. The integration of wavelet transforms with CNNs has been shown to enhance interpretability and improve sensitivity to localized changes [37], [38]. Although wavelet-assisted deep learning is frequently employed in vibration analysis and fault detection, most existing research compartmentalizes wavelet-based numerical modeling and wavelet-enhanced data-driven analysis into distinct areas. One-dimensional convolutional neural networks have been shown to effectively classify cracks in composite beams by directly extracting damage-sensitive features from raw vibration data [39].

In another study, wavelet packet analysis coupled with an autoencoder neural network was developed to localize structural damage under varying temperature conditions by filtering environmental effects from wavelet packet energy ratio features [40]. This integration allows for robust damage detection models, especially when applied to complex structures such as composite beams and plates, where both natural frequencies and mode shapes are sensitive to damage [39], [41]. However, selecting the optimal mother wavelet function remains a significant challenge, often requiring extensive trial and error or heuristic approaches [41].

Wavelets are commonly utilized for the time-frequency decomposition of vibration signals before classification, while their application as numerical basis functions for solving structural equations remains confined to independent analytical investigations. Consequently, the integration of both perspectives within a cohesive framework, where wavelets simultaneously underpin mathematical modeling and serve as a preprocessing tool for machine learning, has been relatively scarce [42], [43], [44].

In this context, the Haar wavelet method presents a distinct advantage, due to its orthogonality, computational simplicity and precise temporal localization, rendering it suitable not only for the numerical discretization of governing equations but also for highlighting localized damage-induced transients within vibration data [27]. These attributes establish a coherent mathematical link between the deterministic modeling and data-driven constituents of the current investigation, thus forming the bedrock for the integrated wavelet framework developed herein. This thesis, therefore, embarks on a novel exploration by unifying these typically disparate applications of wavelets, demonstrating their synergistic potential in both structural modeling and data-driven damage identification [41], [45]. Specifically, this study leverages the Haar Wavelet Method to solve the inverse problem of crack identification in vibrating beams, a technique that allows for the prediction of crack depth and location by analyzing changes in vibrational characteristics [46]. This unique integration bridges the gap between physics-based modeling and data-driven approaches, offering a comprehensive and robust framework for structural health monitoring that overcomes limitations inherent in standalone methodologies. The approach capitalizes on the localized sensitivity of mode shapes to damage, utilizing wavelet transforms to identify singularities indicative of crack presence and quantify their severity [47]. This allows for a baseline free damage detection strategy, where the absolute structural response is sufficient for damage localization, eliminating the need for comparisons with an undamaged state [48]. Furthermore, wavelet-based damage detection methods often rely on analyzing changes in wavelet coefficients, which exhibit singularities at damage locations, thereby facilitating precise spatial localization [49].

1.4 Research Objectives and Novelty

Main goal is to develop and evaluate wavelet-based methodologies for the mathematical modeling and numerical analysis of engineering problems. The main objective can be achieved by performing the following subtasks:

1. Develop and validate the Haar Wavelet Method for solving the equations of motion that govern the vibration and transient dynamics of structural elements.
2. Extend the HWM to the Higher Order Haar Wavelet Method to enhance accuracy and convergence, applying it to functionally graded and nanostructured materials that incorporate nonlocal elasticity.

3. Apply the HWM and HOHWM to transient nonlinear problems, specifically the flight dynamics of fragments subjected to aerodynamic drag, to demonstrate their capability in handling time-dependent coupled systems.
4. Integrate the Haar wavelet transform with Convolutional Neural Network architectures for vibration-based damage detection in composite plates, evaluating the impact of wavelet preprocessing on classification performance and interpretability.
5. Compare and synthesize findings across all applications to assess the effectiveness of Haar-based approaches in modeling, simulation and Structural Health Monitoring.

The novelty of this thesis stems from its establishment of a cohesive framework that bridges deterministic, wavelet-based numerical modeling with data-driven damage identification. On the deterministic side, the Higher Order Haar Wavelet Method is applied to Timoshenko beams, functionally graded Rayleigh-Bishop nanorods, and nonlinear fragment dynamics, representing some of the few studies employing this formulation for multiscale and transient structural problems. This methodology illustrates that the underlying mathematical principles employed for discretizing differential equations are equally effective in augmenting feature extraction from empirical vibration data. Consequently, this research closes the gap between analytical techniques and contemporary machine learning, thereby contributing significantly to both numerical mechanics and intelligent structural monitoring.

Beyond the development of wavelet-based numerical and hybrid models, this research also extends toward a decision-based analytical framework for evaluating material properties and reliability under uncertainty. The integration of fuzzy multi-criteria methods, such as the Analytic Hierarchy Process and the VIKOR technique [50], [51], [52], provides a systematic means of prioritizing parameters and assessing performance when experimental or computational data contain inherent variability. The coupling of deterministic accuracy with fuzzy decision making enhances the interpretability of results, allowing the proposed framework to serve not only as a computational tool but also as a decision support methodology for material characterization and structural assessment. This comprehensive approach offers a robust framework for structural integrity assessment, especially when dealing with complex systems and incomplete information.

1.5 Research Questions

The challenges identified in modeling and analyzing structural dynamics, particularly those concerning accuracy, computational efficiency and data scarcity, serve as the motivation for the research questions explored in this thesis. These questions are formulated to bridge the divide between mathematical modeling, numerical implementation and data-driven analysis using the Haar wavelet framework:

1. How can the Haar Wavelet Method and its higher order formulation be systematically derived and effectively implemented to achieve efficient and highly accurate numerical solutions for the governing differential equations of structural dynamic systems?
2. What distinct convergence behavior is demonstrated by the Higher Order Haar Wavelet Method in comparison to the standard Haar formulation when

applied to diverse problems, including beam vibration, graded nanorods and nonlinear transient problems?

3. How do material gradation, geometric variation and nonlocal elasticity influence the dynamic response and wave-propagation characteristics of structures modeled using the Higher Order Haar Wavelet Method?
4. Can Haar wavelet based preprocessing enhance the learning stability and classification accuracy of convolutional neural network models trained on limited and noisy vibration datasets for damage detection in composite structures?
5. How can Haar based numerical modeling and wavelet-enhanced deep learning be integrated into a unified multiscale computational framework for structural analysis and health monitoring?

In addressing these questions, it is hypothesized that the Higher Order Haar Wavelet Method will exhibit superior convergence properties and enhanced numerical precision relative to the standard Haar formulation, all while maintaining computational efficiency. It is further anticipated that the incorporation of geometric variation, material gradation and nonlocal elasticity within the Haar-based framework will accurately capture scale-dependent effects in structural dynamics. For the data-driven analyses, Haar wavelet preprocessing is posited to improve the training stability and classification reliability of CNNs, particularly in the context of small and noisy datasets. Collectively, these advancements are expected to establish a unified, multiscale methodology that integrates physics-based modeling with data-driven feature learning, thereby ensuring robust structural analysis and damage detection capabilities.

1.6 Scope and Structure of the Thesis

This thesis covers theoretical, numerical and data-driven investigations within the domain of structural analysis. The scope includes the formulation of wavelet-based methods, their application to diverse structural systems and their integration with modern learning algorithms for damage identification.
The structure is as follows:

- Chapter 2 outlines the mathematical and numerical framework of the Haar and Higher Order Haar Wavelet Methods, about their derivation, the treatment of boundary conditions and a comprehensive convergence analysis.
- Chapter 3 details the selected case studies, which include the free vibration of beams and plates, the vibration of functionally graded nanorods, the dynamics of fragments and vibration-based damage detection utilizing a Haar-CNN hybrid model. Each case study is presented with its physical motivation, underlying modeling assumptions and computational setup.
- Chapter 4 presents the findings and subsequent discussions for all conducted case studies, with particular emphasis on assessing accuracy, convergence, computational efficiency and diagnostic performance.
- Chapter 5 concludes the thesis by summarizing the principal findings and outlining promising avenues for future research.

The subsequent chapters will further elaborate on methodologies and results, providing a comprehensive understanding of developed techniques and their implications for structural engineering.

2 Mathematical and Numerical Framework

This section provides an explanation of the mathematical foundations underpinning the Haar Wavelet Method and the Higher Order Haar Wavelet Method, detailing their formulation for solving differential equations and approximating functions [11], [17], [53], [54].

2.1 Haar Wavelet Method (HWM)

The Haar Wavelet Method offers an effective numerical solution for differential equations frequently encountered in structural dynamics. This technique relies on expanding the highest order derivative within the governing equation using orthogonal Haar basis functions, thereby converting the problem into a system of algebraic equations via analytical integration. The formulation of Haar wavelet family is based on notation used in [11]. This approach is particularly advantageous due to its computational efficiency and straightforward implementation, making it suitable for a wide range of engineering applications [13].

The discontinuous Haar wavelet is a foundational element among wavelets, notable for its step-like discontinuity and its classification within a particular family of discrete orthonormal wavelets. This primary wavelet generates a basis of additional wavelets, each of which is orthonormal and normalized to unit length. This inherent property facilitates the independent computation of wavelet coefficients. The Haar functions are formally expressed as:

$$h_i(x) = \begin{cases} 1 & \text{for} \quad x \in \left[\xi_1(i), \xi_2(i)\right) \\ -1 & \text{for} \quad x \in \left[\xi_2(i), \xi_3(i)\right) \\ 0 & \text{elsewhere} \end{cases}, \tag{1}$$

where

$$\begin{matrix} \xi_1(i) = A + 2k\mu\Delta x \\ \xi_2(i) = A + (2k+1)\mu\Delta x, \\ \xi_3(i) = A + 2(k+1)\mu\Delta x \end{matrix} \qquad i = m + k + 1, \qquad \mu = \frac{M}{m}, \qquad \Delta x = \frac{B-A}{2M}, \tag{2}$$

where $k = 0, 1, \ldots, m-1$ specifying the square wave's location and $m = 2^j$ represents the maximum number of square waves within the interval $[A, B]$. Assuming that a function $f(x)$ is square integrable and finite within the interval, it can be expanded into a series of Haar wavelets as follows:

$$f(x) = \sum_{i=1}^{2M} a_i h_i(x), \tag{3}$$

where $h_i(x)$ denotes the Haar function and a_i is the corresponding coefficient. Subsequently, the integrals of the Haar functions of order n can be presented as:

$$p_{n,i}(x)=\begin{cases}0 & x\in[A,\xi_1(i))\\ \dfrac{(x-\xi_1(i))^n}{n!} & x\in[\xi_1(i),\xi_2(i))\\ \dfrac{(x-\xi_1(i))^n-2(x-\xi_2(i))^n}{n!} & x\in[\xi_2(i),\xi_3(i))\\ \dfrac{(x-\xi_1(i))^n-2(x-\xi_2(i))^n+(x-\xi_3(i))^n}{n!} & x\in[\xi_3(i),B)\\ 0 & else\ where\end{cases}. \quad (4)$$

The piecewise constant nature of the Haar basis functions ensures that the resulting matrices are sparse and well-conditioned. The boundary conditions are directly integrated by modifying the relevant rows of the algebraic system, thereby circumventing the need for auxiliary methods such as Lagrange multipliers or transformation matrices. The Haar Wavelet Method exhibits a second order convergence rate, rendering it suitable for solutions characterized by discontinuities or piecewise smoothness.

2.2 Higher Order Haar Wavelet Method (HOHWM)

To achieve enhanced accuracy and smoothness, the Haar basis functions can undergo multiple integrations prior to forming the approximation, which gives rise to the Higher Order Haar Wavelet Method. This methodology, initially introduced in studies of vibration and wave propagation, offers a continuous, higher order representation while retaining the inherent simplicity of the original Haar basis [17].

This advancement enables higher orders of convergence, specifically achieving a fourth order, sixth order rate, which significantly reduces computational errors without a substantial increase in algorithmic complexity compared to the standard Haar Wavelet Method [55].

As previously established, higher order Haar wavelet techniques facilitate a more precise analysis of complex data patterns by meticulously capturing minute details and subtle fluctuations. This enhanced resolution proves particularly beneficial in scenarios where a high degree of information is crucial for accurately interpreting and comprehending the underlying dynamics. The higher order wavelet expansion is formally introduced as:

$$f(x)=\frac{d^{n+2s}u(x)}{dx^{n+2s}}=\sum_{i=1}^{\infty}a_i h_i(x)\,,s=1,2,\dots\ . \quad (5)$$

The approximate solution is then expressed as:

$$f(x)=\frac{d^{n+2s}u(x)}{dx^{n+2s}}=a^T H(i,x), \quad (6)$$

where a^T is the transposed coefficient vector and $H(i,x)$ is the Haar matrix. It is important to note that in a formulation based on HOHWM, the number of integration constants increases. This issue can be mitigated by incorporating additional boundary and initial conditions, periodicity conditions, or by applying the equation itself at grid or collocation points.

2.3 Evaluation Criteria for Accuracy and Convergence

The accuracy and convergence of wavelet-based methods are critical aspects for assessing their reliability and efficiency in numerical simulations, particularly when applied to complex engineering problems. The precision and convergence characteristics of both the Haar Wavelet Method and the Higher Order Haar Wavelet Method were consistently validated across all investigations by comparing their outcomes with analytical solutions or finite element simulations.

For quantitative assessment, the relative error and the numerical convergence rate were employed:

$$\text{Convergence rate} = \log\left(\frac{F_{i-1} - F_e}{F_i - F_e}\right)/\log(2), \tag{7}$$

where F_e is the existing solution based on results from finite element method, other numerical or analytical formulations, or from the literature.

In the analyses of vibration and trajectory, the standard Haar formulation consistently demonstrated a convergence rate approaching second order. This aligns with the inherent piecewise constant characteristic of the Haar basis, which yields first order derivative continuity upon integration. The error trend of the Haar Wavelet Method can be quantitatively described as:

$$e_r \propto N^{-2}, \tag{8}$$

where e_r denotes the relative error, illustrating a quadratic improvement in accuracy as the number of collocation points on a uniform grid increases. While the HWM offers robust solutions for discontinuous or transient responses, its precision in handling smooth higher order derivatives is limited, thus necessitating the development and application of the higher order formulation.

The HOHWM, derived from multiple integrations of the Haar functions, substantially enhances convergence without necessitating an increase in the number of collocation points. The HOHWM therefore follows:

$$e_r \propto N^{-2-2s}, s = 1, 2, \dots \ . \tag{9}$$

This effectively indicates higher order convergence for smooth field variables. The accuracy is predominantly governed by the integration order p rather than the resolution level j. Increasing p enhances the polynomial continuity of the basis, thereby improving approximation quality even when using coarse grids. This characteristic enables highly accurate results with as few as 16–32 collocation points, a notable advantage compared to finite element models that often necessitate several hundred nodes to achieve comparable precision.

2.4 Summary of the Framework

This chapter outlined the mathematical foundations and numerical methodology of the Haar Wavelet Method and its higher order extension, as applied throughout this research. The standard HWM approximates derivatives using orthogonal, piecewise constant Haar functions, achieving a second order accuracy on a uniform grid.

Conversely, the Higher Order Haar Wavelet Method integrates the Haar basis multiple times, generating smooth, continuous functions with fourth order convergence or higher. Both methods produce sparse, well-conditioned algebraic systems and allow

for the direct enforcement of boundary conditions. All computations in this thesis employed uniformly spaced collocation points, thereby confirming that the higher order integration of Haar functions alone is sufficient to achieve high accuracy without adaptive refinement. The subsequent chapter applies these formulations to benchmark problems in vibration, nonlocal elasticity and nonlinear fragment dynamics.

While the Higher Order Haar Wavelet Method offers notable accuracy and accelerated convergence, it is not without specific numerical constraints. The process of integrating discontinuous Haar functions to derive higher order bases can precipitate localized numerical oscillations, particularly in regions characterized by steep gradients or discontinuities within the solution field. These oscillations are a consequence of the inherently piecewise constant nature of the original Haar functions and may subtly impair the smoothness of higher derivatives if the chosen resolution level is suboptimal.

Furthermore, the accumulation of round-off errors during successive integrations, especially at very elevated orders, can lead to minor deviations in the computed coefficients. Consequently, despite the HOHWM's capacity to achieve fourth order convergence or higher and to compute natural frequencies with high accuracy using a comparatively small number of collocation points and precision are dependent upon the careful selection of an appropriate combination of resolution level and integration order tailored to the specific problem under investigation.

3 Case Studies

This chapter presents four exemplary case studies utilized for validating and demonstrating the numerical and hybrid frameworks developed previously. Each case study pertains to a unique class of structural dynamics problems, where the Haar and Higher Order Haar Wavelet Methods are applied. The first three cases address deterministic formulations of governing equations for continuous systems, while the fourth integrates the Haar wavelet transform as a preprocessing stage within convolutional neural network-based damage detection methodologies.

Collectively, these studies substantiate the accuracy, efficiency and adaptability of the Haar-based framework within both analytical and data-driven contexts. Table 1 summarizes the physical system, solution methodology and computational objective associated with each individual case study. The selection of these diverse case studies, ranging from foundational structural elements to advanced material systems and data-intensive damage detection, ensures a thorough assessment of the proposed methodologies across various complexities and application domains.

Table 1. Summary of the case studies.

Case	Physical System	Main Method	Objective
I	Timoshenko beam vibration	HOHWM	Validation of free vibration frequencies and convergence
II	Functionally graded Rayleigh-Bishop nanorod	HOHWM	Study of gradation and nonlocal effects on vibration
III	Flight dynamics of fragments	HWM	Evaluation of nonlinear trajectory prediction
IV	CFRP composite plate vibration data	Haar-CNN	Assessment of wavelet preprocessing in damage detection

3.1 Case I: Vibration Analysis of Structures

This initial case study examines the free vibration characteristics of Timoshenko beams employing the Higher Order Haar Wavelet Method. The primary goal is to validate the accuracy and convergence properties of the HOHWM against established analytical and finite element solutions. The investigation further explores how boundary conditions, beam geometry and resolution levels influence the computed natural frequencies.

Utilizing the Timoshenko beam theory, the fundamental governing differential equations describing the transverse vibration of a beam with specified geometric and material properties are expressed as follows:

$$\frac{\partial}{\partial x}\left[\kappa GA(x)\left(\frac{\partial w(x,t)}{\partial x}-\varphi(x,t)\right)\right]-\rho A\frac{\partial^2 w(x,t)}{\partial t^2}=0 \tag{10}$$

$$\frac{\partial}{\partial x}\left(EI(x)\frac{\partial \varphi(x,t)}{\partial x}\right)+\kappa GA(x)\left(\frac{\partial w(x,t)}{\partial x}-\varphi(x,t)\right)-\rho I\frac{\partial^2 \varphi(x,t)}{\partial t^2}=0 \tag{11}$$

where w and φ are the transverse displacement and rotation. Also, here, E represents Young's modulus, $I(x)$ denotes the second moment of area, $A(x)$ signifies the cross sectional area, G is the shear modulus, k functions as the shear correction factor, here is chosen to be 5/6 and ρ corresponds to the density. In the case of a uniform beam, where $A(x)$ and $I(x)$ are constant, the beam is speculated as homogeneous, isotropic and prismatic. Following a series of transformations, including the homogenization of the governing equation, it becomes feasible to derive an expression for the transverse vibration of the Timoshenko beam that is exclusively dependent on the displacement function, which can be written as:

$$EI\frac{\partial^4 w(x,t)}{\partial x^4}-\left(\frac{EI\rho}{Gk}+I\rho\right)\frac{\partial^4 w(x,t)}{\partial x^2\,\partial t^2}+\frac{I\rho^2}{Gk}\frac{\partial^4 w(x,t)}{\partial t^4}+\rho A\frac{\partial^2 w(x,t)}{\partial t^2}=0. \tag{12}$$

Moreover, in the case of tapered beam, shown in Figure. 1, the cross sectional area $A(x)$ and moment of inertia $I(x)$ are presented as:

$$A(x)=A_0\left(1-\frac{cx}{L}\right), I(x)=I_0\left(1-\frac{cx}{L}\right)^3, \quad x\in[0,L], \tag{13}$$

where *L* is the length of the beam, A_0 and I_0 are area and moment inertia at the base of the beam, respectively.

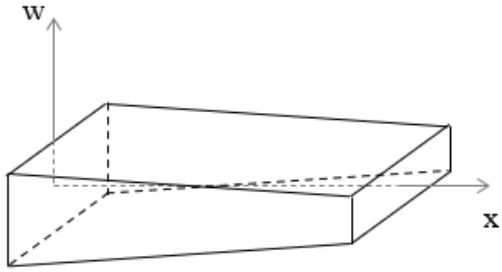

Figure 1. Representation of a tapered beam.

The bending moment, M and shear force, Q, at any given cross section are determined by the following expressions:

$$M=EI(x)\frac{\partial \varphi}{\partial x}, \quad Q=kGA(x)\left(\frac{\partial w}{\partial x}+\varphi\right). \tag{14}$$

Both simply supported and clamped-clamped boundary conditions are taken into consideration and can be expressed as:

$$\begin{aligned}&\text{For the clamped edge: } w=0, \quad \varphi=0\\ &\text{For the pinned edge: } w=0, \quad M=0.\end{aligned} \tag{15}$$

The solution serves as benchmark problems for evaluating convergence behavior in Chapter 4.

3.2 Case II: Dynamic Behavior of Functionally Graded Nanorods

This particular case study extends the application of the Higher Order Haar Wavelet Method to the modeling of longitudinal vibrations within functionally graded nanorods. The primary objective is to assess how material gradation and nonlocal elasticity collectively influence dynamic behavior, with a specific focus on the interplay between microstructural scale and variations in stiffness.

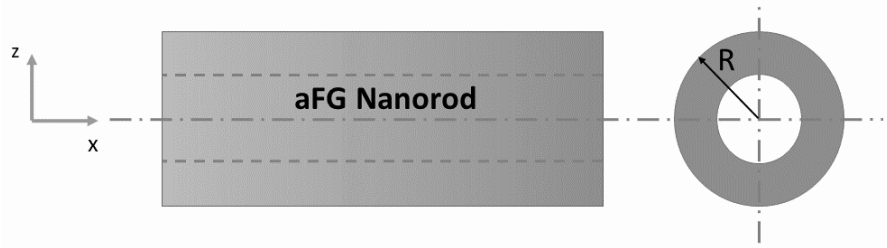

Figure 2. Schematic of Axially Graded Nanorod.

According to the Rayleigh-Bishop rod model, the longitudinal and lateral displacements of the rod can be expressed as follows:

$$u = u(x,t)$$
$$w = w(x,t) = r\underbrace{\left(\frac{E(x)}{2G(x)} - 1\right)}_{\eta}\frac{\partial u(x,t)}{\partial x}, \tag{16}$$

where η is the Poisson's ratio for nanorod and r denotes the distance of the lateral displacement of a particle from the x-axis.

To represent the continuous material variation along the nanorod axis, the elastic and inertial parameters together with the nonlocal parameter are defined using a unified power-law function as follows:

$$\begin{bmatrix} E(x) \\ G(x) \\ \rho(x) \\ e(x) \end{bmatrix} = \begin{bmatrix} E_1 - E_0 \\ G_1 - G_0 \\ \rho_1 - \rho_0 \\ e_1 - e_0 \end{bmatrix} x^k + \begin{bmatrix} E_0 \\ G_0 \\ \rho_0 \\ e_0 \end{bmatrix} \quad and \quad \begin{bmatrix} E_1 \\ \rho_1 \\ e_1 \end{bmatrix} = s \begin{bmatrix} E_0 \\ \rho_0 \\ e_0 \end{bmatrix} \tag{17}$$

where E_0, G_0, ρ_0, e_0 and E_1, G_1, ρ_1, e_1 are the properties at the left and right ends of the nanorod, respectively. Also, k denotes the material-gradation or power-law index, e refers to the nonlocal length-scale parameter in Eringen's nonlocal elasticity theory and s describes the material properties at the right side of nanorod.

The total kinetic and potential energies can be defined in accordance with nonlocal elasticity theory, [56], [57], [58], as presented:

$$E_K = \int_0^L \rho(x)A\left(\frac{\partial u(x,t)}{\partial t}\right)^2 dx + \int_0^L (e(x)a)^2 A\left[\frac{\partial}{\partial x}\left(\rho(x)\frac{\partial u(x,t)}{\partial t}\right)\right]\left(\frac{\partial^2 u(x,t)}{\partial x \partial t}\right) dx + \int_0^L \rho(x)\eta^2 I_P\left(\frac{\partial^2 u(x,t)}{\partial x \partial t}\right)^2 dx + \int_0^L (e(x)a)^2 \eta^2 I_P\left[\frac{\partial}{\partial x}\left(\rho(x)\frac{\partial^2 \delta u(x,t)}{\partial x \partial t}\right)\right]\left(\frac{\partial^3 u(x,t)}{\partial x^2 \partial t}\right) dx \quad (18)$$

$$E_P = \int_0^L E(x)A\left(\frac{\partial u(x,t)}{\partial x}\right)^2 dx + \int_0^L \eta^2 G(x) I_P\left(\frac{\partial^2 u(x,t)}{\partial x^2}\right)^2 dx, \quad (19)$$

where a is the distance between two atoms in the nanorod structure, I_P is the polar moment of inertia of nanorod and is equal to $\frac{\pi}{2}\left({R_2}^4 - {R_1}^4\right)$, R_1 and R_2 are the inner and outer radius of carbon nanotube, respectively. Thus, the Governing equation of motion for the nonlocal Rayleigh-Bishop rod model, [57], can be expressed as:

$$\frac{\partial}{\partial x}\left(E(x)A\frac{\partial u(x,t)}{\partial x}\right) - \frac{\partial^2}{\partial x^2}\left(\eta^2 G(x) I_P \frac{\partial^2 u}{\partial x^2}\right) = \frac{\partial}{\partial t}\left(\rho(x)A\frac{\partial u}{\partial t}\right) - A\frac{\partial^2}{\partial x \partial t}\left((e(x)a)^2\frac{\partial}{\partial x}\left(\rho(x)\frac{\partial u(x,t)}{\partial t}\right)\right) - \eta^2 I_P \frac{\partial^2}{\partial x \partial t}\left(\rho(x)\left(\frac{\partial^2 u(x,t)}{\partial x \partial t}\right)\right) + \eta^2 I_P \frac{\partial^3}{\partial x^2 \partial t}\left((e(x)a)^2\frac{\partial}{\partial x}\left(\rho(x)\frac{\partial^2 u(x,t)}{\partial x \partial t}\right)\right). \quad (20)$$

By assuming the harmonic wave function, $(u(x,t) = U(x)\, sin\, \omega t)$, and dimensionless distance in the nanorod's lattice structure, it can be rewritten as:

$$A\left(\frac{\partial E(X)}{\partial X}\frac{\partial U(X)}{\partial X}\right) + A\left(E(X)\frac{\partial^2 U(X)}{\partial X^2}\right) - \eta^2 I_P \frac{\partial^2}{\partial x^2}\left(G(X)\frac{\partial^2 U(X)}{\partial X^2}\right) = -\omega^2 A\left(\rho(X)U(X)\right) + \omega^2 A\left(\frac{\partial e(X)}{\partial X}\frac{\partial}{\partial X}\left(\rho(X)U(X)\right) + e(X)\frac{\partial^2}{\partial X^2}\left(\rho(X)U(X)\right)\right) + \omega^2\eta^2 I_P\left(\frac{\partial \rho(X)}{\partial x}\left(\frac{\partial U(X)}{\partial x}\right) + \rho(X)\frac{\partial^2 U(X)}{\partial X^2}\right) - \omega^2\eta^2 I_P\left(\frac{\partial^2 e(X)}{\partial X^2}\frac{\partial}{\partial X}\left(\rho(X)\frac{\partial U(X)}{\partial X}\right) + 2\frac{\partial e(X)}{\partial x}\frac{\partial^2}{\partial x^2}\left(\rho(X)\frac{\partial U(X)}{\partial X}\right) + e(X)\frac{\partial^3}{\partial X^3}\left(\rho(X)\frac{\partial U(X)}{\partial X}\right)\right). \quad (21)$$

By implementing forth order Higher Order Haar wavelet method, the displacement function of the nonorod will be obtained as:

$$U(X) = a^T P_4(i,x) + C_1 \frac{X^3}{6} + C_2 \frac{X^2}{2} + C_3 X + C_4, \tag{22}$$

where $P_4(i,x)$ represents the integration matrices, and C_i denotes the integration constants, which are determined by applying the boundary conditions. The boundary conditions considered for this analysis are clamped-free and clamped-clamped. The resulting equations are subsequently resolved utilizing the HOHWM, as detailed in Chapter 4, to thoroughly investigate the frequency response and convergence properties.

3.3 Case III: Flight Dynamics of Fragments

Case III involves the application of the Haar Wavelet Method to simulate the nonlinear dynamics of high velocity fragments under the influence of aerodynamic drag and gravitational forces. The objective is to evaluate the method's stability and computational efficiency in addressing coupled, nonlinear, time-dependent systems.

Prior to developing the numerical formulation, it is essential to determine the initial coordinates and velocities related to the fragments' positions. The ANSYS AUTODYN solver, which is founded on the finite element approach and stochastic failure theory, simulates the natural fragmentation of projectiles. For estimating fragment flight, a fixed coordinate system is adopted, where the x-axis and the unfragmented projectile's axis of symmetry intersect on the projectile's rear surface at a height of one meter. Fragmentation of the projectile occurs at a 60 degree angle relative to the ground. The x-y plane denotes the Earth's surface and the fragments commence their flight at $t = 0$ following the explosion [59].

The trajectory of a fragment subjected to both aerodynamic drag and gravitational forces can be accurately predicted through the application of the point mass trajectory model and presented as:

$$\begin{aligned} x'' &= -\frac{A\rho C_D}{2m}\sqrt{x'^2 + y'^2 + z'^2}\cdot x' \\ y'' &= -\frac{A\rho C_D}{2m}\sqrt{x'^2 + y'^2 + z'^2}\cdot y' \\ z'' &= -\frac{A\rho C_D}{2m}\sqrt{x'^2 + y'^2 + z'^2}\cdot z' - g \end{aligned} \tag{23}$$

where x', y' and z' represent the velocities in their respective directions and $\rho = 1.20\ kg/m^3$ denotes the air density and $g = 9.81\ m/s^2$ is the gravitational acceleration, A is the fragment reference area, and m is the fragment mass. Additionally, C_D signifies the drag coefficient, which is typically influenced by the Mach number. However, for simplicity, a constant drag coefficient is assumed in this study [60]. To develop a solution for the system of differential equations, various mathematical operations are performed:

$$\frac{x''}{x'} = \frac{y''}{y'} \quad \longrightarrow \quad y = cx + d\ ;\ c = \frac{y_0'}{x_0'}\ , d = y_0 - \frac{y_0'}{x_0'}\cdot x_0\ . \tag{24}$$

Quasilinearization is a numerical technique that iteratively solves a series of linearized problems to approximate the solution of a nonlinear differential system. This process involves linearizing the nonlinear problem around the current estimated solution at each iteration, solving the resulting linearized problem and then updating the estimate of the solution to the original nonlinear problem. This iterative procedure continues until convergence is achieved. Subsequently, the system of three equations can be reduced to two. As expressed as:

$$\text{substitute } \frac{A\rho C_D}{2m} = k \rightarrow \quad \begin{aligned} x'' &= -k\sqrt{(1+c^2)x'^2 + z'^2}\, x' = f_1(x', z') \\ z'' &= -k\sqrt{(1+c^2)x'^2 + z'^2}\, z' - g = f_2(x', z') \end{aligned} \tag{25}$$

To linearize the nonlinear systems, a Taylor Series expansion has been utilized. Which can be written as:

$$\begin{aligned} x''_{n+1} &= f_1(x'_n, z'_n) + (x'_{n+1} - x'_{\mathrm{n}})\frac{\partial f_1}{\partial x'_{\mathrm{n}}} + (z'_{\mathrm{n}+1} - z'_{\mathrm{n}})\frac{\partial f_1}{\partial z'_{\mathrm{n}}} \\ z''_{n+1} &= f_2(x'_n, z'_n) + (z'_{n+1} - z'_{\mathrm{n}})\frac{\partial f_2}{\partial z'_{\mathrm{n}}} + (x'_{\mathrm{n}+1} - x'_{\mathrm{n}})\frac{\partial f_2}{\partial x'_{\mathrm{n}}} \end{aligned} \tag{26}$$

where

$$\begin{aligned} \frac{\partial f_1}{\partial x'} &= -k\left[\frac{(1+c^2)x' \cdot x'}{\sqrt{(1+c^2)x'^2 + z'^2}} + \sqrt{(1+c^2)x'^2 + z'^2}\right] \\ \frac{\partial f_1}{\partial z'} &= -k\left[\frac{x' \cdot z'}{\sqrt{(1+c^2)x'^2 + z'^2}}\right] \\ \frac{\partial f_2}{\partial x'} &= -k\left[\frac{(1+c^2)x' \cdot z'}{\sqrt{(1+c^2)x'^2 + z'^2}}\right] \\ \frac{\partial f_2}{\partial z'} &= -k\left[\frac{z' \cdot z'}{\sqrt{(1+c^2)x'^2 + z'^2}} + \sqrt{(1+c^2)x'^2 + z'^2}\right] \end{aligned} \tag{27}$$

In order to solve the system of equations, the HWM is employed:

$$\begin{aligned} x''_{n+1} &= a^{\top}H & z''_{n+1} &= b^{\top}H \\ x'_{n+1} &= a^{\top}P_1 + x_0 & z'_{n+1} &= b^{\top}P_1 + z_0 \end{aligned} \tag{28}$$

where leads to:

$$\begin{aligned} a^{\top}\left[H - P_1\frac{\partial f_1}{\partial x'_{\mathrm{n}}}\right] &= b^{\top}P_1\frac{\partial f_1}{\partial z'_{\mathrm{n}}} + \underbrace{f_1(x'_{\mathrm{n}}, z'_{\mathrm{n}}) + (x_0 - x'_{\mathrm{n}})\frac{\partial f_1}{\partial x'_{\mathrm{n}}} + (z_0 - z'_{\mathrm{n}})\frac{\partial f_1}{\partial z'_{\mathrm{n}}}}_{g_1} \\ b^{\top}\left[H - P_1\frac{\partial f_2}{\partial z'_{\mathrm{n}}}\right] &= a^{\top}P_1\frac{\partial f_2}{\partial x'_{\mathrm{n}}} + \underbrace{f_2(x'_{\mathrm{n}}, z'_{\mathrm{n}}) + (z_0 - z'_{\mathrm{n}})\frac{\partial f_2}{\partial z'_{\mathrm{n}}} + (x_0 - x'_{\mathrm{n}})\frac{\partial f_2}{\partial x'_{\mathrm{n}}}}_{g_2} \end{aligned} \tag{29}$$

The problem is solved numerically in Chapter 4 to test computational convergence and error evolution.

3.4 Case IV: Damage Detection in Composite Plates Using Haar-CNN Hybrid Model

This particular case study extends the existing wavelet-based modeling framework into the domain of data-driven analysis by integrating the Haar wavelet transform with convolutional neural networks for detecting damage through vibration analysis in CFRP composite plates. The primary objective is to investigate how multilevel Haar wavelet preprocessing affects feature extraction and, consequently, classification accuracy, especially when dealing with small, experimentally obtained datasets that are inherently subject to noise.

Two experimental datasets, [61], [62], are analyzed. The initial dataset comprises vibration response signals acquired from CFRP plates that had attached masses, thereby simulating localized reductions in stiffness. Each signal within this dataset corresponds to a specific mass configuration, recorded under identical excitation and boundary conditions [63], [64], [65]. The second dataset consists of frequency response function measurements obtained from similar CFRP plates, which contained controlled delamination defects [66], [67], [68], [69], [70]. Both datasets encompass a healthy reference case alongside several damaged conditions, thus framing them as multi-class classification problems. In both investigations, the Haar wavelet transform was employed to decompose each vibration or FRF signal into multiresolution approximation and detail coefficients. This process serves to highlight local variations while simultaneously filtering out low-frequency trends. The decomposition depth was systematically varied between levels 5 and 10 to thoroughly examine the impact of signal resolution on the performance of the CNN.

Two distinct CNN architectures were developed to process the transformed data, each corresponding to one of the two datasets.

The first architecture, specifically applied to the vibration dataset, implemented a two dimensional CNN configuration. Each vibration signal underwent decomposition using the stationary Haar wavelet transform, and the resultant approximation and detail coefficients were subsequently arranged into a two dimensional coefficient map, which then served as the input for the CNN. The network architecture featured two convolutional layers with rectified-linear activation functions, followed by max-pooling, dropout regularization, and two fully connected layers, culminating in a softmax classifier. The model was trained using the Adam optimizer, with a learning rate of 0.001 and categorical cross-entropy loss. To enhance convergence and mitigate overfitting, batch normalization and early stopping techniques were applied. This configuration was specifically optimized for small datasets, ensuring stable learning and generalization capabilities even with limited training data.

The second architecture, designed for the FRF dataset, utilized a comparable CNN structure but was tailored to process Haar-transformed frequency-response matrices. Each FRF magnitude spectrum was decomposed up to level 10, and the approximation and detail components were then stacked to create a two dimensional grayscale representation indicative of the signal's spectral energy distribution. This network incorporated two convolutional layers, featuring 32 and 64 filters respectively, each succeeded by rectified-linear activation, max-pooling, and dropout. The output from the convolutional layers was then flattened and passed through two dense layers, comprising 128 and 64 neurons, before reaching the final softmax classification layer. The same optimization parameters as in the first case were utilized, enabling a direct

comparison of training behavior and classification accuracy. This configuration effectively captures spatial correlations within the wavelet coefficient maps, thereby extracting multiscale vibration patterns that are associated with delamination-induced stiffness changes.

Figure 3 provides a schematic representation of the Haar-CNN hybrid architecture, illustrating the arrangement of convolutional, pooling, and fully connected layers for both datasets.

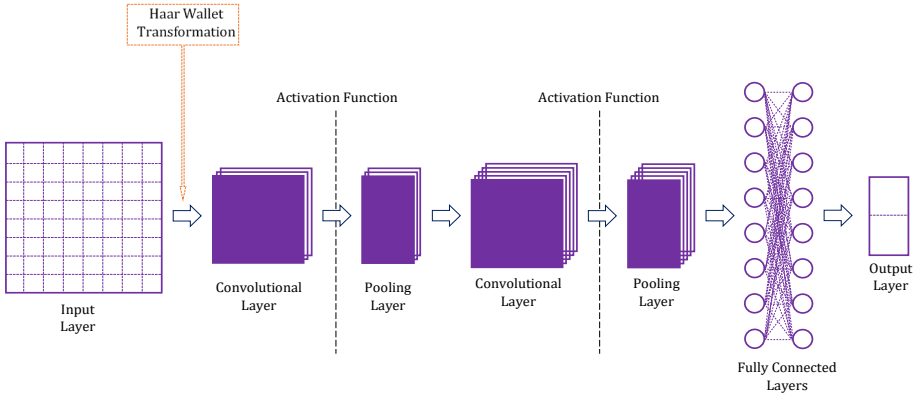

Figure 3. Haar-CNN architecture.

Both networks were evaluated using a comprehensive set of metrics including accuracy, precision, recall and F_1-score, augmented by confusion matrices to ascertain classification consistency across all damage classes. Comparative analyses between raw and Haar-preprocessed inputs unequivocally demonstrated that wavelet decomposition significantly enhances the distinctiveness of features intrinsically linked to localized damage. Furthermore, the influence of the decomposition level was investigated to identify the most efficacious scale for optimal feature separation and network stability.

Consequently, the Haar-CNN hybrid approach establishes a crucial link between physically interpretable signal transformation and automated feature extraction. By synergistically combining the localization ability of the Haar transform with CNN-based learning, this methodology achieves robust and generalizable classification performance on small, experimentally derived vibration datasets, as thoroughly elaborated in Chapter 4.

3.5 Summary

This chapter presented four distinct case studies, each representative of a specific category within structural dynamics problems.

The initial three cases established the governing equations and boundary conditions for deterministic analyses, whereas the fourth case integrated wavelet-based preprocessing with deep learning for vibration-based damage detection in composite plates.

Collectively, these problems underscore the versatility of the Haar and Higher Order Haar Wavelet Methods across diverse domains, ranging from high order differential modeling to hybrid data interpretation.

The subsequent chapter will detail the numerical results, convergence analysis and comparative evaluation for each investigated case.

4 Results and Discussion

This chapter presents the numerical and data-driven results obtained through the application of the Haar Wavelet Method, the Higher Order Haar Wavelet Method and the previously introduced Haar-CNN hybrid framework.

The analyses encompass four distinct problems, which collectively serve to validate the accuracy, stability, and versatility of the proposed methodologies across various physical and computational contexts. The initial three cases focus on deterministic structural dynamics, specifically investigating the free vibration of Timoshenko beams, longitudinal wave propagation in functionally graded nanorods, and the nonlinear motion of fragments. The fourth case extends this framework to address vibration-based damage detection, utilizing wavelet-enhanced convolutional neural networks.

For the deterministic studies, the results include computed natural frequencies and dispersion characteristics, which are compared with analytical and numerical references to assess numerical precision and convergence. The performance of both HWM and HOHWM is evaluated based on relative error, convergence rate, and the smoothness of the computed solutions. The discussion highlights the significant improvements achieved through higher order Haar integration and the consistency of convergence across problems of varying complexity and scale. In the context of the Haar-CNN application, the results primarily concentrate on the classification performance attained both with and without Haar-based preprocessing, exploring how multilevel wavelet decomposition impacts feature separability and model robustness in small experimental datasets.

Throughout this chapter, quantitative comparisons are presented in tables and figures adapted from the author's published works. Each case study provides a brief verification of numerical accuracy, followed by a discussion of the physical interpretation of the results. The analysis demonstrates that the Haar-based numerical formulations maintain an accuracy comparable to spectral or analytical methods, while the hybrid Haar-CNN framework effectively enhances data-driven damage detection by incorporating wavelet-domain feature representations. Collectively, these results establish the reliability and general applicability of the proposed wavelet-based methodologies in the fields of structural dynamics and damage assessment.

4.1 Vibration Analysis of Structures

The Higher Order Haar Wavelet Method was employed to analyze the free vibration characteristics of Timoshenko beams, encompassing both uniform and linearly tapered configurations. The primary objective was to substantiate the convergence and accuracy of this higher order Haar formulation by comparing its results with established analytical solutions.

The governing coupled equations for transverse displacement and rotation, detailed in Chapter 3, were discretized using uniformly distributed collocation points, and boundary conditions were directly integrated into the Haar integration framework. Table 2, as presented in Paper I, presents the dimensionless neutral frequency of a uniform Timoshenko beam under pinned-pinned boundary conditions, calculated using both the conventional Haar Wavelet Method and its higher order counterpart. The findings affirm a strong correlation between the HOHWM and analytical solutions. While the HWM exhibits second order convergence, the HOHWM achieves fourth and sixth order accuracy, underscoring the enhanced precision derived from the higher order integration of the Haar basis.

Table 2. Comparison of HWM and HOHWM for Timoshenko beams under pinned-pinned boundary conditions.

N	HWM			HOHWM 4th ($s = 1$)			HOHWM 6th ($s = 2$)		
	Frequency	A. error	Conv. rate	Frequency	A. error	Conv. rate	Frequency	A. error	Conv. rate
4	10.76068319	1.60E+00		9.16627318	5.59E-03		9.16109539	4.12E-04	
8	9.59208533	4.31E-01	1.8954	9.16088118	1.98E-04	4.0580	9.16069124	8.05E-06	5.2583
16	9.27047366	1.10E-01	1.9742	9.16069928	1.61E-05	4.0268	9.16068333	1.48E-07	5.6800
32	9.18825306	2.76E-02	1.9935	9.16068724	4.06E-06	4.0244	9.16068322	3.68E-08	5.7820
64	9.16758331	6.90E-03	1.9983	9.16068383	6.42E-07	4.0240	9.16068319	6.74E-10	5.9221
128	9.16240869	1.73E-03	1.9995	9.16068327	8.79E-08	4.0133	9.16068318	1.73E-11	5.9850
256	9.16111459	4.31E-04	1.9998	9.16068320	1.74E-08	4.0054	9.16068318	3.90E-12	6.0130
Exact solution: 9.16068318									

Table 2 shows the convergence behavior of the HWM and HOHWM for increasing Haar resolution levels, previously reported in Paper I. The rapid convergence of the HOHWM signifies that a limited number of collocation points is sufficient to attain high accuracy, thereby substantially decreasing computational demands when compared to conventional finite element method discretization. To further validate the method's versatility, clamped-clamped and clamped-pinned configurations were analyzed, see Table 3, as presented in Paper II.

Table 3. Comparison of HWM and HOHWM for Timoshenko beams under various boundary conditions.

	N	HWM			HOHWM 4th ($s = 1$)			HOHWM 6th ($s = 2$)		
		Frequency	A. error	Conv. rate	Frequency	A. error	Conv. Rate	Frequency	A. error	Conv. rate
Clamped-Pinned	4	12.16296846	1.08E+00		11.12396203	4.15E-02		11.08476457	2.27E-03	
	8	11.67284507	5.90E-01	2.0085	11.08552579	3.03E-03	4.0017	11.08257904	7.99E-05	6.1932
	16	11.16717818	8.47E-02	2.0065	11.08280853	3.09E-04	4.0153	11.08249987	6.91E-07	6.1877
	32	11. 08814918	5.65E-03	2.0050	11.08250835	9.17E-06	4.0153	11. 08249920	2.00E-08	6.1326
	64	11. 08267527	1.76E-04	2.0043	11.08249969	5.14E-07	4.0010	11. 08249919	5.82E-09	6.1049
	128	11.08254898	4.98E-05	2.0042	11.08249985	6.72E-07	4.0099	11.08249918	4.24E-10	6.0573
	256	11.08250581	6.63E-06	2.0024	11.08249918	4.96E-09	4.0002	11.08249918	3.35E-11	6.0547
	Exact solution: 11.08249918									
Clamped-Clamped	4	13.96275845	1.28e-01		13.84197845	7.22e-03		13.83477975	2.13e-05	
	8	13.86655612	3.18e-02	2.0091	13.83519214	4.34e-04	4.0576	13.83476001	1.56e-06	5.4358
	16	13.84269132	7.93e-03	2.003	13.83478525	2.68e-05	4.0146	13.83475854	8.43e-08	5.7522
	32	13.83674066	1.98e-03	2.0007	13.83476012	1.67e-06	4.0036	13.83475846	1.51e-09	5.9467
	64	13.83525392	4.95e-04	2.00019	13.83475856	1.04e-07	4.0009	13.83475846	7.71e-10	5.9955
	128	13.83488232	1.24e-04	2.00004	13.83475846	6.53e-09	4.0002	13.83475845	4.08e-11	5.9999
	256	13.83478942	3.10e-05	2.00001	13.83475845	4.08e-10	4.0000	13.83475845	1.40e-13	6.0000
	Exact solution: 13.83475845									

The consistent agreement observed across all boundary conditions corroborates the robustness of the HOHWM formulation.

To further evaluate the method's versatility, it was applied to a linearly tapered Timoshenko beam. The stiffness and mass distributions were directly incorporated into the governing equations without modifying the underlying Haar framework. Table 4, as presented in Paper II, summarizes the fundamental nondimensional frequencies for various taper ratios. The results indicate that the HOHWM accurately captures the frequency reduction attributed to tapering, maintaining minimal deviation from the existing solution.

Table 4. Effect of taper ratio on non-dimensional natural frequencies of the clamped-clamped Timoshenko beam.

	N	HWM			HOHWM 4th			HOHWM 6th		
		Frequency	A. error	Conv. rate	Frequency	A. error	Conv. Rate	Frequency	A. error	Conv. rate
c=0.4	4	13.38213007	9.60E-01		12.42216412	3.56E-02		12.42216313	4.40E-03	
	8	12.51071171	8.85E-02	2.0154	12.45779287	7.62E-03	4.3451	12.42655937	7.71E-04	6.0527
	16	12.43177774	9.61E-03	2.0095	12.42293499	7.72E-04	4.0623	12.42217245	9.32E-06	6.0129
	32	12.42292193	7.59E-04	2.0037	12.42221943	5.63E-05	4.0103	12.42216313	4.41E-07	6.0099
	64	12.42223492	7.18E-05	2.0018	12.42978489	9.92E-07	4.0096	12.42293432	4.36E-09	6.0042
	128	12.42218071	1.76E-05	2.0008	12.42216317	4.02E-08	4.0073	12.42216357	7.28E-10	6.0017
	256	12.42216626	3.13E-06	2.0003	12.42216313	4.39E-09	4.0023	12.42216313	2.71E-11	6.0009
	Existing result = 12.422163									
c=0.8	4	10.77014610	1.04E+00		9.738846102	1.17E-02		9.727997702	8.52E-04	
	8	10.28714610	5.60E-01	2.0994	9.727886102	7.40E-04	4.0807	9.727181202	3.51E-05	6.0698
	16	9.782096102	5.50E-02	2.0848	9.727219602	7.35E-05	4.0713	9.727147068	9.66E-07	6.0695
	32	9.728230102	1.08E-03	2.0631	9.727157102	1.10E-05	4.0466	9.727146185	8.28E-08	6.0606
	64	9.727253202	1.07E-04	2.0480	9.727151332	5.23E-06	4.0402	9.727146103	6.74E-10	6.0326
	128	9.727156532	1.04E-05	2.0279	9.727146886	7.84E-07	4.0198	9.727146102	4.75E-11	6.0050
	256	9.727147652	1.55E-06	2.0051	9.727146151	4.90E-08	4.0074	9.727146102	6.84E-12	6.0007
	Exact solution= 9.727146									

The consistent accuracy of the HOHWM across both uniform and tapered geometries highlights the method's adaptability in addressing spatially varying stiffness properties without compromising precision. The strong correlation between HOHWM, analytical, and existing results corroborates the theoretical framework, affirming that the method achieves higher order convergence while retaining the inherent simplicity and sparsity of the Haar framework. These findings position the HOHWM as a dependable and computationally efficient alternative to traditional high order numerical approaches for structural vibration analysis.

4.2 Dynamic Behavior of Functionally Graded Nanorods

The Higher Order Haar Wavelet Method underwent validation through its application to the longitudinal vibration analysis of homogeneous Rayleigh-Bishop nanorods, considering both local and nonlocal formulations. The numerical accuracy and fourth order convergence of the HOHWM, particularly when compared to the standard Haar Wavelet Method, were substantiated by the computed nondimensional frequencies, absolute errors, and convergence rates presented in Table 5. More detailed investigation of these findings are presented in paper III.

Table 5. Comparison of HWM and HOHWM for Homogenous Rayleigh-Bishop Rod.

	N	HWM			HOHWM 4th		
		Frequency	A. error	Conv. rate	Frequency	A. error	Conv. Rate
e_0=0	4	2.319104	1.78e-02	---	2.302340	1.02e-03	---
	8	2.305855	4.53e-03	1.9714	2.301383	6.21e-05	4.0372
	16	2.302459	1.14e-03	1.9937	2.301324	3.85e-06	4.0096
	32	2.301605	2.85e-04	1.9984	2.301321	2.41e-07	4.0024
	64	2.301392	7.13e-05	1.9996	2.301320	1.50e-08	4.0006
	128	2.301338	1.78e-05	1.9999	2.301320	9.39e-10	4.0001
	256	2.301325	4.45e-06	1.9999	2.301320	5.87e-11	4.0000
	Existing result = 2.30132095212840503962						
e_0=0.1	4	2.210516	1.50e-02	---	2.196385	8.60e-04	---
	8	2.199350	3.82e-03	1.9706	2.195577	5.24e-05	4.0374
	16	2.196485	9.61e-04	1.9935	2.195528	3.25e-06	4.0097
	32	2.195765	2.40e-04	1.9984	2.195525	2.03e-07	4.0024
	64	2.195585	6.01e-05	1.9996	2.195525	1.27e-08	4.0006
	128	2.195540	1.50e-05	1.9999	2.195525	7.92e-10	4.0001
	256	2.195528	3.76e-06	1.9999	2.195525	4.75e-11	4.0000
	Exact solution= 2.195525123273453						

The data substantiate a fourth order convergence rate for the HOHWM, whereas the conventional HWM exhibits second order convergence. The utilization of the higher order formulation leads to an approximate two order of magnitude reduction in absolute error, with computed frequencies closely aligning with exact reference values, demonstrating negligible deviation. These outcomes affirm the accuracy and efficacy of the HOHWM in characterizing the longitudinal dynamics of both local and nonlocal homogeneous Rayleigh-Bishop nanorods.

4.3 Flight Dynamics of Fragments

The nonlinear equations of motion fragments, subject to aerodynamic drag and gravity, were analyzed using both the Haar Wavelet Method and the Higher Order Haar Wavelet Method. The convergence and accuracy of these methods were assessed by comparing their results against a numerical Runge-Kutta reference solution.

For a case study, a projectile weighing $12\ kg$ and diameter of $105\ mm$ was simulated. This simulation generated approximately 3950 fragments during the $0.14\ ms$; the initial position and velocity of one fragment were selected, and its position and velocity in all directions were subsequently calculated at various time intervals using the formulation presented previously, as detailed in Table 6 previously reported in Paper V.

Table 6. Position and velocities based on the HWM for a chosen fragment.

t	x	y	z	x'	y'	z'
initial	0.1143	-0.1703	0.8062	-24.2968	-1121.0214	69.5044
1.0	-11.2112	-524.3401	29.8954	-6.14743	-285.0912	11.4625
2.0	-15.8341	-738.8114	34.3712	-3.5065	-162.7054	-1.2054
3.0	-18.7624	-874.7501	29.0023	-2.4553	-113.9810	-9.1834
4.0	-20.9146	-974.7061	16.4569	-1.8853	-87.5647	-15.7229

Table 7, as presented in Paper IV, presents the velocity and location for a chosen fragment calculated with HWM and also HOHWM.

Table 7. Comparison of HWM and HOHWM for a chosen fragment at $t = 2.5s$.

	N	HWM			HOHWM 4th		
		Value	A. error	Conv. rate	Value	A. error	Conv. rate
x	4	-17.29994925	1.28E-01		-17.42072359	7.23E-03	
	8	-17.39615158	3.18E-02	2.0103933	-17.42751557	4.34E-04	4.0576692
	16	-17.42001639	7.93E-03	2.0030078	-17.42792242	2.68E-05	4.0146075
	32	-17.42596710	1.98E-03	2.0007748	-17.42794758	1.67E-06	4.0036622
	64	-17.42745378	4.95E-04	2.0001951	-17.42794915	1.04E-07	4.0009162
	128	-17.42782539	1.24E-04	2.0000489	-17.42794924	6.53E-09	4.0002289
	256	-17.42791828	3.10E-05	2.0000122	-17.42794925	4.08E-10	4.0000549
	Runge-Kutta method: -17.42794925						
x'	4	-2.78958350	9.85E-02		-2.88349768	4.63E-03	
	8	-2.86413772	2.40E-02	2.0383492	-2.88784956	2.78E-04	4.0581877
	16	-2.88213661	5.99E-03	2.0015815	-2.88811028	1.72E-05	4.0142098
	32	-2.88663071	1.50E-03	2.0009089	-2.88812641	1.07E-06	4.0046429
	64	-2.88775339	3.74E-04	2.0003872	-2.88812741	6.69E-08	4.0008970
	128	-2.88803396	9.35E-05	2.0000500	-2.88812748	4.18E-09	4.0002293
	256	-2.88810410	2.34E-05	2.0000246	-2.88812748	2.61E-10	4.0000268
	Runge-Kutta method: -2.88812748						

The absolute error and convergence rates for both the HWM and HOHWM were determined using the exact Runge-Kutta reference solution.

The numerical results, presented in Table 7, validate that the HOHWM consistently achieves fourth order convergence, while the conventional HWM maintains second order accuracy. This method consistently produces stable and smooth solutions for the intricate nonlinear equations of motion, demonstrating accuracy comparable to the analytical Runge-Kutta reference solution. These findings collectively affirm the applicability of the higher order Haar formulation for accurately modeling fragment trajectories under the influence of aerodynamic drag.

4.4 Damage Detection in Composite Plates Using Haar-CNN Hybrid Model

A convolutional neural network model, employing Haar wavelets, was assessed using two experimental datasets derived from vibration analyses of carbon fiber reinforced polymer composite plates. The initial dataset encompassed mass attachment scenarios, indicative of various damage classifications, while the second dataset pertained to delamination cases identified via frequency response function measurements. Both datasets underwent processing through stationary Haar wavelet decomposition across multiple levels, specifically ranging from 5 to 10.

The primary objective was to quantify the influence of the decomposition level on the CNN's capacity to categorize distinct damage conditions and to ascertain the optimal wavelet resolution for enhancing feature separability and model generalization.

For each dataset, two distinct models were trained:

1. A Baseline CNN: This model was trained directly using raw signals or frequency response function inputs.
2. A Haar-CNN Hybrid: This model was trained on Haar-decomposed coefficients, which were subsequently reconstructed into two-dimensional matrices.

The network architecture, as previously discussed in Chapter3, incorporated convolutional layers, featuring ReLU activation, max-pooling, dropout regularization, and fully connected dense layers, culminating in a softmax output layer. The Adam optimizer was utilized with a learning rate set at 0.001, and categorical cross-entropy served as the chosen loss function. Training proceeded for 100/200 epochs, with batch normalization applied between convolutional layers, employing a 70-15-15 data split for training, validation, and testing purposes.

4.4.1 Case 1: Mass-Attachment Dataset

The initial dataset comprises vibration signals collected from a carbon fiber reinforced polymer plate configured with various mass attachments. Each configuration signifies a distinct damage scenario characterized by localized stiffness reduction. However, the dataset's limited size, offering only a few samples per configuration, poses a significant hurdle for data-driven modeling. This scarcity of examples restricts the convolutional neural network's generalization capability and heightens the training process's susceptibility to initialization variability and noise.

Figure 4 illustrates a representative signal, decomposed up to level 10, displaying the detail coefficients D_5-D_{10} and the approximation component A_{10}. This decomposition effectively demonstrates how the Haar transform isolates transient, high-frequency components, indicative of local disturbances, in the upper detail levels, while preserving the global vibration trend in the lower approximation.

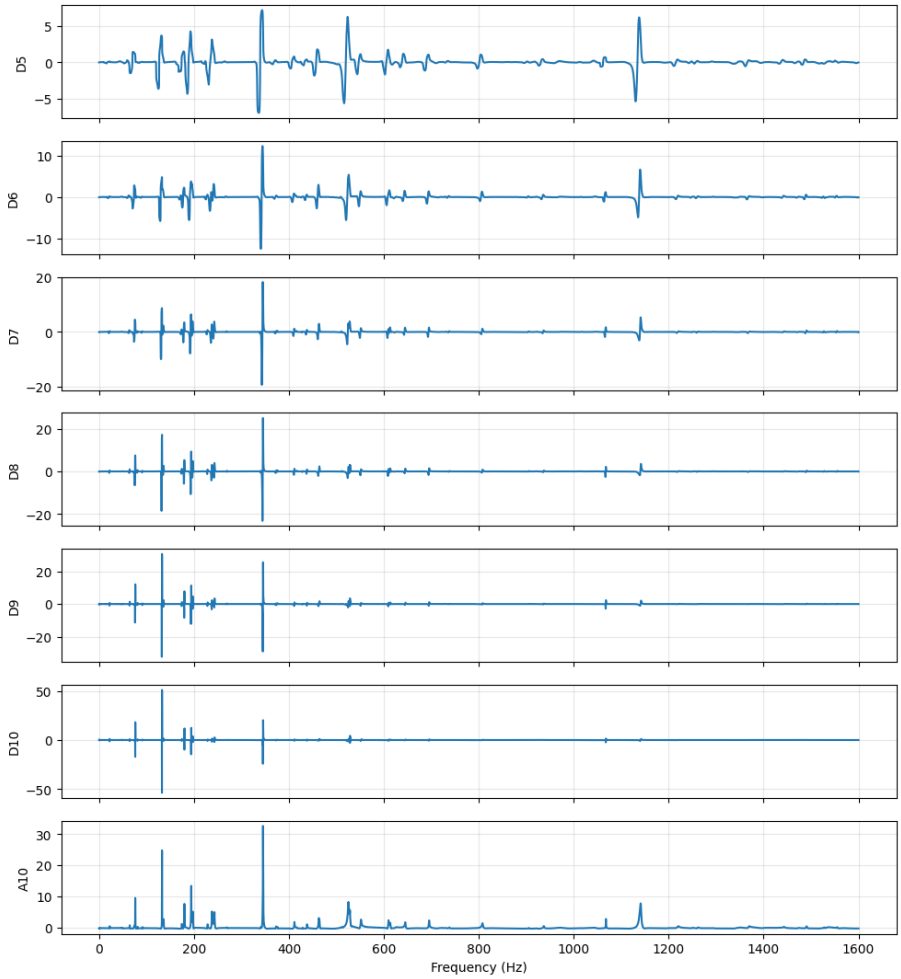

Figure 4. Stationary Haar wavelet transform of a representative vibration signal.

Two models were evaluated under identical hyperparameter configurations: a baseline CNN trained directly on raw vibration signals and a Haar-CNN model trained on Haar-transformed coefficients derived from decomposition level 8. Both models shared the same network architecture, activation functions, optimizer, and training duration, ensuring that any observed discrepancies stemmed solely from the preprocessing stage.

Figure 5 illustrates a comparative analysis of the training and validation accuracy for both the baseline CNN and the Haar-CNN. While both networks exhibited progressive accuracy improvements over epochs, the baseline model displayed more pronounced fluctuations and a clear divergence between its training and validation curves. In contrast, the Haar-CNN model demonstrated smoother convergence and reduced disparity between its training and validation accuracy. Although the ultimate accuracy remained moderate, this limitation is primarily attributable to the exceptionally small dataset and the inherent spectral similarity among certain mass-attachment cases, which complicates class separation. The Haar-CNN's smoother convergence corroborates that wavelet representation stabilizes the learning process by filtering redundant information and accentuating the most energetic transient components within the vibration signal.

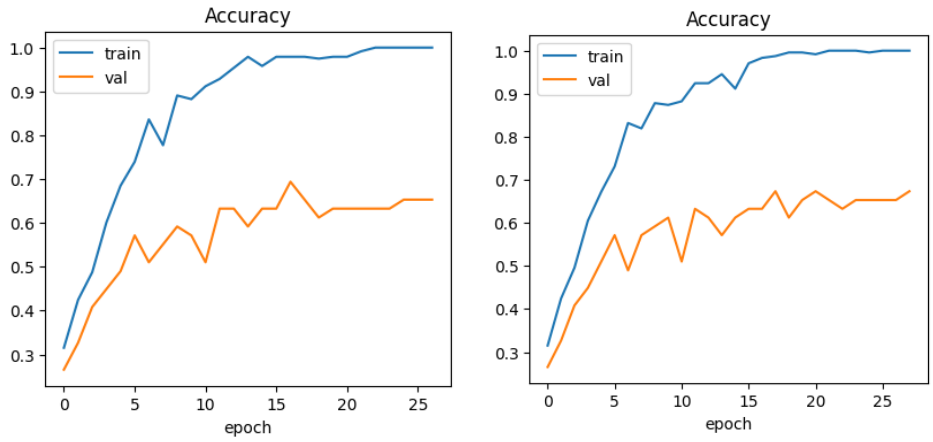

Baseline CNN Haar-CNN

Figure 5. Training and validation accuracy for baseline CNN and Haar-CNN at Haar level 8 for the mass-attachment dataset.

Figure 6 presents the confusion matrices for both models. The baseline CNN revealed considerable overlap between adjacent classes, particularly in the mid-range damage states where vibration patterns are spectrally analogous. Following Haar preprocessing, the diagonal dominance increased, and off-diagonal elements diminished, indicating enhanced recognition consistency across categories. This improvement reflects the Haar transform's capacity to highlight localized frequency alterations associated with subtle stiffness variations.

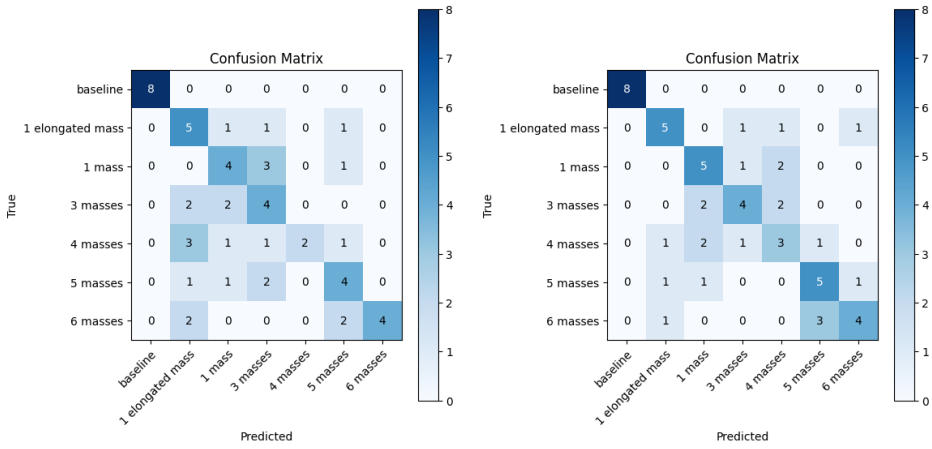

Baseline CNN Haar-CNN

Figure 6. Confusion matrices for baseline CNN and Haar-CNN at Haar level 8 for the mass-attachment dataset.

In conclusion, despite the inherent limitations on absolute accuracy imposed by the smaller dataset size, the comparative enhancement achieved through Haar decomposition suggests that integrating multiscale preprocessing can partially offset sparse data challenges by improving feature clarity and network stability.

4.4.2 Case 2: Delamination Dataset

This case study examines the impact of Haar wavelet preprocessing on the performance of convolutional neural networks in classifying delamination within carbon fiber reinforced polymer plates. The dataset comprises vibration response signals representing three structural conditions: two distinct delamination sizes and a healthy configuration. Each signal segment captures the steady state and transient frequency response of the plate under consistent boundary and excitation conditions.

Figure 7 illustrates a representative vibration signal segment from the dataset. The broadband, irregular pattern observed reflects the complex dynamic response characteristic of composite materials, where multiple vibration modes often overlap. Prior to analysis, the signal was standardized to eliminate scaling bias and emphasize relative variations.

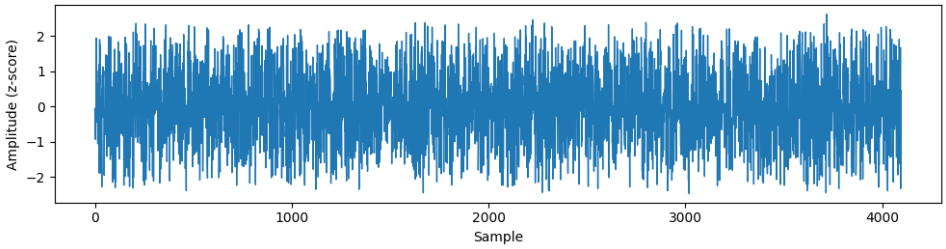

Figure 7. Original vibration signal segment from the delamination dataset.

Subsequently, the stationary Haar wavelet transform was applied at a decomposition depth of eight levels, generating a multiresolution representation depicted in Figure 8. This band-stack visualization effectively demonstrates how energy is distributed across detail and approximation components (D_1-D_8 and A_8). Specifically, the higher levels capture localized, high-frequency fluctuations associated with damage-induced discontinuities, while the lower levels retain global modal behavior. This decomposition technique allows for the simultaneous representation of vibration features in both the time and frequency domains, thereby forming the input for the neural network.

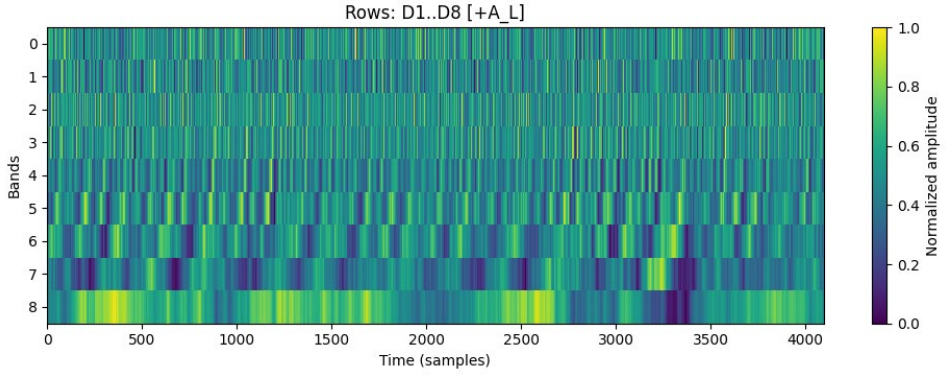

Figure 8. Stationary Haar wavelet transform (Haar, $L = 10$).

For comparative evaluation, two models were trained. The first network was trained directly using the normalized vibration signals, whereas the second utilized Haar-transformed coefficients at level eight as its input. Both networks shared a similar

architecture, incorporating convolutional layers with rectified-linear activation and max-pooling, followed by dropout regularization and fully connected layers culminating in a softmax output. Training and validation data were partitioned identically to ensure that any observed performance differences stemmed from the preprocessing stage rather than architectural or parameter variations.

Figure 9 presents the results for the network trained on raw signals. The loss and F_1-score histories indicate that while the model achieved consistent improvement, the validation curve remained highly variable, suggesting sensitivity to data imbalance and class similarity. The confusion matrix further reveals substantial overlap between the two delamination cases, reflecting the close spectral resemblance of their vibration signatures. Conversely, the healthy state, characterized by a distinct global frequency pattern, was classified more reliably. These results underscore the inherent difficulty of directly learning discriminative features from raw signals when faced with overlapping spectral characteristics.

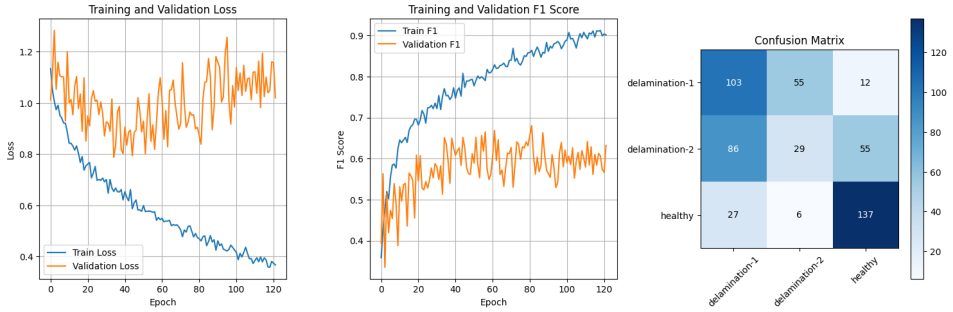

Figure 9. Training, validation loss, F_1-score and confusion matrix for the baseline CNN.

Figure 10 illustrates the results obtained when the vibration data underwent Haar wavelet preprocessing before CNN training. The training and validation curves exhibit smoother convergence and reduced divergence between datasets, signifying improved learning stability. The corresponding confusion matrix demonstrates clearer diagonal dominance, indicating more distinct classification boundaries among the three structural states. The Haar preprocessing effectively enhanced the network's ability to isolate frequency-localized patterns and mitigate the spectral overlap observed during raw-signal training.

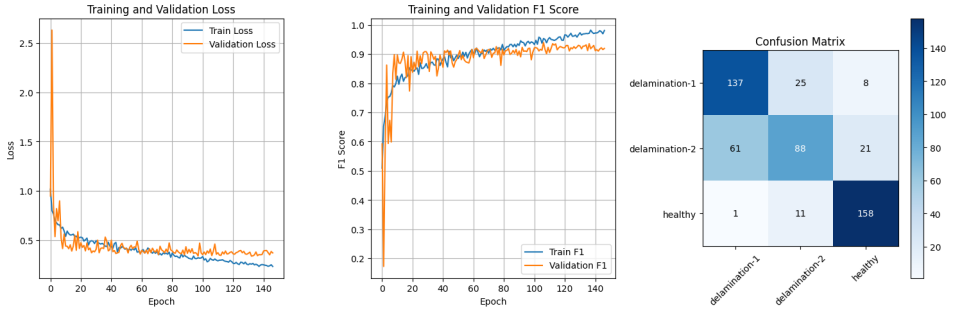

Figure 10. Training, validation loss, F_1-score and confusion matrix for the Haar-CNN.

In conclusion, the overall comparison confirms that integrating Haar wavelet decomposition prior to CNN training substantially improves both convergence behavior and classification consistency. The wavelet representation adeptly captures the local transient behavior associated with delamination while simultaneously preserving the global vibration characteristics of the healthy state. Consequently, the Haar-CNN hybrid approach offers a more robust and physically interpretable method for vibration-based detection of delamination in composite plates, particularly in scenarios with limited dataset size.

4.5 Summary of the Results

This section detailed the development and validation of the Haar Wavelet Method and its higher-order variant for structural dynamics problems, alongside introducing the Haar-CNN framework for data-driven damage detection. The Haar-based methodologies consistently demonstrated high accuracy and rapid convergence across diverse analyses, including free vibration, wave propagation and nonlinear transient analyses. Notably, the HOHWM achieved higher order convergence determined by method parameter, yielding smooth, continuous field approximations with a reduced number of collocation points. Furthermore, the Haar-CNN hybrid model extended this approach to experimental composite data, where multilevel Haar preprocessing significantly enhanced feature localization and classification accuracy. Collectively, these findings underscore the robustness and adaptability of the proposed Haar-based techniques for both deterministic and data-driven structural analysis.

5 Conclusions and Future Work

5.1 Summary of Main Contributions

This chapter concludes the thesis by summarizing the key outcomes and methodological contributions of the Haar-based numerical and data-driven frameworks. The comprehensive analyses confirmed the accuracy, convergence and broad applicability of the proposed methodologies across different physical scales and problem types.

For enhanced accuracy and smoothness, Haar basis functions can be subjected to multiple integrations before forming an approximation, thereby establishing the Higher Order Haar Wavelet Method. This approach initially developed for studies in vibration and wave propagation, provides a continuous, higher order representation while maintaining the intrinsic simplicity and orthogonality of the original Haar basis.

The initial case study investigated the free vibration of Timoshenko beams, validating the higher order Haar formulation against analytical and finite element benchmarks. The incorporation of higher order Haar functions yielded smooth displacement and rotation fields, underscoring higher order convergence with a reduced number of collocation points. It should be mentioned that current formulation is among the few where the Higher Order Haar Wavelet Method was evaluated with sixth-order convergence (method parameter $s = 2$) and was applied to Timoshenko beams, accurately representing shear deformation effects.

The second case study focused on longitudinal wave propagation in functionally graded Rayleigh-Bishop nanorods within the framework of nonlocal elasticity. The results indicated that the HOHWM accurately captured the influence of nonlocal parameters on natural frequencies and wave dispersion characteristics. The method confirmed the expected softening behavior with increasing nonlocal length scale and verified the convergence rate observed in the beam problem, affirming the higher order formulation's generality for graded and nanoscale structures. This is one of the few applications of the Higher Order Haar Wavelet Method at the nanoscale, developed for functionally graded Rayleigh-Bishop nanorods with nanoparticle material.

The third case study examined the nonlinear flight dynamics of fragments, employing the HWM and HOHWM to solve coupled trajectory equations under aerodynamic drag. The HOHWM exhibited rapid convergence towards the Runge-Kutta reference solution, reducing numerical error by two orders of magnitude compared to the standard formulation. These findings validated the method's efficiency in transient problems and its capacity to maintain stability under nonlinear and time-dependent conditions. This case verified that the Higher Order Haar Wavelet Method maintains higher convergence in nonlinear flight problems, with input parameters obtained with finite element simulations in ANSYS.

The fourth case study extended the Haar framework to data-driven damage identification using convolutional neural networks. The Haar-CNN hybrid approach was assessed using two experimental datasets of composite plates: one involving vibration-based mass-attachment and another a delamination-based frequency-response dataset. In both instances, Haar wavelet preprocessing improved feature localization and enhanced convergence stability compared to training on raw data. The optimal wavelet decomposition level was identified within the 7 to 9 range, offering the best balance between feature richness and computational efficiency. The hybrid model demonstrated reliable class separation, even with limited datasets, confirming the practical benefits of integrating multiscale signal analysis with deep-learning-based classification.

All the research questions formulated in Chapter 1 have been addressed through the numerical, analytical and data-driven investigations presented in this thesis.

Collectively, across all four studies, the Haar-based formulations exhibited robust numerical stability, rapid convergence, and consistent accuracy over a wide spectrum of structural problems. The higher order Haar extensions effectively improved smoothness and precision in continuous domain analyses, while the wavelet-enhanced CNN framework strengthened feature extraction and pattern recognition capabilities in experimental datasets. Together, these results highlight the versatility of Haar wavelet formulations as a unifying tool for both deterministic and data-driven modeling in structural dynamics and damage detection.

5.2 Theoretical and Computational Contributions

The thesis theoretically advanced the formulation of the HWM and HOHWM for structural dynamics problems governed by ordinary and partial differential equations. The higher order framework achieved higher order convergence while maintaining the simplicity and orthogonality inherent in the original Haar basis. The methods underwent validation across both local and nonlocal continua, accurately reproducing analytical benchmarks with minimal computational overhead.

Numerical findings confirmed that the HOHWM generates continuous displacement and stress fields, exhibits stable convergence and produces sparse algebraic matrices. Its performance remained consistent across a spectrum of linear and nonlinear problems, encompassing transient fragment motion, graded nanostructures and classical vibration analysis. The uniform grid formulation effectively eliminated the complexities associated with adaptive meshing, all while preserving high accuracy and computational efficiency.

These results position the HOHWM as a compact yet highly precise solver for dynamic systems, capable of serving as an alternative to more computationally demanding finite element or spectral methods in analyses requiring moderate resolution.

This study notably contributes to the literature by demonstrating that the Higher Order Haar Wavelet Method achieved higher order of convergence, thereby underscoring its exceptional numerical precision.

5.3 Integration of Wavelet-Based Modeling and Machine Learning

A significant contribution of this research involves the integration of wavelet-based signal processing with deep learning for structural health monitoring. By employing stationary Haar wavelet decomposition on datasets comprising vibration and frequency response data, the convolutional neural network models successfully extracted localized, multiscale features directly correlated with various structural damage patterns. The analysis of two composite plate datasets, one related to localized mass attachment and the other to delamination, demonstrated that Haar wavelet preprocessing improved CNN learning stability, mitigated overfitting and enhanced feature separability, even with limited data. An optimal decomposition depth was determined to be between seven and nine levels, a range that effectively preserved transient and modal information without introducing redundant noise. This fusion of Haar-based preprocessing with CNN architectures bridges physics-informed modeling and data-driven learning, enabling deep networks to process physically interpretable features derived from the same mathematical foundation used in numerical modeling.

5.4 Practical Implications for Structural Dynamics and SHM

The present research findings offer direct implications for the comprehensive analysis, intricate simulation and continuous monitoring of diverse structural systems. Specifically, the HOHWM presents a computationally efficient alternative for dynamic simulations where both precision and stability are paramount, such as in vibration-based design, advanced nano-mechanical modeling and complex fragment dynamics. Its inherent sparse and orthogonal matrix structure renders it highly suitable for integration into large-scale simulations and embedded numerical solvers.

Furthermore, the Haar-CNN framework extends the applicability of wavelet methodologies to experimental and operational monitoring contexts. Its multiresolution preprocessing step markedly improves feature extraction from inherently noisy vibration data, thereby enhancing the robustness of classification models utilized for identifying damage, delamination, or other forms of structural degradation. This approach proves particularly advantageous for datasets that are small or incomplete, where conventional deep-learning techniques often encounter difficulties in generalization.

Collectively, these methodologies constitute a coherent computational toolset that effectively integrates the interpretability characteristic of physics-based models with the adaptability inherent in machine-learning frameworks. This synergy facilitates reliable diagnostics and sophisticated predictive modeling in both laboratory-scale and field-scale structural applications.

In summation, these findings corroborate that the research objectives, as outlined in Chapter 1, have been comprehensively fulfilled. Each inquiry was addressed through theoretical development, numerical validation or data-driven experimentation, thereby affirming the capability of Haar based methods to integrate modeling accuracy, computational efficiency and learning-driven damage detection within the domain of structural dynamics.

5.5 Future Research

Future research endeavors can expand upon the current work in several key areas:

1. Extension of the Higher Order Haar Wavelet Method: Applying higher order Haar formulations to intricate coupled multi-field systems, such as thermo-mechanical and piezoelectric problems, to assess their efficacy in multiphysics modeling.
2. Adaptive Wavelet Frameworks: Developing adaptive or hybrid grid schemes within the Haar formulation to enhance computational efficiency for localized nonlinear effects while preserving orthogonality.
3. Uncertainty Quantification: Integrating stochastic approaches with Haar-based solvers to meticulously analyze the influence of material and boundary uncertainties on dynamic responses.
4. Deep Learning Generalization: Expanding the Haar-CNN framework to encompass 3D structural geometries and large-scale sensor networks, incorporating transfer learning or physics-informed architectures to achieve superior generalization under diverse operational conditions.
5. Real Time Structural Health Monitoring Implementation: Embedding Haar-based preprocessing into onboard diagnostic systems for real time vibration analysis and automated damage detection in critical industrial and aerospace structures.

These proposed directions aim to drive Haar-based modeling from theoretical validation towards practical deployment within intelligent structural systems. The continued integration of wavelet mathematics with data-driven techniques holds significant promise for developing interpretable, efficient, and generalizable solutions to complex challenges in structural dynamics and health monitoring.

List of Figures

List of Tables

References

[1] K. Vijaya Sundravel, R. Jagadeesan, A. Dhanush, and A. Sanjay Kumar, “A Review of Innovations, Challenges, and Future Directions in Structural Health Monitoring Using Smart Materials,” *Journal of Environmental Nanotechnology*, vol. 14, no. 1, pp. 464–478, 2025, doi: 10.13074/jent.2025.03.2511163.

[2] F. Falcetelli, N. Yue, R. Di Sante, and D. Zarouchas, “Probability of detection, localization, and sizing: The evolution of reliability metrics in Structural Health Monitoring,” *Struct Health Monit*, vol. 21, no. 6, pp. 2990–3017, 2022, doi: 10.1177/14759217211060780.

[3] S. , Cheng and H. Zhou, *Advances in Research on Structural Dynamics and Health Monitoring*. MDPI-Multidisciplinary Digital Publishing Institute, 2025. doi: 10.3390/books978-3-7258-3030-5.

[4] A. G. Sanchez-Rivadeneira and C. A. Duarte, “A high-order generalized Finite Element Method for multiscale structural dynamics and wave propagation,” *Comput Methods Appl Mech Eng*, vol. 384, p. 113934, 2021, doi: 10.1016/j.cma.2021.113934.

[5] J. Andrej *et al.*, “High-performance finite elements with MFEM,” *Int J High Perform Comput Appl*, vol. 38, no. 5, pp. 447–467, 2024, doi: 10.1177/10943420241261981.

[6] T. Gerasimov and L. De Lorenzis, “On penalization in variational phase-field models of brittle fracture,” *Comput Methods Appl Mech Eng*, vol. 354, pp. 990–1026, 2019, doi: 10.1016/j.cma.2019.05.038.

[7] H. Ren, X. Zhuang, N. T. Trung, and T. Rabczuk, “A nonlocal operator method for finite deformation higher-order gradient elasticity,” *Comput Methods Appl Mech Eng*, vol. 384, p. 113963, 2021, doi: 10.1016/j.cma.2021.113963.

[8] H. Hein and L. Jaanuska, “Quantification of cracks in beams on the Pasternak foundation using Haar wavelets and machine learning,” *Proceedings of the Estonian Academy of Sciences*, vol. 71, no. 1, pp. 16–29, 2022, doi: 10.3176/proc.2022.1.02.

[9] R. Hou, X. Wang, Q. Xia, and Y. Xia, “Sparse Bayesian learning for structural damage detection under varying temperature conditions,” *Mech Syst Signal Process*, vol. 145, p. 106965, 2020, doi: 10.1016/j.ymssp.2020.106965.

[10] Y. Lee, H. Kim, S. Min, and H. Yoon, “Structural damage detection using deep learning and FE model updating techniques,” *Sci Rep*, vol. 13, no. 1, p. 18694, 2023, doi: 10.1038/s41598-023-46141-9.

[11] Ü. Lepik and H. Hein, *Haar wavelets: with applications*. Cham: Springer International Publishing, 2014. doi: 10.1007/978-3-319-04295-4_2.

[12] J. Majak, M. Pohlak, M. Eerme, and T. Lepikult, “Weak formulation based Haar wavelet method for solving differential equations,” *Appl Math Comput*, vol. 211, no. 2, pp. 488–494, 2009, doi: 10.1016/j.amc.2009.01.089.

[13] J. Majak, B. Shvartsman, K. Karjust, M. Mikola, A. Haavajõe, and M. Pohlak, “On the accuracy of the Haar wavelet discretization method,” *Compos B Eng*, vol. 80, pp. 321–327, 2015, doi: 10.1016/j.compositesb.2015.06.008.

[14] H. Gökdağ and O. Kopmaz, “A new damage detection approach for beam-type structures based on the combination of continuous and discrete wavelet transforms,” *J Sound Vib*, vol. 324, no. 3–5, pp. 1158–1180, 2009, doi: 10.1016/j.jsv.2009.02.030.

[15] Y. Wang, T. Deng, J. Huang, M. Cao, and D. Sumarac, “A Noise-Robust, Baseline-Free, and Adaptive Damage Indicator of Plate-like Structures Based on the Multicomponent Information Separation of High-Resolution Mode Shapes Using Wavelets,” *Sensors*, vol. 25, no. 9, p. 2669, 2025, doi: 10.3390/s25092669.

[16] J. Majak, M. Ratas, K. Karjust, and B. Shvartsman, “Higher Order Haar Wavelet Method for Solving Differential Equations,” in *IntechOpen eBooks*, IntechOpen, 2020, p. 349. doi: 10.5772/intechopen.94520.

[17] J. Majak, M. Pohlak, K. Karjust, M. Eerme, J. Kurnitski, and B. S. Shvartsman, “New higher order Haar wavelet method: Application to FGM structures,” *Compos Struct*, vol. 201, pp. 72–78, 2018, doi: 10.1016/j.compstruct.2018.06.013.

[18] M. Ratas, A. Salupere, and J. Majak, “Solving nonlinear PDEs using the higher order Haar wavelet method on nonuniform and adaptive grids,” *Mathematical Modelling and Analysis*, vol. 26, no. 1, pp. 147–169, 2021, doi: 10.3846/mma.2021.12920.

[19] M. Ratas, J. Majak, and A. Salupere, “Solving Nonlinear Boundary Value Problems Using the Higher Order Haar Wavelet Method,” *Mathematics*, vol. 9, no. 21, p. 2809, 2021, doi: 10.3390/math9212809.

[20] L. Chouinard, V. Shahsavari, and J. Bastien, “Reliability of Wavelet Analysis of Mode Shapes for the Early Detection of Damage in Beams,” *Front Built Environ*, vol. 5, 2019, doi: 10.3389/fbuil.2019.00091.

[21] X. Song, D. Li, and C. Cho, “Image-based machine learning approach for structural damage detection through wavelet transforms,” *Urban Lifeline*, vol. 2, no. 1, p. 4, 2024, doi: 10.1007/s44285-023-00010-z.

[22] J. L. C. R. Vila, S. H. S. Carneiro, J. N. V. Goulart, C. T. M. Anflor, and A. B. Jorge, “Wavelet-based numerical investigation on damage localisation and quantification in beams using static deflections and mode shapes,” *European Journal of Mechanics - A/Solids*, vol. 107, p. 105351, 2024, doi: 10.1016/j.euromechsol.2024.105351.

[23] T. Q. Nguyen, D. P. Nguyen, P. T. Nguyen, and T. T. Nguyen, “Advanced structural damage detection in steel beams using discrete wavelet transform and fast Fourier transform,” *Journal of Low Frequency Noise, Vibration and Active Control*, vol. 44, no. 2, pp. 800–816, 2025, doi: 10.1177/14613484241303557.

[24] J. Zhao, Z. Zhou, D. Guan, and J. Guo, “A wavelet based data coupling method for spatial damage detection in beam-type structures,” *PLoS One*, vol. 18, no. 8, p. e0290265, 2023, doi: 10.1371/journal.pone.0290265.

[25] R. Hou and Y. Xia, “Review on the new development of vibration-based damage identification for civil engineering structures: 2010–2019,” *J Sound Vib*, vol. 491, p. 115741, 2021, doi: 10.1016/j.jsv.2020.115741.

[26] R. K. Shinagam, D. R. K. Vengalasetti, and T. Maruvada, “Crack detection and localization in composite plates by intersection of first three normalized mode shape curves from experimental modal analysis,” *World Journal of Engineering*, vol. 22, no. 5, pp. 968–977, 2024, doi: 10.1108/WJE-09-2023-0412.

[27] L. Jaanuska and H. Hein, “Delamination Quantification by Haar Wavelets and Machine Learning,” *Mechanics of Composite Materials*, vol. 58, no. 2, pp. 249–260, 2022, doi: 10.1007/s11029-022-10025-2.

[28] R. Boccagna, M. Bottini, M. Petracca, A. Amelio, and G. Camata, “Unsupervised Deep Learning for Structural Health Monitoring,” *Big Data and Cognitive Computing*, vol. 7, no. 2, p. 99, 2023, doi: 10.3390/bdcc7020099.

[29] S. S. Eshkevari, M. Takáč, S. N. Pakzad, and M. Jahani, “DynNet: Physics-based neural architecture design for nonlinear structural response modeling and prediction,” *Eng Struct*, vol. 229, p. 111582, 2021, doi: 10.1016/j.engstruct.2020.111582.

[30] X. Zhou and Y. He, “Dynamic displacement estimation of structures using one-dimensional convolutional neural network,” *Front Phys*, vol. 11, p. 1290880, 2023, doi: 10.3389/fphy.2023.1290880.

[31] Y.-J. Cha, R. Ali, J. Lewis, and O. Büyüköztürk, “Deep learning-based structural health monitoring,” *Autom Constr*, vol. 161, p. 105328, 2024, doi: 10.1016/j.autcon.2024.105328.

[32] H. Amanollah, A. Asghari, M. Mashayekhi, and S. M. Zahrai, “Damage detection of structures based on wavelet analysis using improved AlexNet,” *Structures*, vol. 56, p. 105019, 2023, doi: 10.1016/j.istruc.2023.105019.

[33] H. Hein and L. Jaanuska, “Comparison of machine learning methods for crack localization,” *Acta et Commentationes Universitatis Tartuensis de Mathematica*, vol. 23, no. 1, pp. 125–142, 2019, doi: 10.12697/ACUTM.2019.23.13.

[34] R. Zhang, Y. Liu, and H. Sun, “Physics-guided convolutional neural network (PhyCNN) for data-driven seismic response modeling,” *Eng Struct*, vol. 215, p. 110704, 2020, doi: 10.1016/j.engstruct.2020.110704.

[35] L. Rosafalco, A. Manzoni, S. Mariani, and A. Corigliano, “Fully convolutional networks for structural health monitoring through multivariate time series classification,” *Adv Model Simul Eng Sci*, vol. 7, no. 1, p. 38, 2020, doi: 10.1186/s40323-020-00174-1.

[36] H. Khodabandehlou, G. Pekcan, and M. S. Fadali, “Vibration-based structural condition assessment using convolution neural networks,” *Struct Control Health Monit*, vol. 26, no. 2, p. e2308, 2019, doi: 10.1002/stc.2308.

[37] D. Łuczak, “Machine Fault Diagnosis through Vibration Analysis: Continuous Wavelet Transform with Complex Morlet Wavelet and Time–Frequency RGB Image Recognition via Convolutional Neural Network,” *Electronics (Basel)*, vol. 13, no. 2, p. 452, 2024, doi: 10.3390/electronics13020452.

[38] G. Azuara, M. Ruiz, and E. Barrera, “Damage Localization in Composite Plates Using Wavelet Transform and 2-D Convolutional Neural Networks,” *Sensors*, vol. 21, no. 17, p. 5825, 2021, doi: 10.3390/s21175825.

[39] M. I. Shirazi, S. Khatir, D. Boutchicha, and M. A. Wahab, “Feature extraction and classification of multiple cracks from raw vibrational responses of composite beams using 1D-CNN network,” *Compos Struct*, vol. 327, p. 117701, 2024, doi: 10.1016/j.compstruct.2023.117701.

[40] Q. Ma, J. Xu, X. Gao, and M. Liu, “Structural damage localization based on wavelet packet analysis under varying environment effects,” *J Civ Struct Health Monit*, vol. 15, no. 6, pp. 2037–2057, 2025, doi: 10.1007/s13349-025-00926-w.

[41] M. Saadatmorad, R.-A. Jafari-Talookolaei, M.-H. Pashaei, and S. Khatir, “Damage detection on rectangular laminated composite plates using wavelet based convolutional neural network technique,” *Compos Struct*, vol. 278, p. 114656, 2021, doi: 10.1016/j.compstruct.2021.114656.

[42] N. I. Pérez-Quezadas, H. Benítez-Pérez, and A. Durán-Chavesti, “Proposal of a Methodology Based on Using a Wavelet Transform as a Convolution Operation in a Convolutional Neural Network for Feature Extraction Purposes,” *Algorithms*, vol. 18, no. 4, p. 221, 2025, doi: 10.3390/a18040221.

[43] G. Michau, G. Frusque, and O. Fink, “Fully learnable deep wavelet transform for unsupervised monitoring of high-frequency time series,” *Proceedings of the National Academy of Sciences*, vol. 119, no. 8, 2022, doi: 10.1073/pnas.2106598119.

[44] J. M. Alam, “Wavelet Transforms and Machine Learning Methods for the Study of Turbulence,” *Fluids*, vol. 8, no. 8, p. 224, 2023, doi: 10.3390/fluids8080224.

[45] Y. L. Alemu, T. Lahmer, and C. Walther, “Damage Detection with Data-Driven Machine Learning Models on an Experimental Structure,” *Eng*, vol. 5, no. 2, pp. 629–656, 2024, doi: 10.3390/eng5020036.

[46] L. Feklistova and H. Hein, “Crack Identification in Vibrating Beams Using Haar Wavelets and Neural Networks,” *Applied Mechanics and Materials*, vol. 420, pp. 62–67, 2013, doi: 10.4028/www.scientific.net/AMM.420.62.

[47] L.-F. Zhu, L.-L. Ke, X.-Q. Zhu, Y. Xiang, and Y.-S. Wang, “Crack identification of functionally graded beams using continuous wavelet transform,” *Compos Struct*, vol. 210, pp. 473–485, 2019, doi: 10.1016/j.compstruct.2018.11.042.

[48] L. F. Zhu, L. L. Ke, Y. Xiang, and X. Q. Zhu, “Free vibration and damage identification of cracked functionally graded plates,” *Compos Struct*, vol. 250, p. 112517, 2020, doi: 10.1016/j.compstruct.2020.112517.

[49] M.-L. J. Manuel, B. Andrea, M. Stefano, and G. Luigi, “Wavelets-based damage localization on beams under the influence of moving loads,” *Mechanics & Industry*, vol. 14, no. 2, pp. 107–113, 2013, doi: 10.1051/meca/2012036.

[50] K. Karjust, M. Mehrparvar, S. Kaganski, and T. Raamets, “Development of a Sustainability-Oriented KPI Selection Model for Manufacturing Processes,” *Sustainability*, vol. 17, no. 14, p. 6374, 2025, doi: 10.3390/su17146374.

[51] M. Mehrparvar, J. Majak, and K. Karjust, “Effect of aggregation methods in fuzzy technique for prioritization of criteria of automated vehicle system,” 2024, *AIP Publishing LLC*. doi: 10.1063/5.0189323.

[52] M. Mehrparvar, J. Majak, and K. Karjust, “A comparative analysis of Fuzzy AHP and Fuzzy VIKOR methods for prioritization of the risk criteria of an autonomous vehicle system,” *Proceedings of the Estonian Academy of Sciences*, vol. 73, no. 2, pp. 116–123, 2024, doi: 10.3176/proc.2024.2.04.

[53] J. Majak, M. Ratas, K. Karjust, and B. Shvartsman, “Higher Order Haar Wavelet Method for Solving Differential Equations,” in *Wavelet Theory*, IntechOpen, 2020, p. 349. doi: 10.5772/intechopen.94520.

[54] S. K. Jena, S. Chakraverty, and M. Malikan, “Implementation of Haar wavelet, higher order Haar wavelet, and differential quadrature methods on buckling response of strain gradient nonlocal beam embedded in an elastic medium,” *Eng Comput*, vol. 37, no. 2, pp. 1251–1264, 2021, doi: 10.1007/s00366-019-00883-1.

[55] J. Majak, M. Pohlak, M. Eerme, and B. Shvartsman, “Solving ordinary differential equations with higher order Haar wavelet method,” 2019, *AIP Publishing LLC*. doi: 10.1063/1.5114340.

[56] S. Adali, “Variational principles for multi-walled carbon nanotubes undergoing buckling based on nonlocal elasticity theory,” *Phys Lett A*, vol. 372, no. 35, pp. 5701–5705, 2008, doi: 10.1016/j.physleta.2008.07.003.

[57] M. Arda, “Axial dynamics of functionally graded Rayleigh-Bishop nanorods,” *Microsystem Technologies*, vol. 27, no. 1, pp. 269–282, 2021, doi: 10.1007/s00542-020-04950-2.

[58] M. Arda, “Evaluation of optimum length scale parameters in longitudinal wave propagation on nonlocal strain gradient carbon nanotubes by lattice dynamics,” *Mechanics Based Design of Structures and Machines*, vol. 50, no. 12, pp. 4363–4386, 2022, doi: 10.1080/15397734.2020.1835488.

[59] M. Mehrparvar, L. Kivistik, M. Eerme, and K. Karjust, “Haar wavelet based analysis of dynamics of flight of the fragments,” 2025, *AIP Publishing LLC*. doi: 10.1063/5.0287481.

[60] B. Zecevic and J. Terzic, “Characterization of distribution parameters of fragment mass and number for conventional projectiles,” *14Th Seminar on New Trends in Research of Energetic Materials*, no. APRIL, 2011.

[61] N. Dwek, D. Janssens, and E. Deckers, “LMSD 2021 Dataset for Damage Identification in Plates,” 2024, *Zenodo*.

[62] M. M. Azad and H. S. Kim, “Vibration Data for Laminated Composite Structures: Healthy and Delamination States,” 2025, *Mendeley Data*.

[63] N. Dwek, D. Janssens, V. Dimopoulos, M. Kirchner, E. Deckers, and F. Naets, “Frequency response function data of a composite plate under various damage identification scenarios,” *Data Brief*, vol. 59, p. 111385, 2025, doi: 10.1016/j.dib.2025.111385.

[64] V. Dimopoulos, W. Desmet, and E. Deckers, “Sparse Damage Detection with Complex Group Lasso and Adaptive Complex Group Lasso,” *Sensors*, vol. 22, no. 8, p. 2978, 2022, doi: 10.3390/s22082978.

[65] N. Dwek, V. Dimopoulos, D. Janssens, M. Kirchner, E. Deckers, and F. Naets, “Damage Identification in Plate-Like Structures Using Frequency-Coupled L1-Based Sparse Estimation,” *Mech Syst Signal Process*, vol. 224, p. 112084, 2025, doi: 10.1016/j.ymssp.2024.112084.

[66] M. M. Azad and H. S. Kim, “Hybrid deep convolutional networks for the autonomous damage diagnosis of laminated composite structures,” *Compos Struct*, vol. 329, p. 117792, 2024, doi: 10.1016/j.compstruct.2023.117792.

[67] M. M. Azad and H. S. Kim, “An explainable artificial intelligence-based approach for reliable damage detection in polymer composite structures using deep learning,” *Polym Compos*, vol. 46, no. 2, pp. 1536–1551, 2025, doi: 10.1002/pc.29055.

[68] M. M. Azad and H. S. Kim, “Noise robust damage detection of laminated composites using multichannel wavelet-enhanced deep learning model,” *Eng Struct*, vol. 322, p. 119192, 2025, doi: 10.1016/j.engstruct.2024.119192.

[69] M. M. Azad, P. Kumar, and H. S. Kim, “Delamination detection in CFRP laminates using deep transfer learning with limited experimental data,” *Journal of Materials Research and Technology*, vol. 29, pp. 3024–3035, 2024, doi: 10.1016/j.jmrt.2024.02.067.

[70] M. M. Azad, S. Kim, and H. S. Kim, “Autonomous data-driven delamination detection in laminated composites with limited and imbalanced data,” *Alexandria Engineering Journal*, vol. 107, pp. 770–785, 2024, doi: 10.1016/j.aej.2024.09.004.

Acknowledgements

I would like to express my deepest gratitude to Professor Majak for his continuous guidance, encouragement and trust throughout this research. From the very beginning, he inspired me to pursue independent inquiry and supported my decision to define my own path within the broader field of structural dynamics. His insight, patience and confidence in my work have been invaluable in shaping both the technical and intellectual foundation of this thesis.

I also wish to thank Professor Karjust for his support and for providing an academic environment that enabled this work to progress within the wider context of our research group.

My heartfelt thanks go to my family, whose constant encouragement and understanding sustained me despite the distance that separated us. Their belief in my work and their quiet strength have been my foundation throughout this long journey. I am equally grateful to my friends and colleagues, whose companionship, humor and understanding provided balance and a much needed perspective along the way.

Finally, I dedicate a special acknowledgment to Bijou, my cat, companion, and, by all rights, unofficial co-author of this thesis. Her patient presence beside me through countless hours of writing and computation brought warmth and calm to every stage of this work. Her curiosity, quiet insistence on attention, and gentle companionship made this journey immeasurably lighter and far more meaningful.

During the PhD studies, this work has been supported by “Increasing the knowledge intensity of Ida-Viru entrepreneurship”, ÕÜF9, co–funded by the European Union and VEU22048 “Master of Science in Smart, Secure and Interconnected Systems” (1.10.2022−30.09.2026); Tallinn University of Technology (partner); Financier: European Commission.

Abstract

Mathematical Modeling and Numerical Analysis of Structural Dynamics with Applications to Damage Detection

Precise modeling of structural dynamic behavior and reliable identification of the damage in structures remain central challenges in engineering design and maintenance. Modern structures, from large-scale constructions to micro- and nanoscale components, work under progressively complex dynamic conditions and are often made of advanced and/or functionally graded materials. These new developments have brought with them nonlinear behavior, spatial inhomogeneity and multiscale effects that in some cases could exceed the analytical capacity of classical methods. On the other hand, vibration based SHM relies on noisy and limited experimental data interpretation. This thesis addresses both challenges and introduces a unified Haar wavelet-based framework that integrates mathematical modeling, numerical analysis and data-driven interpretation of structural dynamics. The approach proposed demonstrates that the same wavelet family can be employed for both solving governing differential equations and enhancing vibration-based damage detection through deep learning algorithms.

The theoretical foundation is based on the formulation of the Haar Wavelet Method that approximates differential operators using piecewise-constant orthogonal functions. This results in sparse and well-conditioned system matrices and facilitates easy application of the boundary conditions. A Higher Order Haar Wavelet Method is then constructed by integrating the Haar functions repeatedly to obtain continuous higher order approximations with improved smoothness and faster rates of convergence. They are evaluated in terms of accuracy, convergence rate and computation efficiency.

Haar wavelets based methods are implemented for four representative problems chosen to illustrate their flexibility in various physical scales and computational contexts. The first three problems are covered be deterministic numerical modeling and the fourth combines wavelet preprocessing with a convolutional neural network for vibration-based damage detection.

The first case study examines the free vibration analysis of both uniform and tapered beams under various boundary conditions according to Timoshenko's shear deformation theory. The Higher Order Haar Wavelet Method Formulation exhibits improved accuracy and faster convergence compared to the reference HWM based solution.

The second case study extends the method to the nonlocal Rayleigh-Bishop theory, incorporating shear deformation and lateral inertia to study the longitudinal wave propagation in axially graded nanorods. The Higher Order Haar Wavelet Method is used to solve the governing motion equations, incorporating a nonlocal parameter within the material graduation. The method is used to compute the natural frequencies and evaluate the influence of the nonlocal parameter on the dynamic behavior of the nanorod.

The third case utilizes the Higher Order Haar wavelet method for the transient nonlinear motion of fragments generated by high-pressure rupture, where the equations of motion, including aerodynamic drag and gravitational effects, are discretized on the Higher Order Haar wavelet basis and time-integrated. The results are in good agreement with Runge-Kutta method, and the trajectory errors remained low, which verifies that the developed formulation can accurately capture nonlinear, time-dependent responses and yet retain numerical stability for systems with discontinuous acceleration histories.

The final case integrates the Haar wavelet transform with a convolutional neural network to improve vibration-based damage detection in composite plates. Two different experimental datasets of frequency response functions for a composite plate with various damage configurations are considered. Experimentally measured vibration and frequency response data from carbon fiber reinforced polymer (CFRP) plates in various damage conditions are analyzed using two CNN configurations: one trained on raw input signals and another trained on Haar-decomposed representations. The wavelet transformation emphasized localized transients and frequency variations while suppressing noise, producing clearer and more distinctive input features. Both models shared identical architectures and training parameters to isolate the effect of wavelet preprocessing. The results indicate that Haar-based multiresolution filtering enhances feature separability, improves model stability and provides a more robust representation of structural response, particularly for small and noisy experimental datasets used in vibration-based structural health monitoring.

The thesis demonstrates that wavelet-based numerical and hybrid methods can function as an effective connection between classical mechanics as well as modern data-driven structural analysis. The proposed framework increases the accuracy and stability of numerical simulations and enhances the interpretability of vibration-based diagnostics. In addition, it offers attractive properties in the sense of mathematical modeling and simulation as well as structural damage identification for systems in the presence of small data and complex dynamical behaviors. The results indicate that further integration of higher-dimensional wavelet formulations and adaptive learning architectures can extend this methodology to large-scale monitoring systems, advancing the application of wavelet mathematics in structural health monitoring and dynamic analysis.

Lühikokkuvõte

Konstruktsioonide dünaamika matemaatiline modelleerimine ja numbriline analüüs kahjustuste tuvastamise rakendusnäidetega

Konstruktsioonide dünaamilise käitumise täpne modelleerimine ja kahjustuste usaldusväärne tuvastamine konstruktsioonides on jätkuvalt keskseks väljakutseks insenerteaduses, nii projekteerimisel kui hooldusel. Kaasaegsed konstruktsioonid, alates suurtest ehitistest kuni mikro- ja nanomastaabis komponentideni, töötavad järjest keerukamates dünaamilistes tingimustes ning on sageli valmistatud kõrgtehnoloogilistest ja/või funktsionaalselt gradueeritud materjalidest. Need arengud toovad kaasa reeglina mittelineaarse käitumise, ruumilise ebaühtluse ja mitmemõõtmelisuse efektid, mis võivad ületada klassikaliste meetodite analüütilised võimalused. Samal ajal tugineb vibratsioonipõhine konstruktsioonide seisundi seire (SHM) sageli mürarikkale ja piiratud eksperimentaalsete andmete tõlgendamisele. Käesolev doktoritöö käsitleb mõlemat probleemi võttes kasutusele Haari lainikute põhise raamistiku, ühendades matemaatilise modelleerimise, numbrilise analüüsi ja andmepõhist konstruktsiooni dünaamika tõlgendamise. Väljatöötatud lähenemine võimaldab kasutada Haari lainikute perekonda nii diferentsiaalvõrrandite lahendamiseks kui ka vibratsioonipõhiste kahjustuste tuvastamise algoritmide täiustamiseks süvaõppemeetodite abil.

Uurimistöö teoreetiline alus tugineb Haar'i lainikute meetodi formuleeringule, mis lähendab diferentsiaaloperaatoreid kasutades tükiti konstantseid ortogonaalseid funktsioone. Tulemusena saadakse hõredad ja hästi konditsioneeritud maatriksid ning lihtne rajatingimuste rakendamine. Seejärel rakendatakse kõrgemat järku Haar'i lainikute meetodit, integreerides Haar'i funktsioone korduvalt, et saada pidevad kõrgema järgu lähendid parema siledusastme ja kiirema koonduvuskiirusega. Meetodeid hinnatakse täpsuse, koonduvuskiiruse ja arvutusmahu alusel.

Haari lainikutel põhinevaid meetodeid rakendatakse nelja probleemi lahendamiseks, mis on valitud nende paindlikkuse demonstreerimiseks erinevatel füüsikalistel ja arvutuslikel tasanditel. Esimesed kolm probleemi sisaldavad deterministlikku numbrilist modelleerimist, neljas ühendab Haari lainikute põhise eeltöötluse konvolutsioonilise närvivõrguga, eesmärgiga parandada vibratsioonipõhist kahjustuste tuvastamist.

Esimene juhtumuuring käsitleb ühtlaste ja koonuseliste ristlõigetega talade vabavibratsioonianalüüsi erinevate rajatingimuste korral, tuginedes Timoshenko nihkedeformatsiooni teooriale. Kõrgemat järku Haar'i lainepõhine meetod näitab kõrgemat täpsust ja kiiremat koonduvuskiirust võrreldes võrdlusbaasiks kasutatava HWM-ga.

Teine juhtumuuring laiendab kõrgemat järku Haari lanikute meetodit mitte-lokaalsele Rayleigh-Bishopi teooriale, hõlmates nihkedeformatsiooni ja külgjõu inertsiefekte, et uurida pikilainete levikut aksiaalselt gradueeritud nanovarrastes. Kõrgemat järku Haar'i lainikute põhist meetodit kasutatakse liikumisvõrrandite lahendamiseks, võttes arvesse funktsionaalselt gradueeritud mitte-lokaalset parameetrit. Meetodi abil arvutatakse nanovarda omasagedused ja hinnatakse mitte-lokaalse parameetri mõju dünaamilisele käitumisele.

Kolmas juhtumuuring kasutab kõrgemat järku Haar'i lainikute põhist meetodit kõrgsurve purunemisel tekkivate fragmentide mittelineaarsete liikumiste simuleerimiseks, kus liikumisvõrrandid (sh aerodünaamiline takistus ja gravitatsioon) diskretiseeritakse

kõrgemat järku lainikute põhisel meetodil ning integreeritakse ajas. Tulemused on heas kooskõlas Runge Kutta meetodi abil saadud tulemustega ning trajektoorivead püsivad väikesed. Tulemused kinnitavad, et välja töötatud formulatsioon suudab täpselt jäädvustada mittelineaarseid ajas muutuvaid funktsioone ja säilitada arvutusliku stabiilsuse süsteemides.

Neljas juhtumuuring ühendab Haar'i lainikute põhise teisenduse konvolutsioonilise närvivõrguga, et parandada vibratsioonipõhist kahjustuste tuvastamist komposiitmaterjalist plaatide korral. Kasutatakse kahte erinevat eksperimentaalset sageduse funktsioonide andmestikku komposiitplaadi kohta, millel on erinevad kahjustuste konfiguratsioonid. Katsetulemused süsinikkiuga tugevdatud polümeerplaatide (CFRP) vibratsiooni- ja sagedusreaktsioonide kohta erinevates kahjustustingimustes analüüsitakse kahe CNN-mudeliga: üks treenitakse töötlemata sisenditel, teine Haar'i lanikute abil teisendatud sisenditel. Lainikutepõhine teisendus rõhutas lokaliseeritud siirdelisi ja sagedusmuutusi, vähendades samas müra ning luues selgemaid ja eristatavamaid sisendomadusi. Mõlemal mudelil olid identsed arhitektuurid ja treeningparameetrid, et eraldada lainikupõhise eeltöötluse mõju. Tulemused näitavad, et Haar'i lainikutepõhine mitmeresolutsiooniline filtreerimine parandab omaduste eristatavust, suurendab mudeli stabiilsust ja annab vastupidavama struktuurivastuse esituse, eriti väikeste ja mürarikaste andmestike korral, mida kasutatakse vibratsioonipõhises konstruktsioonide seisundiseires.

Doktoritöö tulemusena selgub, et lainikutepõhised arvutus- ja hübriidmeetodid võivad toimida tõhusa sillana klassikalise mehaanika ja kaasaegse andmepõhise struktuurianalüüsi vahel. Esitatud raamistik suurendab arvutussimulatsioonide täpsust ja stabiilsust ning parandab vibratsioonipõhiste diagnostikate tõlgendatavust. Lisaks pakub see atraktiivseid omadusi matemaatilise modelleerimise, simulatsiooni ja kahjustuste tuvastamise seisukohalt, eriti väikese andmemahu ja keerulise dünaamilise käitumisega süsteemides. Tulemused viitavad, et mitmemõõtmeliste Haari lainikutepõhiste formulatsioonide ja adaptiivsete õppearhitektuuride edasine integreerimine võib laiendada seda metoodikat suurobjektide seireks, edendades lainikutepõhise matemaatika rakendusi konstruktsioonide seisundiseires ja dünaamilises analüüsis.

Appendix

Publication I

M. Mehrparvar, J. Majak, K. Karjust, and M. Arda, “Free vibration analysis of tapered Timoshenko beam with higher order Haar wavelet method,” *Proceedings of the Estonian Academy of Sciences*, vol. 71, no. 1, p. 77, 2022, doi: https://doi.org/10.3176/proc.2022.1.07.

Proceedings of the Estonian Academy of Sciences,
2022, **71**, 1, 77–83
https://doi.org/10.3176/proc.2022.1.07
Available online at www.eap.ee/proceedings

COMPUTATIONAL
MECHANICS

Free vibration analysis of tapered Timoshenko beam with higher order Haar wavelet method

This paper is dedicated to the 100th birthday of Professor Ülo Lepik.
This study can be considered as a continuation of the research in the area of Haar wavelet methods started by Professor Ülo Lepik

Marmar Mehrparvar*, Jüri Majak, Kristo Karjust and Mustafa Arda

Department of Mechanical and Industrial Engineering, Tallinn University of Technology, Ehitajate tee 5, 19086 Tallinn, Estonia

Received 11 November 2021, accepted 4 January 2022, available online 15 February 2022

Abstract. In the current study, the higher order Haar wavelet method based formulation is developed for the analysis of the free vibrations of the tapered Timoshenko beam. The clamped-clamped and clamped-pinned boundary conditions are explored and the results with the 4th order and the 6th order of convergence are presented. The results are found to be in good agreement with the corresponding results of the Ritz method. The proposed approach can be considered as the principal improvement of the widely used Haar wavelet method providing the same accuracy with the several magnitudes lower mesh. Thus, the higher order Haar wavelet method has reduced the computational cost in comparison with the widely used Haar wavelet method since the computational complexity of both methods is determined by the mesh used. In the case of the fixed equal mesh used for both methods, the higher order Haar wavelet method results in the several magnitudes lower absolute error without a remarkable increase in computational complexity. The cost needed to pay for higher accuracy is hidden in a certain increase in the implementation complexity compared with the widely used Haar wavelet method.

Key words: higher order Haar wavelet method, tapered Timoshenko beam, free vibration.

1. INTRODUCTION

Development and adaptation of computational methods and mathematical modelling techniques are rapidly evolving research areas with the main focus on finding more accurate, less time-consuming, and simpler approximations.

The Haar wavelet method (HWM) was first introduced in [1–2]. According to Chen and Hsiao's approach, the highest order of derivatives included in a differential equation is expanded into a series of Haar functions [1–2]. This method is applied to solving differential and integro-differential equations covering applications in various research areas such as engineering, natural sciences, etc. [3–9]. Furthermore, this method is used as a numerical solution to linear and nonlinear delay differential equations [10], and space derivatives are obtained through the Haar wavelet collocation method to solve 1D and 2D cubic nonlinear Schrodinger equations [11]. In [12] the accuracy and convergence results of the HWM are presented. Based on the obtained

* Corresponding author, marmar.mehrparvar@taltech.ee

results, it can be concluded that despite its simple implementation, the HWM needs refinement in order to compete with such widely used numerical methods as the finite difference method and the differential quadrature method.

Recently, the higher order Haar wavelet method (HOHWM) was introduced in [13] in order to improve the accuracy and convergence of the previously proposed Haar wavelet method. The HOHWM has been applied with success to solving differential equations, vibration, and buckling response of beams [14–18]. Theoretical and numerical analyses of the free and forced vibration of homogeneous and functionally graded Timoshenko beams have been performed [19–22]. In the case of tapered beams, many approaches have been used for analysing the Timoshenko beam that has a non-uniform cross-section [23–26].

The HOHWM is applied with success to the analysis of plate and shell structures using Euler–Bernoulli and zig-zag theories. In this paper the HOHWM approach is adapted to the Timoshenko beam theory.

2. HOHWM APPROACH TO FREE VIBRATION ANALYSIS OF THE TIMOSHENKO BEAM

In this section, the formulation of the free vibration of the tapered Timoshenko beam and boundary conditions are introduced.

2.1. Free vibration of the Timoshenko beam

A schematic view of the Timoshenko beam with a non-uniform cross-section along the length, *x*-direction, is shown in Fig. 1.

Herein, free vibration of homogeneous tapered Timoshenko beams has been investigated. The material properties of the beams are assumed to be constant. Firstly, the cross-sectional area $A(x)$ and the moment of inertia $I(x)$ are presented as

$$A(x) = A_0\left(1-\frac{cx}{L}\right), I(x) = I_0\left(1-\frac{cx}{L}\right)^3, \quad x \in [0, L], \tag{1}$$

where A_0 and I_0 are the area and the moment of inertia at the base of the beam, respectively. L is the length of the beam, E denotes Young's modulus, G refers to shear modulus, ρ represents mass density, and k is the shear correction factor which is chosen to be 5/6. For the described Timoshenko beam, the basic governing differential equations for transverse vibration of the tapered beam can be presented as

$$\begin{gathered}\frac{\partial}{\partial x}\left(EI(x)\frac{\partial \varphi}{\partial x}\right)+\kappa GA(x)\left(\frac{\partial w}{\partial x}-\varphi\right)-\rho I\frac{\partial^2 \varphi}{\partial t^2}=0 \\ \frac{\partial}{\partial x}\left[\kappa GA(x)\left(\frac{\partial w}{\partial x}-\varphi\right)\right]-\rho A\frac{\partial^2 w}{\partial t^2}=0\end{gathered}, \tag{2}$$

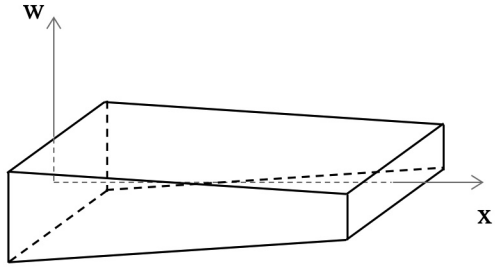

Fig. 1. Schematic view of a tapered beam.

where w and φ are the transverse deflection and rotation of the cross-section, respectively. The bending moment M and the shear force Q at any cross-section can be read as

$$M = EI(x)\frac{\partial\varphi}{\partial x}, \quad Q = kGA(x)\left(\frac{\partial w}{\partial x} + \varphi\right). \tag{3}$$

The boundary conditions for the beam can be expressed

$$\begin{array}{l} \text{for the clamped edge as: } w = 0, \quad \varphi = 0, \\ \text{for the pinned edge as: } w = 0, \quad M = 0. \end{array} \tag{4}$$

2.2. Higher order Haar wavelet method

The higher order Haar wavelet method (HOHWM) is developed as an improvement of the widely used Haar wavelet method (HWM) [13].

The n-th order ordinary differential equation, in general, can be presented as

$$G(x, u, u', u'', \ldots u^{(n-1)}, u^{(n)}) = 0, \tag{5}$$

where n represents the order of the highest derivative involved in the differential equation. In the HOHWM, in comparison to the Haar wavelet method, the order of expansion is increased by $2s$, Eq. (6). Based on the Haar wavelet, the expansion is presented as

$$f(x) = \frac{d^{n+2s}u(x)}{dx^{n+2s}} = \sum_{i=1}^{\infty} a_i h_i(x), s = 1,2, \ldots, \tag{6}$$

in which $h_i(x)$ is the Haar function [18]

$$h_i(x) = \begin{cases} 1 & \text{for} \quad x \in [\xi_1(i), \xi_2(i)) \\ -1 & \text{for} \quad x \in [\xi_2(i), \xi_3(i)), \\ 0 & \text{elsewhere} \end{cases} \tag{7}$$

where $i = m + k + 1$, $m = 2^j$ is a maximum number of square waves arranged in the interval $[A,B]$ and the parameter k indicates the location of the particular square wave [18]

$$\begin{array}{lll} \xi_1(i) = A + 2k\mu\Delta x, & \xi_2(i) = A + (2k+1)\mu\Delta x, & \xi_3(i) = A + 2(k+1)\mu\Delta x, \\ \mu = M/m, & \Delta x = (B-A)/(2M). & \end{array} \tag{8}$$

The integrals of the Haar functions (7) of order n can be expressed as [13]

$$p_{n,i}(x) = \begin{cases} 0 & x \in [A, \xi_1(i)) \\ \frac{(x-\xi_1(i))^n}{n!} & x \in [\xi_1(i), \xi_2(i)) \\ \frac{(x-\xi_1(i))^n - 2(x-\xi_2(i))^n}{n!} & x \in [\xi_2(i), \xi_3(i)) \\ \frac{(x-\xi_1(i))^n - 2(x-\xi_2(i))^n + (x-\xi_3(i))^n}{n!} & x \in [\xi_3(i), B) \\ 0 & elsewhere \end{cases} \quad for \tag{9}$$

The differential equation can be satisfied in selected uniform grid points

$$x_{iL} = \frac{i}{2M}, \; x_{iR} = 1 - \frac{i}{2M}, i = 0, \ldots, s-1, \tag{10}$$

where L and R are the added collocation points on the left and right boundary, respectively. Then the numerical order of the convergence of the method can be estimated by

$$\text{Convergence rate} = \frac{\log\left(\frac{F_{i-1} - F_{Ref}}{F_i - F_{Ref}}\right)}{\log(2)}, \tag{11}$$

where F_{Ref} is the existing solution, which in the current solution is obtained from the Ritz method [21].

3. NUMERICAL RESULTS

In order to showcase the accuracy of the formulation proposed above, the values of natural frequencies of the Timoshenko beam under two arbitrary boundary conditions are presented. Table 1 presents the effect of

Table 1. Effect of taper ratio on non-dimensional natural frequencies of the C-C Timoshenko beam

	N	HWM			HOHWM 4th			HOHWM 6th		
		Frequency	A. error	Conv. rate	Frequency	A. error	Conv. rate	Frequency	A. error	Conv. rate
$c = 0$	4	13.96275845	1.28e-01		13.84197845	7.22e-03		13.83477975	2.13e-05	
	8	13.86655612	3.18e-02	2.0091	13.83519214	4.34e-04	4.0576	13.83476001	1.56e-06	5.4358
	16	13.84269132	7.93e-03	2.003	13.83478525	2.68e-05	4.0146	13.83475854	8.43e-08	5.7522
	32	13.83674066	1.98e-03	2.0007	13.83476012	1.67e-06	4.0036	13.83475846	1.51e-09	5.9467
	64	13.83525392	4.95e-04	2.00019	13.83475856	1.04e-07	4.0009	13.83475846	7.71e-10	5.9955
	128	13.83488232	1.24e-04	2.00004	13.83475846	6.53e-09	4.0002	13.83475845	4.08e-11	5.9999
	256	13.83478942	3.10e-05	2.00001	13.83475845	4.08e-10	4.0000	13.83475845	1.40e-13	6.0000
	Existing result = 13.834758									
$c = 0.4$	4	13.38213007	9.60E-01		12.42216412	3.56E-02		12.42216313	4.40E-03	
	8	12.51071171	8.85E-02	2.0154	12.45779287	7.62E-03	4.3451	12.42655937	7.71E-04	6.0527
	16	12.43177774	9.61E-03	2.0095	12.42293499	7.72E-04	4.0623	12.42217245	9.32E-06	6.0129
	32	12.42292193	7.59E-04	2.0037	12.42221943	5.63E-05	4.0103	12.42216313	4.41E-07	6.0099
	64	12.42223492	7.18E-05	2.0018	12.42978489	9.92E-07	4.0096	12.42293432	4.36E-09	6.0042
	128	12.42218071	1.76E-05	2.0008	12.42216317	4.02E-08	4.0073	12.42216357	7.28E-10	6.0017
	256	12.42216626	3.13E-06	2.0003	12.42216313	4.39E-09	4.0023	12.42216313	2.71E-11	6.0009
	Existing result = 12.422163									
$c = 0.8$	4	10.7701461	1.04E+00		9.738846102	1.17E-02		9.727997702	8.52E-04	
	8	10.2871461	5.60E-01	2.0994	9.727886102	7.40E-04	4.0807	9.727181202	3.51E-05	6.0698
	16	9.782096102	5.50E-02	2.0848	9.727219602	7.35E-05	4.0713	9.727147068	9.66E-07	6.0695
	32	9.728230102	1.08E-03	2.0631	9.727157102	1.10E-05	4.0466	9.727146185	8.28E-08	6.0606
	64	9.727253202	1.07E-04	2.0480	9.727151332	5.23E-06	4.0402	9.727146103	6.74E-10	6.0326
	128	9.727156532	1.04E-05	2.0279	9.727146886	7.84E-07	4.0198	9.727146102	4.75E-11	6.0050
	256	9.727147652	1.55E-06	2.0051	9.727146151	4.90E-08	4.0074	9.727146102	6.84E-12	6.0007
	Existing result = 9.727146									

A. error – Absolute error

Table 2. Effect of boundary conditions on non-dimensional natural frequencies of the tapered Timoshenko beam ($c = 0.2$)

	N	HWM			HOHWM 4th			HOHWM 6th		
		Frequency	A. error	Conv. rate	Frequency	A. error	Conv. rate	Frequency	A. error	Conv. rate
C-P	4	12.48688739	1.80E+00		11.05355589	3.67E-01		10.77030682	8.34E-02	
	8	11.05808739	3.70E-01	2.3120	10.73676607	6.99E-02	4.8521	10.68746912	5.82E-04	7.6790
	16	10.75601079	6.91E-02	2.0624	10.6877406	8.53E-03	4.0629	10.68692751	4.01E-05	6.6293
	32	10.69501206	8.12E-03	2.0039	10.6869284	4.10E-04	4.0132	10.68688961	2.22E-06	6.0872
	64	10.68781264	9.25E-04	2.0007	10.68688976	2.37E-05	4.0083	10.6868877	3.06E-07	6.0034
	128	10.68715151	2.64E-04	2.0003	10.68688778	3.94E-06	4.0019	10.6868874	9.28E-09	6.0012
	256	10.68695081	6.30E-05	2.00002	10.6868874	7.31E-07	4.0005	10.68688739	2.79E-10	6.0008
	Existing result = 10.68689									
C-C	4	14.32226684	1.10E+00		13.26456684	4.23E-02		13.22543684	3.17E-03	
	8	13.95226684	7.30E-01	2.0906	13.22523684	2.97E-03	4.1523	13.22233484	6.80E-05	6.0228
	16	13.28756684	6.53E-02	2.0746	13.22246484	1.98E-04	4.0945	13.22226727	4.35E-07	6.0197
	32	13.22697684	4.71E-03	2.0595	13.22227401	7.17E-06	4.0840	13.22226686	1.76E-08	6.0131
	64	13.22245884	1.92E-04	2.0164	13.22226732	4.83E-07	4.0570	13.22226684	6.23E-09	6.0109
	128	13.22232314	5.63E-05	2.0117	13.22226737	5.34E-07	4.0338	13.22226684	6.31E-10	6.0072
	256	13.22227227	5.43E-06	2.0021	13.22226684	4.85E-09	4.0013	13.22226684	5.02E-11	6.0020
	Existing result = 13.222267									

taper ratio (c) for the beam under clamped-clamped (C-C) boundary conditions. The results are compared with the existing results obtained from the Ritz method and alternative methods employed in [22,25].

As expected, for the beam with the taper ratio other than $c = 0$, the non-dimensional natural frequency decreases for the higher value of c. Moreover, as it can be observed, the results of the higher order Haar wavelet method prove that in the case of the 4th and the 6th order of convergence, the absolute error reduces much faster by increasing the number of terms in the Haar wavelet method. This matter could be essential in the case of more complex problems, thus the accurate result can be obtained faster and with a smaller number of terms.

The effect of boundary conditions is shown in Table 2. For the tapered Timoshenko beam ($c = 0.2$), the results of two boundary conditions – clamped-clamped (C-C) and clamped-pinned (C-P) – are produced, which prove the above-mentioned point for the higher order Haar wavelet method. In the future study, the HOHWM is planned to be applied to design optimization of plate and shell structures [27–31].

4. CONCLUSIONS

During the last two years, the HOHWM has been applied with success to the analysis of plate and shell structures by using Euler–Bernoulli and zig-zag theories. In the current study, the HOHWM is extended to the vibration analysis of Timoshenko beams. The solution has been used to analyse the beam under two boundary conditions, clamped-clamped and clamped-pinned. The results for beams with different taper ratios prove that the higher order Haar wavelet method is accurate, and for the versions with the higher order of convergence (4th and 6th order) the absolute error drops extremely fast. These results can be translated to a faster, simpler, and more accurate solution for other structural analyses where the analytical solution is difficult to obtain.

ACKNOWLEDGEMENTS

The study was supported by the Estonian Centre of Excellence in Zero Energy and Resource Efficient Smart Buildings and Districts, ZEBE, TK146 funded by the European Regional Development Fund (grant 2014-2020.4.01.15-0016); Smart Industry Centre (SmartIC) funded by the Estonian Research Council TT2; Estonian Research Council project MOBJD704 "Development of numerical methods for analysis of advanced composite and nanostructures"; AR20013 Smart City Centre of Excellence (1.01.2020–31.08.2023). The publication costs of this article were covered by the Estonian Academy of Sciences.

REFERENCES

1. Chen, C. F. and Hsiao, C. H. Haar wavelet method for solving lumped and distributed-parameter systems. *IEE Proc. Control Theory Appl.*, 1997, **144**(1), 87–94.
2. Hsiao, C. H. State analysis of the linear time delayed systems via Haar wavelets. *Math. Comput. Simul.*, 1997, **44**(5), 457–470.
3. Lepik, Ü. Buckling of elastic beams by the Haar wavelet method. *Estonian J. Eng.*, 2011, **17**(3), 271–284.
4. Lepik, Ü. Numerical solution of differential equations using Haar wavelets. *Math. Comput. Simul.*, 2005, **68**(2), 127–143.
5. Lepik, Ü. Numerical solution of evolution equations by the Haar wavelet method. *Appl. Math. Comput.*, 2007, **185**(1), 695–704.
6. Hein, H. and Feklistova, L. Computationally efficient delamination detection in composite beams using Haar wavelets. *Mech. Syst. Signal Process.*, 2011, **25**(6), 2257–2270.
7. Hein, H. and Feklistova, L. Free vibrations of non-uniform and axially functionally graded beams using Haar wavelets. *Eng. Struct.*, 2011, **33**(12), 3696–3701.
8. So, S.-R., Yun, H., Ri, Y., O, R. and Yun, Y.-I. Haar wavelet discretization method for free vibration study of laminated composite beam under generalized boundary conditions. *J. Ocean Eng. Sci.*, 2021, **6**(1), 1–11.
9. Aziz, I. and Šarler, B. The numerical solution of second-order boundary-value problems by collocation method with the Haar wavelets. *Math. Comput. Model.*, 2010, **52**(9–10), 1577–1590.
10. Aziz, I. and Amin, R. Numerical solution of a class of delay differential and delay partial differential equations via Haar wavelet. *Appl. Math. Model.*, 2016, **40**(23–24), 10286–10299.
11. Pervaiz, N. and Aziz, I. Haar wavelet approximation for the solution of cubic nonlinear Schrodinger equations. *Physica A*, 2020, **545**, 123738.
12. Majak, J., Shvartsman, B., Karjust, K., Mikola, M., Haavajõe, A. and Pohlak, M. On the accuracy of the Haar wavelet discretization method. *Compos. B. Eng.*, 2015, **80**, 321–327.
13. Majak J., Pohlak, M., Karjust, K., Eerme, M., Kurnitski, J. and Shvartsman, B. S. New higher order Haar wavelet method: Application to FGM structures. *Compos. Struct.*, 2018, **201**, 72–78.
14. Majak, J., Pohlak, M., Eerme, M. and Shvartsman, B. Solving ordinary differential equations with higher order Haar wavelet method. *AIP Conf. Proc.*, 2019, **2116**, 330002.
15. Majak, J., Shvartsman, B., Ratas, M., Bassir, D., Pohlak, M., Karjust, K. and Eerme, M. Higher-order Haar wavelet method for vibration analysis of nanobeams. *Mater. Today Commun.*, 2020, **25**, 101290.
16. Jena, S. K., Chakraverty, S. and Malikan, M. Implementation of Haar wavelet, higher order Haar wavelet, and differential quadrature methods on buckling response of strain gradient nonlocal beam embedded in an elastic medium. *Eng. Comput.*, 2021, **37**(2), 1251–1264.
17. Ratas, M., Salupere, S. and Majak, J. Solving nonlinear PDEs using the higher order Haar wavelet method on nonuniform and adaptive grids. *Math. Model. Anal.*, 2021, **26**(1), 147–169.
18. Sorrenti, M., Di Sciuva, M., Majak, J. and Auriemma, F. Static response and buckling loads of multilayered composite beams using the refined zigzag theory and higher-order Haar wavelet method. *Mech. Compos. Mater.*, 2021, **57**(1), 1–18.
19. Majkut, L. Free and forced vibrations of Timoshenko beams described by single difference equation. *J. Theor. Appl. Mech.*, 2009, **47**(1),193–210.
20. Shahba, A., Attarnejad, R., Marvi, M. T. and Hajilar, S. Free vibration and stability analysis of axially functionally graded tapered Timoshenko beams with classical and non-classical boundary conditions. *Compos. B. Eng.*, 2011, **42**(4), 801–808.
21. Zhou, D. and Cheung, Y. K. Vibrations of tapered Timoshenko beams in terms of static Timoshenko beam functions, *J. Appl. Mech*., 2001, **68**(4), 596–602.
22. Pradhan, K. K. and Chakraverty, S. Free vibration of Euler and Timoshenko functionally graded beams by Rayleigh–Ritz method. *Compos. B. Eng.*, 2013, **51**,175–184.
23. Attarnejad, R., Semnani, S. J. and Shahba, A. Basic displacement functions for free vibration analysis of non-prismatic Timoshenko beams. *Finite Elem. Anal. Des.*, 2010, **46**(10), 916–929.
24. Sohani, F. and Eipakchi, H. R. Analytical solution for modal analysis of Euler–Bernoulli and Timoshenko beam with an arbitrary varying cross-section. *Math. Model. Eng.*, 2018, **4**(3), 164–174.

25. Tang, A.-Y., Wu, J.-X., Li, X.-F. and Lee, K. Y. Exact frequency equations of free vibration of exponentially non-uniform functionally graded Timoshenko beams. *Int. J. Mech. Sci.*, 2014, **89**, 1–11.
26. Huang, Y., Yang, L.-E. and Luo, Q.-Z. Free vibration of axially functionally graded Timoshenko beams with non-uniform cross-section. *Compos. B. Eng.*, 2013, **45**(1), 1493–1498.
27. Guessasma, S. and Bassir, D. Optimization of the mechanical properties of virtual porous slids using a hybrid approach. *Acta Mater.*, 2010, **58**(2), 716–725.
28. Guessasma, S. and Bassir, D. Identification of mechanical properties of biopolymer composites sensitive to interface effect using hybrid approach. *Mech. Mater.*, 2010, **42**(3), 344–353.
29. Snatkin, A., Eiskop, T., Karjust, K. and Majak, J. Production monitoring system development and modification. *Proc. Estonian Acad. Sci.*, 2015, **64**(4S), 567–580.
30. Guessasma, S., Bassir, D. and Hedjazi, L. Influence of interphase properties on the effective behaviour of a starch-hemp composite. *Mater. Des.*, 2015, **65**, 1053–1063.
31. Abouzaid, K., Bassir, D., Guessasma, S. and Yue, H. Modelling the process of fused deposition modelling and the effect of temperature on the mechanical, roughness, and porosity properties of resulting composite products. *Mech. Compos. Mater.*, 2021, **56**, 805–816.

Muutuva ristlõikega Timoshenko tala vabavõnkumiste analüüs kõrgemat järku Haari lainikute meetodi abil

Marmar Mehrparvar, Jüri Majak, Kristo Karjust ja Mustafa Arda

Viimase kahe aasta jooksul on rakendatud kõrgemat järku Haari lainikute meetodit plaatide ja koorikute analüüsiks, kasutades peamiselt Euler-Bernoulli teooriat, ühes artiklis ka zig-zag teooriat. Käesolevas töös on laiendatud kõrgemat järku Haari lainikute meetod Timoshenko tala vabavõnkumiste analüüsiks. Töös on kasutatud jäik-jäik ja jäik-vaba (vaba toetus) rajatingimusi. Analüüsitud on erivate ristlõike muutumise koefitsentidele vastavaid lahendusi. Kõrgemat järku Haari lainikute meetod osutus täpseks ja kiireks nii 4. kui 6. järku koonduvuse korral (koonduvuse järk on määratud meetodi parameetriga). Saadud tulemused on üldistatavad laiema plaatide/koorikute vabavõnkumisi käsitlevate ülesannete klassi jaoks, kattes ka juhtusid, kus analüütiline lahend puudub. Saadud tulemused on kooskõlas laiemalt kasutatava Haari lainikute meetodi ja Ritzi meetodi abil saadud tulemustega. Kõrgemat järku Haari lainikute meetodit võib vaadelda kui Haari lainikute meetodi edasiarendust, mis tagab kõrgemat järku koonduvuskiiruse ja väiksema absoluutse vea.

Publication II

M. Mehrparvar, J. Majak, and K. Karjust, “Free vibration analysis of Timoshenko beam by higher-order Haar wavelet method,” *AIP Conference Proceedings*, vol. 2849, no. 1, p. 250007, 2023, doi: https://doi.org/10.1063/5.0162269.

Free Vibration Analysis of Timoshenko Beam by Higher-Order Haar Wavelet Method

Marmar Mehrparvar[a)], Jüri Majak[b)] and Kristo Karjust[c)]

Department of Mechanical and Industrial Engineering, Tallinn University of Technology, Tallinn, Estonia

[a)] *Corresponding Author: marmar.mehrparvar@taltech.ee*
[b)] *Juri.Majak@ttu.ee*
[c)] *kristo.karjust@ttu.ee*

Abstract. The current study aims to develop a numerical algorithm based on the higher-order Haar wavelet method (HOHWM) to accurately investigate the free vibrations of the Timoshenko beam. The proposed solution is implemented for beams with three different boundary conditions. Results of two specific cases of HOHWM, 4th and 6th order of convergence, are presented and are compared with the well-known Haar wavelet method (HWM) and the existing exact solution.

INTRODUCTION

Various numerical methods and algorithms have been used by engineers and researchers to pave the way for solving complex scientific problems. In engineering problems, utilizing modern numerical methods, for instance the Haar wavelet method, is one of the most common approaches to analyze all sorts of structures. The Haar wavelet method (HWM) was first introduced by Chen and Hsiao [1] to solve ordinary differential equations in which the highest order derivative in the differential equations will be expanded into Haar wavelets. Pioneering studies have been done by Ü.Lepik in this area covering wide class of solid mechanics problems [2-3]. The HWM was recognized as a method simple to implement and it was adapted for solving various differential [3-14] and integral/integro-differential equations [15-17]. However, according to convergence theorem proved for HWM in 2015 in [18], the rate of convergence of the Chen and Hsiao approach based HWM is equal to two. Thus, the HWM needs improvement in order to compete with mainstream numerical methods used in engineering.

The higher order Haar wavelet method (HOHWM) was introduced in 2018 in [19] as principal improvement of the HWM. The HOHWM has been implemented successfully for vibration analysis of Euler-Bernoulli beams, composites plates, linear and nonlinear differential equations, vibration analysis of nanobeams, etc [20-26].

FORMULATION

In this section, the formulation for free vibration analysis of Timoshenko beams is presented, and then the essence of the Haar wavelet method (HWM) and higher-order Haar wavelet method (HOHWM) are provided.

Timoshenko Beam

The Timoshenko model is an extension of the Euler-Bernoulli model by taking into account the shearing force effect and the rotary motion effect. Consider a Timoshenko beam of length L, with bending stiffness of EI, shear stiffness of GA, distributed rotational inertia per unit length of ρI, and distributed mass of ρA per unit length which all are dependent on the axial coordinate x measured from the end of the beam. Also, k is the shear correction factor which in the current study chosen to be 5/6. For a beam with the given geometry and material properties, by employing the Timoshenko beam theory, basic governing differential equations for transverse vibration of beams read:

$$\begin{aligned} \rho A\frac{\partial^2 w(x,t)}{\partial t^2} - GkA\left(\frac{\partial^2 w(x,t)}{\partial x^2} - \frac{\partial \varphi(x,t)}{\partial x}\right) = 0 \\ EI\frac{\partial^2 \varphi(x,t)}{\partial x^2} + GkA\left(\frac{\partial y(x,t)}{\partial x} - \varphi(x,t)\right) - I\rho\frac{\partial^2 \varphi(x,t)}{\partial t^2} = 0 \end{aligned} \tag{1}$$

where w and φ are the transverse deflection and rotation of cross-section at the neutral surface, respectively. After some transformations, like the transformation of the homogeneous equation, it is possible to obtain an equation for the transverse vibration of the Timoshenko beam that is only dependent on the displacement function $w(x,t)$.

$$EI\frac{\partial^4 w(x,t)}{\partial x^4} - \left(\frac{EI\rho}{Gk} + I\rho\right)\frac{\partial^4 w(x,t)}{\partial x^2\,\partial t^2} + \frac{I\rho^2}{Gk}\frac{\partial^4 w(x,t)}{\partial t^4} + \rho A\frac{\partial^2 w(x,t)}{\partial t^2} = 0 \tag{2}$$

Higher-order Haar Wavelet Method

The Haar wavelet, a special class of discrete orthonormal wavelets, is one of the most basic wavelets which is discontinuous and similar to a step function. The other wavelets produced from the identical main wavelet form a basis whose elements are orthonormal to each other and are normalized to unit length. This property allows each wavelet coefficient to be computed independently of other wavelets. The Haar functions are given as

$$h_i(x) = \begin{cases} 1 & \text{for} \quad x \in [\xi_1(i), \xi_2(i)) \\ -1 & \text{for} \quad x \in [\xi_2(i), \xi_3(i)) \\ 0 & \text{elsewhere} \end{cases} \tag{3}$$

In (1) $i = m + k + 1, m = 2^j$ is a maximum number of square waves deployed in the interval $[A, B]$ and the parameter k indicates the location of the particular square wave

$$\begin{aligned} \xi_1(i) = A + 2k\mu\Delta x, \qquad \xi_2(i) = A + (2k+1)\mu\Delta x, \qquad \xi_3(i) = A + 2(k+1)\mu\Delta x, \\ \mu = M/m, \qquad \Delta x = (B-A)/(2M) \end{aligned} \tag{4}$$

The integrals of the Haar functions (3) of order n can be expressed as [8]

$$p_{n,i}(x) = \begin{cases} 0 & x \in [A, \xi_1(i)) \\ \dfrac{(x-\xi_1(i))^n}{n!} & x \in [\xi_1(i), \xi_2(i)) \\ \dfrac{(x-\xi_1(i))^n - 2(x-\xi_2(i))^n}{n!} & x \in [\xi_2(i), \xi_3(i)) \\ \dfrac{(x-\xi_1(i))^n - 2(x-\xi_2(i))^n + (x-\xi_3(i))^n}{n!} & x \in [\xi_3(i), B) \\ 0 & else\ where \end{cases} \quad for \tag{5}$$

Recently, the higher-order Haar wavelet method approach has been introduced [19]. The higher-order wavelet expansion is introduced as:

$$f(x) = \frac{d^{n+2s}u(x)}{dx^{n+2s}} = \sum_{i=1}^{\infty} a_i h_i(x)\,, s = 1,2,\ldots \tag{6}$$

NUMERICAL RESULTS

To study the accuracy and speed of the method employed in this paper, the free vibration of Timoshenko beams under different boundary conditions is presented in this section.

TABLE 1. Comparison of the dimensionless natural frequencies of Timoshenko beams with three different boundary conditions

		HWM			HOHWM 4th ($s=1$)			HOHWM 6th ($s=2$)		
	N	Frequency	A. error	Conv. rate	Frequency	A. error	Conv. rate	Frequency	A. error	Conv. rate
Pinned-Pinned Exact: 9.16068318	4	10.76068319	1.60E+00		9.16627318	5.59E-03		9.16109539	4.12E-04	
	8	9.59208533	4.31E-01	1.8954	9.16088118	1.98E-04	4.0580	9.16069124	8.05E-06	5.2583
	16	9.27047366	1.10E-01	1.9742	9.16069928	1.61E-05	4.0268	9.16068333	1.48E-07	5.6800
	32	9.18825306	2.76E-02	1.9935	9.16068724	4.06E-06	4.0244	9.16068322	3.68E-08	5.7820
	64	9.16758331	6.90E-03	1.9983	9.16068383	6.42E-07	4.0240	9.16068319	6.74E-10	5.9221
	128	9.16240869	1.73E-03	1.9995	9.16068327	8.79E-08	4.0133	9.16068318	1.73E-11	5.9850
	256	9.16111459	4.31E-04	1.9998	9.16068320	1.74E-08	4.0054	9.16068318	3.90E-12	6.0130
Clamped-Pinned Exact: 11.08249918	4	12.16296846	1.08E+00		11.12396203	4.15E-02		11.08476457	2.27E-03	
	8	11.67284507	5.90E-01	2.0085	11.08552579	3.03E-03	4.0017	11.08257904	7.99E-05	6.1932
	16	11.16717818	8.47E-02	2.0065	11.08280853	3.09E-04	4.0153	11.08249987	6.91E-07	6.1877
	32	11. 08814918	5.65E-03	2.0050	11.08250835	9.17E-06	4.0153	11. 08249920	2.00E-08	6.1326
	64	11. 08267527	1.76E-04	2.0043	11.08249969	5.14E-07	4.0010	11. 08249919	5.82E-09	6.1049
	128	11.08254898	4.98E-05	2.0042	11.08249985	6.72E-07	4.0099	11.08249918	4.24E-10	6.0573
	256	11.08250581	6.63E-06	2.0024	11.08249918	4.96E-09	4.0002	11.08249918	3.35E-11	6.0547
Clamped-Clamped Exact: 13.83475845	4	13.96275845	1.28e-01		13.84197845	7.22e-03		13.83477975	2.13e-05	
	8	13.86655612	3.18e-02	2.0091	13.83519214	4.34e-04	4.0576	13.83476001	1.56e-06	5.4358
	16	13.84269132	7.93e-03	2.003	13.83478525	2.68e-05	4.0146	13.83475854	8.43e-08	5.7522
	32	13.83674066	1.98e-03	2.0007	13.83476012	1.67e-06	4.0036	13.83475846	1.51e-09	5.9467
	64	13.83525392	4.95e-04	2.00019	13.83475856	1.04e-07	4.0009	13.83475846	7.71e-10	5.9955
	128	13.83488232	1.24e-04	2.00004	13.83475846	6.53e-09	4.0002	13.83475845	4.08e-11	5.9999
	256	13.83478942	3.10e-05	2.00001	13.83475845	4.08e-10	4.0000	13.83475845	1.40e-13	6.0000

Table 1 exhibits the dimensionless neutral frequencies of a homogeneous beam under three arbitrary boundary conditions, pinned-pinned, pinned-clamped, and clamped-clamped. Also, the results are validated by the given exact solution which is calcuated by authors. As it can be seen the used method is proven to be accurate and by utilizing HOHWM the solution converges faster which can be crucial for more complicated problems. However due to some limitations in order to obtain the desired convergence rate some extra measures have been taken.

In the future study, the design optimization of the Timoshenko beam is planned based on previous long time experience of the workgroup in area of traditional and evolutionary optimization [27-29]. First interest is related to maximization of the fundamental frequency value. Development of optimization algorithms for wide class of engineering structures is planned in cooperation with workgroup from Université Paris-Saclay [30-33]. Another challenge is adaption of the HOHWM for analysis of nanostructures in cooperation with Trakya University [34-37].

CONCLUSION

In the current study, the higher order Haar wavelet method has been adapted for free vibration analysis of a homogenous Timoshenko beam. The dimensionless natural frequencies of Timoshenko beam under three different boundary conditions were evaluated. An analysis of the results allows confirming that the proposed HOHWM provides principal improvement of accuracy and the rate of convergence in comparison with widely used HWM.

ACKNOWLEDGMENTS

Estonian Centre of Excellence in Zero Energy and Resource Efficient Smart Buildings and Districts, ZEBE, TK146 funded by the European Regional Development Fund (grant 2014-2020.4.01.15-0016); Smart Industry Centre (SmartIC) funded by the Estonian Research Council TT2; AR20013 Smart City Center of Excellence (1.01.2020−31.08.2023)

REFERENCES

1. C.F. Chen, C.H. Hsiao, IEE Proc Contr Theor Appl, **144**(1), 87-94 (1997)
2. Ü.Lepik, Math. Comput. Simulat. **68**(2), 127-143 (2005)
3. Ü.Lepik, Proc. Estonian Acad. Sci. **56**(1), 28-46 (2007)
4. H.Hein, L. Feklistova, Mech Syst Signal Pr **25** (6), 2257-70 (2011)
5. L. Jaanuska, H. Hein, Int. J. of Mechanics, **10**, 281-287 (2016)
6. L. Feklistova, H. Hein, Comp. Assisted Meth. in Eng. and Sci., **19** (4), 351-360 (2012)
7. Ü. Lepik, H. Hein, Haar wavelets: with applications (Springer, New York, 2014)
8. J. Majak, B. Shvartsman, M. Pohlak, K. Karjust, M. Eerme, E. Tungel AIP Conf. Proc. **1738**, 480110 (2016)
9. N. Pervaiz, I. Aziz, Physica A: Statistical Mechanics and its Applications **545**,123738 (2020)
10. M. Ratas, AIP Conference Proceedings, **2116**, 330004 (2019).
11. Ö. Oruç, Computers and Mathematics with Applications, **77**(7), 1799-1820 (2019)
12. S. Saleem, I. Aziz, M.Z. Hussain, Eng with Computers, **232**, (2019)
13. I. Aziz, Siraj-ul-Islam, M. Nisar, Calcolo **53**, 4, 621-633 (2016)
14. L. Jaanuska, H. Hein, Acta et Commentationes Universitatis Tartuensis de Mathematica, **23** (1), 125−142 (2019)
15. I Aziz, I., Khan, International Journal of Computational Methods **15**(6),1850047 (2018)
16. S.U. Islam, I. Aziz, A.S. Al-Fhaid. Journal of Comp. and Appl. Math. **260**, 449–469 (2014)
17. S.U. Islam, I. Aziz, M. Fayyaz, International Journal of Computer Mathematics, **90** (9), 1971–1989 (2013)
18. J. Majak J, B.S. Shvartsman, M. Kirs, M. Pohlak, H. Herranen, Compos. Struct. **126**, 227-32 (2015)
19. J. Majak, M. Pohlak, K. Karjust, M. Eerme, J. Kurnitski, B.S. Shvartsman, Compos. Struct. **201**, 72-78 (2018)
20. J. Majak, B. Shvartsman, M. Ratas, D. Bassir, M. Pohlak, K. Karjust, M. Eerme, Mater. Today Commun. **25**, 101290 (2020)
21. M. Ratas, A. Salupere, Math. Modelling and Analysis, **25** (2), 271-288 (2020)
22. J. Majak, M. Pohlak, M. Eerme, B. Shvartsman, AIP Conference Proceedings, **2116**, 330002 (2019)
23. M Sorrenti, M. Di Sciuva, J Majak, F Auriemma, Mechanics of Composite Materials **57** (1), 1-18 (2021)
24. M. Ratas, AIP Conference Proceedings, **2116**, 330004 (2019)
25. S.K. Jena, S. Chakraverty, European Physical Journal Plus **134** (10), 538 (2019)
26. M Ratas, A Salupere, J Majak, Mathematical Modelling and Analysis **26** (1), 147-169 (2021)
27. J. Lellep, J. Majak, Structural Optimization, **14** (2-3), 116-120 (1997)
28. J. Lellep, J. Majak, Mechanics of Composite Materials, **36** (4), 261−266 (2000)
29. A. Snatkin, T. Eiskop, K. Karjust, J. Majak, Proc. of the Estonian Academy of Sciences, **64**, 567−580 (2015)
30. J. Zhu, W.Zhang, L.Xia, Q.Zhang, D. Bassir, Journal of Intelligent and Robitic System, **67**(3-4), 185-199 (2012)
31. K. Abouzaid, S. Guessasma, S. Belhabib, D. Bassir, A. Chouaf, European Polymer Journal, **108**, 262-273 (2018)
32. W.H. Zhang, M. Domasxewski, D. Bassir, Structural Optimization, **17**,2, 219-225 (1999)
33. S. Guessasma, D. Bassir, L. Hedjazi, Materials & Design, **65**, 1053-1063 (2015)
34. M. Arda, M. Aydogdu, Advances in Science and Technology-Research Journal, **9** (26), 28–33 (2015)
35. M. Arda, M. Aydogdu, Journal of Vibration and Control, **25** (4), 820-833 (2019)
36. M. Arda, M. Aydogdu, International Journal of Engineering & Applied Sciences (IJEAS) **9** (2), 22-38 (2017)
37. M Arda, M Aydogdu M Arda, M Aydogdu, Solid State Phenomena **267**, 151-156 (2017)

Publication III

M. Arda, J. Majak, and M. Mehrparvar, "Longitudinal Wave Propagation in Axially Graded Raylegh–Bishop Nanorods," *Mechanics of Composite Materials*, vol. 59, no. 6, pp. 1109–1128, Jan. 2024, doi: https://doi.org/10.1007/s11029-023-10160-4.

DOI 10.1007/s11029-023-10160-4
Mechanics of Composite Materials, Vol. 59, No. 6, January, 2024

LONGITUDINAL WAVE PROPAGATION IN AXIALLY GRADED RAYLEGH–BISHOP NANORODS

M. Arda,[1,2*] J. Majak,[1] and M. Mehrparvar[1]

Keywords: *longitudinal wave propagation, Haar wavelet method, axially graded, Raylegh–Bishop rod, nonlocal elasticity*

Longitudinal wave propagation in axially graded nanotubes was explored. The effect of shear deformation and lateral inertia on nanorods was considered using the nonlocal Raylegh–Bishop rod theory. As a novel approach, a nonlocal parameter was assumed in the graded formulation. The higher order Haar wavelet method was utilized for solving the governing equation of motion. The effects of material grading power-law index and nonlocal parameters on the longitudinal wave response of axially graded nanorods were investigated. Phase and group velocity variations of the axially graded nanorod were obtained. The present study may be useful in the modeling of advanced functional composite nanowires.

1. Introduction

Carbon nanotubes are one of the most impressive nanomaterials, which have superior physical properties for a one-dimensional structure. Besides the wide range of application areas, nanotubes can be improved with functionally graded material (FGM). With the high conductivity characteristics and interaction with magnetic fields, carbon nanotubes are the best candidate for nanowire applications. Designing a material in graded composition gives a huge advantage in specific applications. Recently, graded nanotubes have been used as semiconductor alloy nanowires, which were produced in an axially graded composition in single-walled carbon nanotubes [1].

Continuum modeling of the nano-sized structures can be achieved with the size-dependent gradient theories, which consider the small-scale effects and long-range interactions in the nanostructure. One of these size-dependent theories

[1]Tallinn University of Technology, Department of Mechanical and Industrial Engineering, 19086 Tallinn, Estonia
[2]Trakya University, Department of Mechanical Engineering, 22130 Edirne, Turkey
[*]Corresponding author; tel.: +90 505 4317096; e-mail: mustafaarda@trakya.edu.tr

Original article submitted July 5, 2023; revision submitted October 2, 2023.

Fig 1. Axially graded nanorod continuum model.

is the nonlocal stress gradient elasticity theory, which was proposed by Eringen [2, 3]. It has been mostly used theory in statics and dynamics analysis of nanostructures [4-14]. Also, higher order [15] and shear deformation [16] beam models have been developed for the analysis of nanotubes.

Nanorods can be modeled as continuous hollow rods with the help of nonlocal elasticity. In addition to the strain and stress resultants in the axial direction, the lateral motion of particles has affected the nanorod dynamics. Bishop [17] considered these effects by adding shear strain and rotational inertia terms in his model, which is the well-known Rayleigh–Bishop model.

A comparison of longitudinal wave propagation with several rod models was carried out in [18, 19]. A similar comparison was made by Aydogdu [20] for the nanorods by considering unimodal theories. Validation and calibration of small-scale parameters for various models in wave propagation were carried out by using lattice dynamics results. Longitudinal wave propagation and vibration of nanorods were investigated by Li et al. [21] with nonlocal unimodal rod theories. Hosseini et al. used the Bishop rod model with strain gradient theory for modeling the nano-resonator [22] and FG-reinforced composite microrods [23]. Karlicic et al. [24] studied the multiple Bishop nanorod system by utilizing the nonlocal elasticity theory.

Materials with continuously varying properties in the length direction should be named axially functionally graded (aFG) structures [25-28]. The nanoscale application of aFG materials for the wave characteristics of nanostructure was first studied by Kiani who proposed a nonlocal surface energy model for axially graded nanorods [29] and nanobeams [30]. Elastic wave dispersion in FG double nanobeam system under the effect of thermal and magnetic fields was studied by Ebrahimi and Dabbagh [31]. Yao et al. [32] investigated the vibrations and wave propagation of axially moving FG nonlocal Timoshenko microbeams. In addition, continuum shell models were used in wave propagation in several papers [33, 34]. Longitudinal and torsional dynamics of porous nanorods, which can be defined in terms of FGM with deformable boundaries, were investigated by Yayli et al. in [35-39]. Vibration analysis of carbon nanotube reinforced composite materials was studied in [40, 41].

In the majority of studies, related to axially graded nanostructures, the nonlocal parameter was assumed constant. However, nonlocality is a material property like elasticity or density that should be considered a variable in the grading directions. The novelty of the present work is that the nonlocal parameter is varied with power-law formulation, like other material properties. Axially FG Rayleigh–Bishop nanorod model was obtained with nonlocal elasticity theory, Rayleigh–Bishop rod theory, and minimum potential energy principle. To the best of the author's knowledge for the first time in the literature, the higher order Haar wavelet method (HOHWM) has been applied for the numerical solution of the wave propagation problem of the nonlocal differential equation of motion with variable coefficients. Contrasting with the previous work [42], the present study deals with wave propagation in axially graded nanorod structures. Aziz exhibited in several studies that numerical solutions of second-order boundary value problems [43], delay partial differential equations [44] and cubic nonlinear Schrodinger equation could be obtained with the Haar Wavelet method. The HOHWM has been introduced by Majak et al. [45] and has been utilized with success for solving differential and integrodifferential equations [46-54].

Material properties variation has been assumed the power-law function of the axial displacement. Effects of material gradient index and nonlocal parameters were investigated. Results could be useful for the dynamical analysis of advanced functional composite semiconductor alloy nanowires.

2. Analysis

An infinitely long axially FG nanorod is assumed. Cartesian coordinates are considered in which the *x*-axis is in the direction of the length and the *r*-axis is in the cross-sectional radial direction of the nanorod (Fig. 1). The material properties of the nanorod are varying along the *x*-direction.

Longitudinal (*u*) and lateral (*w*) displacements of the rod can be defined as the functions below according to the Raylegh–Bishop rod model:

$$u = u(x,t), \tag{1}$$

$$w = w(x,t) = r\eta \frac{\partial u(x,t)}{\partial x}, \tag{2}$$

where *r* is the distance of the lateral displacement of a particle from the *x*-axis and it is assumed to be proportional to the longitudinal strain. The Poisson's ratio η for the nanorod is defined as:

$$\eta = \frac{E(x)}{2G(x)} - 1, \tag{3}$$

where *E* and *G* are the Young's and shear moduli of the nanorod, respectively.

2.1. Nonlocal elasticity theory

Nonlocal constitutive relation for stress tensor is defined in differential form as below [55]:

$$\left(1 - \left(e(x)a\right)^2 \nabla^2\right)\tau_{kl} = \frac{E(x)\nu}{(1+\nu)(1-2\nu)}\varepsilon_{rr}\delta_{kl} + \frac{E(x)}{(1+\nu)}\varepsilon_{kl}, \tag{4}$$

where τ_{kl} is the nonlocal stress tensor, ε_{rr} is the sum of normal strains $\left(\varepsilon_{rr} = \varepsilon_{11} + \varepsilon_{22} + \varepsilon_{33}\right)$, δ_{kl} is the Kronecker Delta, ε_{kl} is the strain tensor, ν is the Poisson's ratio, $\left(e(x)a\right)^2$ is called the nonlocal parameter, $e(x)$ is the scale parameter, and a is the distance between two atoms in the nanorod structure. For the longitudinal dynamics of an axially graded nanorod, Eq. (4) should be written in the one-dimensional form:

$$\left(1 - \left(e(x)a\right)^2 \frac{\partial^2}{\partial x^2}\right)\sigma = E(x)\varepsilon, \tag{5}$$

where ε and σ are the normal strain and stress, respectively. Integration of the normal stress gives the normal force resultant of nanorod:

$$N = \int_A \sigma \, dA, \tag{6}$$

where A is the cross-sectional area. Nonlocal normal force resultant can be interpreted as below:

$$N^{NL} - \left(e(x)a\right)^2 \frac{\partial^2 N^{NL}}{\partial x^2} = N^L, \tag{7}$$

where the local force resultant is defined in a conventional manner:

$$N^L = E(x) A \varepsilon_{xx} . \tag{8}$$

2.2. Equation of motion for the Raylegh–Bishop nanorod

Governing equation of motion and boundary conditions for axial dynamics of the Raylegh–Bishop nanorod model can be obtained using Hamilton's minimum potential energy principle.

The total kinetic (E_K) and potential (E_P) energies can be defined according to nonlocal elasticity theory in Eq. (4) as below [56-58]:

$$E_K = \int_0^L \rho(x) A \left(\frac{\partial u(x,t)}{\partial t} \right)^2 dx + \int_0^L \left(e(x) a \right)^2 A \left[\frac{\partial}{\partial x} \left(\rho(x) \frac{\partial u(x,t)}{\partial t} \right) \right] \left(\frac{\partial^2 u(x,t)}{\partial x \partial t} \right) dx$$

$$+ \int_0^L \rho(x) \eta^2 I_P \left(\frac{\partial^2 u(x,t)}{\partial x \partial t} \right)^2 dx + \int_0^L \left(e(x) a \right)^2 \eta^2 I_P \left[\frac{\partial}{\partial x} \left(\rho(x) \frac{\partial^2 \delta u(x,t)}{\partial x \partial t} \right) \right] \left(\frac{\partial^3 u(x,t)}{\partial x^2 \partial t} \right) dx, , \tag{9}$$

$$E_P = \int_0^L E(x) A \left(\frac{\partial u(x,t)}{\partial x} \right)^2 dx + \int_0^L \eta^2 G(x) I_P \left(\frac{\partial^2 u(x,t)}{\partial x^2} \right)^2 dx , \tag{10}$$

where ρ is the density, I_P is the polar moment of inertia of the nanorod. It should be noted that E, G, ρ, and e are variated by axial coordinate x. The polar moment of inertia for a hollow cylindrical rod can be defined as:

$$I_P = \frac{\pi}{2} \left(R_2^{\,4} - R_1^{\,4} \right), \tag{11}$$

where R_1 and R_2 are the inner and outer radii of the carbon nanotube. For brevity, variations of the kinetic and potential energies are omitted herein. Interested readers can look [58] for comprehensive formulation. Governing equation of motion for the nonlocal Raylegh–Bishop rod model is [58]:

$$\frac{\partial}{\partial x} \left(E(x) A \frac{\partial u(x,t)}{\partial x} \right) - \frac{\partial^2}{\partial x^2} \left(\eta^2 G(x) I_P \frac{\partial^2 u}{\partial x^2} \right) = \frac{\partial}{\partial t} \left(\rho(x) A \frac{\partial u}{\partial t} \right)$$

$$- A \frac{\partial^2}{\partial x \partial t} \left(\left(e(x) a \right)^2 \frac{\partial}{\partial x} \left(\rho(x) \frac{\partial u(x,t)}{\partial t} \right) \right)$$

$$- \eta^2 I_P \frac{\partial^2}{\partial x \partial t} \left(\rho(x) \left(\frac{\partial^2 u(x,t)}{\partial x \partial t} \right) \right) + \eta^2 I_P \frac{\partial^3}{\partial x^2 \partial t} \left(\left(e(x) a \right)^2 \frac{\partial}{\partial x} \left(\rho(x) \frac{\partial^2 u(x,t)}{\partial x \partial t} \right) \right) \tag{12}$$

and boundary conditions are:

$$\left[\left(E(x) A \frac{\partial u}{\partial x} \right) - \frac{\partial}{\partial x} \left(\eta^2 G(x) I_P \frac{\partial^2 u}{\partial x^2} \right) + \left(\eta^2 \rho(x) I_P \frac{\partial^3 u}{\partial x \partial t^2} \right) \right.$$

$$\left. + \left(A \left(e(x) a \right)^2 \frac{\partial}{\partial x} \left(\rho(x) \frac{\partial^2 u(x,t)}{\partial t^2} \right) \right) - \left(\eta^2 I_P \frac{\partial}{\partial x} \left(\left(e(x) a \right)^2 \frac{\partial}{\partial x} \left(\rho(x) \frac{\partial^3 u(x,t)}{\partial x \partial t^2} \right) \right) \right) \right] \quad \text{or } u , \tag{13}$$

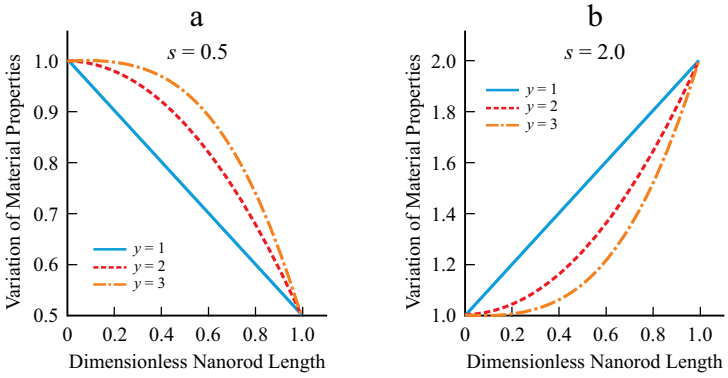

Fig. 2. Material property variations in axially FG nanorod at different value of power-law index y .

$$\left[\left(\eta^2 G(x) I_P \frac{\partial^2 u}{\partial x^2}\right) + \left(\eta^2 I_P \left(e(x)a\right)^2 \frac{\partial}{\partial x}\left(\rho(x)\frac{\partial^3 u(x,t)}{\partial x \partial t^2}\right)\right)\right] \quad \text{or} \quad \frac{\partial u}{\partial x}. \tag{14}$$

Equation (12) is the governing motion equation for longitudinal dynamics of nonlocal axially graded Raylegh–Bishop nanorod. Equation (12) can be turned into a classical continuum Rayleigh rod model if necessary, assumptions ($G = \eta = e = 0$) can be made.

2.3. Functionally graded materials

The functionally graded materials are the result of the combination of two different materials. Variations of the material properties (elasticity modulus, shear modulus, density, and scale parameter) in the axially graded structure are assumed as the power-law function:

$$\begin{bmatrix} E(x) \\ G(x) \\ \rho(x) \\ \mu(x) \end{bmatrix} = \begin{bmatrix} E_1 - E_0 \\ G_1 - G_0 \\ \rho_1 - \rho_0 \\ \mu_1 - \mu_0 \end{bmatrix} x^y + \begin{bmatrix} E_0 \\ G_0 \\ \rho_0 \\ \mu_0 \end{bmatrix} \quad \text{and} \quad \begin{bmatrix} E_1 \\ \rho_1 \\ \mu_1 \end{bmatrix} = s \begin{bmatrix} E_0 \\ \rho_0 \\ \mu_0 \end{bmatrix}, \tag{15}$$

where y is the material grading or power-law index, E_0 , G_0 , ρ_0 , μ_0 and E_1 , G_1 , ρ_1 , μ_1 are the material properties at the left and right side of the nanorod, respectively, s is a coefficient, which determines the material properties at the right side of nanorod. Power-law variations of material properties are shown in Fig. 2. In the present study, dimensionless material properties were assumed. y and s parameters can be determined according to the composition of materials selected and production methods. For the analysis, s is assumed as 0.5, 1, 2 and y is assumed as 1, 2, 3. Besides that, these parameters can be selected from fractional numbers.

With the assumption of the harmonic wave function $\left(u(x,t)=U(x)\sin\omega t\right)$, dimensionless distance $\left(X=\frac{x}{a}\right)$ in the nanorod's lattice structure, and nonlocality function $\left(\mu(X)=e(X)^2\right)$, Eq. (12) turns into:

$$A\left(\frac{\partial E(X)}{\partial X}\frac{\partial U(X)}{\partial X}\right)+A\left(E(X)\frac{\partial^2 U(X)}{\partial X^2}\right)-\eta^2 I_P\frac{\partial^2}{\partial x^2}\left(G(X)\frac{\partial^2 U(X)}{\partial X^2}\right)$$

$$=-\omega^2 A\left(\rho(X)U(X)\right)+\omega^2 A\left(\frac{\partial\mu(X)}{\partial X}\frac{\partial}{\partial X}\left(\rho(X)U(X)\right)+\mu(X)\frac{\partial^2}{\partial X^2}\left(\rho(X)U(X)\right)\right)$$

$$+\omega^2\eta^2 I_P\left(\frac{\partial\rho(X)}{\partial x}\left(\frac{\partial U(X)}{\partial x}\right)+\rho(X)\frac{\partial^2 U(X)}{\partial X^2}\right)-\omega^2\eta^2 I_P\left(\frac{\partial^2\mu(X)}{\partial X^2}\frac{\partial}{\partial X}\left(\rho(X)\frac{\partial U(X)}{\partial X}\right)\right.$$

$$\left.+2\frac{\partial\mu(X)}{\partial x}\frac{\partial^2}{\partial x^2}\left(\rho(X)\frac{\partial U(X)}{\partial X}\right)+e(X)\frac{\partial^3}{\partial X^3}\left(\rho(X)\frac{\partial U(X)}{\partial X}\right)\right). \tag{16}$$

Equation (16) is an ordinary differential equation with variable coefficients and an analytical solution has not been obtained. To solve this equation, a newly developed higher order Haar wavelet method was used in the present work.

2.4. Haar Wavelet Method (HWM)

Haar wavelets were introduced by Hungarian mathematician Alfred Haar in 1910. The Haar wavelets consist of piecewise constant functions and are the simplest among all the wavelet families which is a good feature to integrate them analytically at arbitrary times [59].

Haar wavelets $\left(h_i(x)\right)$ defined as a group of square waves with magnitude ±1 in given intervals and zero elsewhere [59]

$$h_i(x)=\begin{cases}1 \text{ if } x\in\left[\xi_1(i),\xi_2(i)\right]\\ -1 \text{ if } x\in\left[\xi_2(i),\xi_3(i)\right]\\ 0 \text{ elsewhere}\end{cases}, \tag{17}$$

where

$$\xi_1(i)=A+2k\mu\Delta x,$$

$$\xi_2(i)=A+(2k+1)\mu\Delta x \text{ and } \mu=\frac{M}{m},\ \Delta x=\frac{B-A}{2M}, \tag{18}$$

$$\xi_3(i)=A+2(k+1)\mu\Delta x.$$

The wavelet number (i) can be defined as $i=m+k+1$, and m $\left(m=2^j, M=2^J\right)$ is the maximum number of square waves, which can be deployed sequentially in the interval $[A,B]$. J is the maximum level of resolution. The interval $[A,B]$ is divided into $2M$ subintervals of equal length which is Δx.

If the j increases, the wavelet becomes narrower. Because of that, j is called the dilatation parameter. The integer k is called the translation parameter which determines the position of the wavelet in the x-axis.

Equation (18) is valid if $i>1$. In the case of $i=1$, $h_1(x)$ is the scaling function:

$$h_1(x)\equiv 1 \text{ and } m=0,\ \xi_1(1)=A,\ \xi_2(1)=\xi_3(1)=B. \tag{19}$$

The width of the i th wavelet is:

$$\xi_2(i)-\xi_1(i)=2\mu\Delta x=(B-A)m^{-1}=(B-A)2^{-j}. \tag{20}$$

If the maximal level of resolution (J) is assumed, it can be concluded that the Haar wavelets are orthogonal to each other.

Let us assume that $\varphi(x)$ is a square-integrable and a finite function in the interval $[A,B]$. Then, function $\varphi(x)$ can be expanded into Haar wavelets as:

$$\varphi(x)=\sum_{i=1}^{2M}a_i h_i(x), \tag{21}$$

where a_i is the Haar wavelet coefficient.

The integrals of the Haar functions according to α^{th} order can be expressed as [59]

$$P_{\alpha,i}(x)=\begin{cases}0 & \text{if } x<\xi_1(i)\\ \dfrac{1}{\alpha!}\left[x-\xi_1(i)\right]^{\alpha} & \text{if } x\in\left[\xi_1(i),\xi_2(i)\right]\\ \dfrac{1}{\alpha!}\left\{\left[x-\xi_1(i)\right]^{\alpha}-2\left[x-\xi_2(i)\right]^{\alpha}\right\} & \text{if } x\in\left[\xi_2(i),\xi_3(i)\right]\\ \dfrac{1}{\alpha!}\left\{\left[x-\xi_1(i)\right]^{\alpha}-2\left[x-\xi_2(i)\right]^{\alpha}+\left[x-\xi_3(i)\right]^{\alpha}\right\} & \text{if } x>\xi_3(i).\end{cases} \tag{22}$$

Integrals in Eq. (22) can be used for $i>1$. In the case of $i=1$, boundary elements turn into $\xi_1(1)=A$ and $\xi_2(1)=\xi_3(1)=B$. The integral of a function in this case ($i=1$) can be obtained with:

$$P_{\alpha,1}(x)=\frac{1}{\alpha!}\left[x-A\right]^{\alpha}. \tag{23}$$

Derivatives of the functions also may be expanded into the Haar wavelet series. Taking into consideration of the present problem, the higher order derivative of the axial displacement function can be expanded to the Haar wavelet series as below:

$$\varphi(x)=\frac{d^4U(X)}{dX^4}=\sum_{i=1}^{2M}a_i h_i(x). \tag{24}$$

Equation (24) can be expressed in matrix form as below:

$$\frac{d^4U(X)}{dX^4}=a^T H(i,x), \tag{25}$$

where a^T is the transpose of the axial displacement vector of nanorod and $H(i,x)$ is the Haar matrix. If Eq. (25) is integrated analytically four times according to axial x -coordinate, the axial displacement function of the nanorod will be obtained as below:

$$U(X)=a^T P_4(i,x)+C_1\frac{X^3}{6}+C_2\frac{X^2}{2}+C_3X+C_4, \tag{26}$$

where $P_4(i,x)$ are the fourth-order integration matrices and C_i stands for integration constants which can be determined by using boundary conditions.

2.5. Higher order Haar wavelet method (HOHWM)

Higher Order Haar wavelet method has the same theoretical background as HWM, except for the function expansion process. In Eq. (24), the highest order derivative involved in the governing Eq. (16) is expanded to the Haar wavelet series. Higher order HWM increases the order of derivative of the function by even numbers.

$$U(x)=\frac{d^{\nu+2\xi}U(X)}{dX^{\nu+2\xi}}=\sum_{i=1}^{2M}a_i h_i(x). \tag{27}$$

In the case $\xi=1$, the wavelet expansion starts from the 6th order derivative of the function. It has been observed by [45-47, 53, 60] that the HOHWM outperforms HWM by an increased rate of convergence and reduced absolute error. In the case of HOHWM, extra boundary conditions or periodicity conditions can be utilized for determining complementary integration constants. Periodical relations for the wave equation can be obtained by applying Bloch–Floquet theory.

2.6. Bloch–Floquet theory

Bloch–Floquet theory [61] declares that an energy potential in the lattice structure is periodic in the unit length of the lattice. Let us assume $\varphi(x)$ function defines any energy potential in the lattice. Unit length in the lattice is assumed as a. The Bloch–Floquet theory expression for $\varphi(x)$ is:

$$\varphi(x)=\varphi(x+a). \tag{28}$$

For the wave propagation in the lattice structure, the periodicity condition of the Bloch–Floquet theory can be used in the displacement function and its derivatives using the Bloch wave vector as below for the present problem:

$$U(0)e^{in\pi}=U(1), \tag{29}$$

$$\frac{d^{\nu}U(0)}{dX^{\nu}}e^{in\pi}=\frac{d^{\nu}U(1)}{dX^{\nu}}, \tag{30}$$

where i is the complex number ($i=\sqrt{-1}$) and n is the Bloch wave vector. With the help of Eqs. (29) and (30), necessary periodicity conditions for determining the integration constants in Eq. (26) can be obtained.

If the periodicity conditions for the Haar Wavelet method are written in matrix form:

$$\begin{bmatrix} e^{in\pi}-1 & 0 & 0 & 0 \\ -1 & e^{in\pi}-1 & 0 & 0 \\ -1/2 & -1 & e^{in\pi}-1 & 0 \\ -1/6 & -1/2 & -1 & e^{in\pi}-1 \end{bmatrix} \begin{bmatrix} c_1 \\ c_2 \\ c_3 \\ c_4 \end{bmatrix} = \begin{bmatrix} P_1(i,1) \\ P_2(i,1) \\ P_3(i,1) \\ P_4(i,1) \end{bmatrix}. \tag{31}$$

For the higher order Haar wavelet method, the periodicity conditions in matrix form can be expressed as below:

$$\begin{bmatrix} e^{in\pi}-1 & 0 & 0 & 0 & 0 & 0 \\ -1 & e^{in\pi}-1 & 0 & 0 & 0 & 0 \\ -1/2 & -1 & e^{in\pi}-1 & 0 & 0 & 0 \\ -1/6 & -1/2 & -1 & e^{in\pi}-1 & 0 & 0 \\ -1/24 & -1/6 & -1/2 & -1 & e^{in\pi}-1 & 0 \\ -1/120 & -1/24 & -1/6 & -1/2 & -1 & e^{in\pi}-1 \end{bmatrix} \begin{bmatrix} c_1 \\ c_2 \\ c_3 \\ c_4 \\ c_5 \\ c_6 \end{bmatrix} = \begin{bmatrix} P_1(i,1) \\ P_2(i,1) \\ P_3(i,1) \\ P_4(i,1) \\ P_5(i,1) \\ P_6(i,1) \end{bmatrix}. \tag{32}$$

TABLE 1. Validation for Homogenous R–B Rod ($e_0 = 0,\ s = 1$)

J	2^{J+1}	HWM			HOHWM		
		Frequency	True Error	Conv Rate	Frequency	True Error	Conv Rate
1	4	2.319104	1.78×10^{-02}	——	2.302340	1.02×10^{-03}	——
2	8	2.305855	4.53×10^{-03}	1.9714	2.301383	6.21×10^{-05}	4.0372
3	16	2.302459	1.14×10^{-03}	1.9937	2.301324	3.85×10^{-06}	4.0096
4	32	2.301605	2.85×10^{-04}	1.9984	2.301321	2.41×10^{-07}	4.0024
5	64	2.301392	7.13×10^{-05}	1.9996	2.301320	1.50×10^{-08}	4.0006
6	128	2.301338	1.78×10^{-05}	1.9999	2.301320	9.39×10^{-10}	4.0001
7	256	2.301325	4.45×10^{-06}	1.9999	2.301320	5.87×10^{-11}	4.0000
Exact value		2.301320952128405 [41]					

With the help of Bloch–Floquet theory, integration constants can be defined for HWM and HOHWM using Eqs. (31) and (32). Axial displacement function and derivatives for axially graded the nanorod can be inserted into governing equation of motion (Eq. (16)) and wave frequency can be determined.

Phase (V_P) and group velocities (V_G) are important characteristics for traveling waves and can be defined as the velocity of an individual particle that propagates in the structure (Eq. (33)) and the overall shape of the propagation of a group of waves at similar frequency (Eq. (34)), respectively.

$$V_P = \frac{\omega}{n}, \tag{33}$$

$$V_G = \frac{d\omega}{dn}. \tag{34}$$

3. Numerical Results

Longitudinal wave responses of axially graded Raylegh–Bishop nanorods were investigated in the present Section. Dimensionless material properties for the aFG nanorod are considered. The inner radius and thickness of the nanorod are 0.41 and 0.066 nm, respectively. The Poisson ratio for nanotubes is 0.20.

Molecular dynamic simulations and nonlocal continuum models are compared for wave propagation in carbon nanotubes [62]. The higher order Haar wavelet method is a newly developed numerical solution technique and the validation of the present nonlocal Raylegh–Bishop rod model was carried out by using homogenous local and nonlocal rod model results in Tables 1 and 2, respectively.

Very good agreement can be observed with HWM and HOHWM in the “True Error” and “Convergence Rate” parameters, which are defined in Eqs. (35) and (36), respectively. Exact results for local and nonlocal rod models were taken from [56].

$$\varepsilon_t = \left|\omega(J) - \omega(exac)\right|, \tag{35}$$

$$CR = \frac{\log\left|\dfrac{\omega(J-1)-\omega(exac)}{\omega(J)-\omega(exac)}\right|}{\log 2}. \tag{36}$$

TABLE 2. Validation for Nonlocal Homogenous R–B Rod (e_0=0.1, s = 1)

J	2^{J+1}	HWM			HOHWM		
		Frequency	True Error	Conv Rate	Frequency	True Error	Conv Rate
1	4	2.210516	1.50×10^{-02}	—	2.196385	8.60×10^{-04}	—
2	8	2.199350	3.82×10^{-03}	1.9706	2.195577	5.24×10^{-05}	4.0374
3	16	2.196485	9.61×10^{-04}	1.9935	2.195528	3.25×10^{-06}	4.0097
4	32	2.195765	2.40×10^{-04}	1.9984	2.195525	2.03×10^{-07}	4.0024
5	64	2.195585	6.01×10^{-05}	1.9996	2.195525	1.27×10^{-08}	4.0006
6	128	2.195540	1.50×10^{-05}	1.9999	2.195525	7.92×10^{-10}	4.0001
7	256	2.195528	3.76×10^{-06}	1.9999	2.195525	4.75×10^{-11}	4.0000
Exact value		2.195525123273453 [41]					

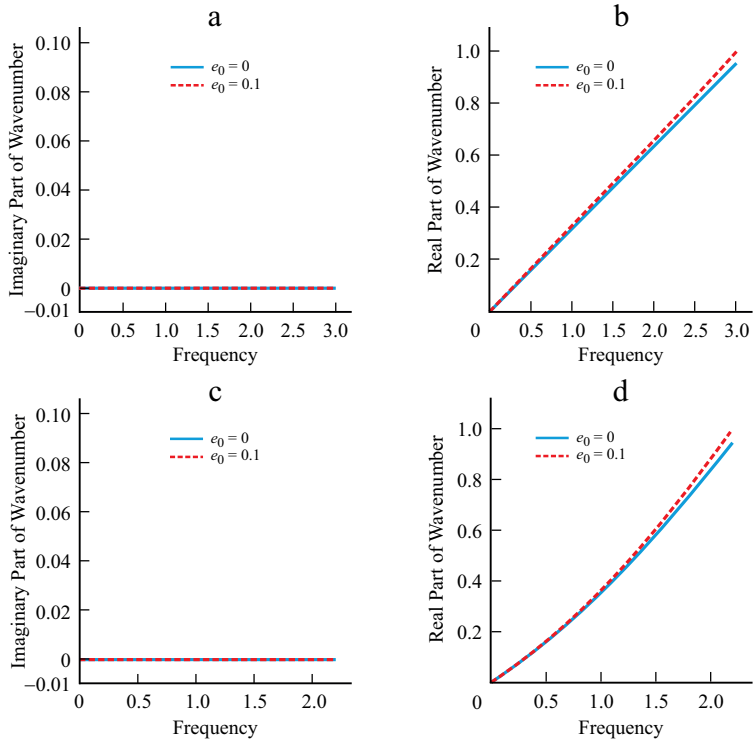

Fig. 3. Nonlocal effect on the imaginary (a, c) and real (b, d) parts of wavenumber of homogenous Rayleigh (a, b) and homogenous Rayleigh-Bishop (c, d) rods at s = 1.

It can be observed from Tables 1 and 2 that, HOHWM has a lower true error than HWM at the same resolution (J). The rate of convergence tends to be 4 and 2, in the case of HOHWM and HWM, respectively.

To see the effect of graded nonlocality, which is pointed out beforehand to be the novelty of the current study, the comparison of wave frequencies of aFG Raylegh–Bishop nanorods are shown in Tables 3 and 4 for constant and graded nonlo-

TABLE 3. Grading Nonlocal Effect on AFG Rayleigh-Bishop NanoRod with HWM ($y = 2$)

J	2^{J+1}	Constant Nonlocality ($e = 0.1$)			Grading Nonlocality ($e_0 = 0.1$)		
		$s = 0.5$	$s = 1$	$s = 2$	$s = 0.5$	$s = 1$	$s = 2$
1	4	2.282941	2.210516	2.180577	2.329669	2.210516	2.193185
2	8	2.276619	2.199350	2.171733	2.323278	2.199350	2.198548
3	16	2.275062	2.196485	2.169437	2.321706	2.196485	2.202387
4	32	2.274675	2.195765	2.168858	2.321315	2.195765	2.203862
5	64	2.274578	2.195585	2.168713	2.321217	2.195585	2.204290
6	128	2.274554	2.195540	2.168677	2.321192	2.195540	2.204402
7	256	2.274548	2.195528	2.168668	2.321186	2.195528	2.204430

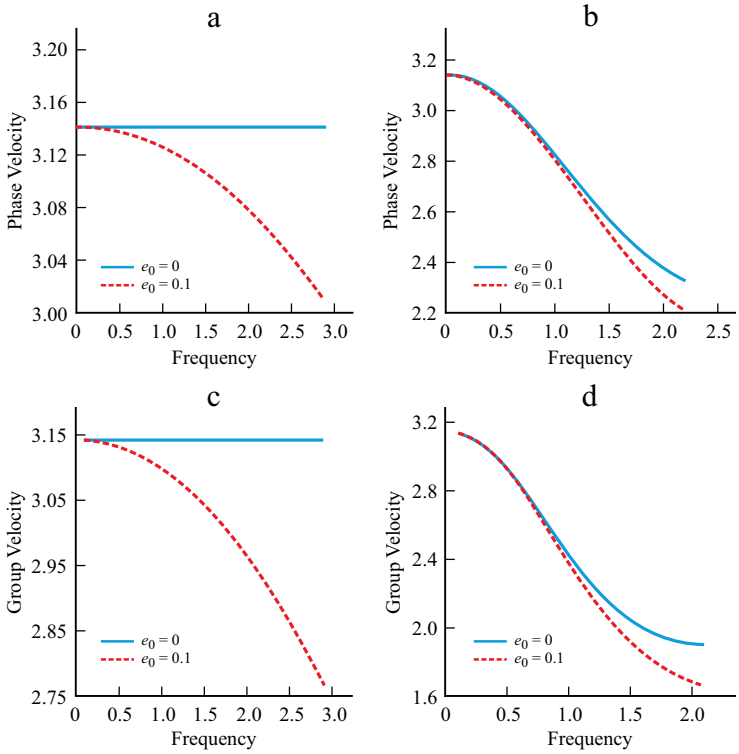

Fig. 4. Nonlocal effect on the phase (a, b) and group (c, d) velocities of the homogenous Rayleigh (a, c) and homogenous Rayleigh-Bishop (b, d) nanorods at $s = 1$.

cal parameters, respectively. Grading nonlocality increases the wave frequency for the enhancing ($s = 2$) material properties case. This behavior can change with second material properties and the power-law parameter. Thus, the grading nonlocality certainly affects the dynamics of the structure.

In Figs. 3, nonlocal effect on wave response of homogenous Rayleigh and Raylegh–Bishop rods can be seen. Wave number has only the real number part in the homogenous rod. The nonlocal effect decreases the wave frequency with the

TABLE 4. Grading Nonlocal Effect on AFG Rayleigh-Bishop NanoRod with HOHWM ($y = 2$)

J	2^{J+1}	Constant Nonlocality ($e = 0.1$)			Grading Nonlocality ($e_0 = 0.1$)		
		$s = 0.5$	$s = 1$	$s = 2$	$s = 0.5$	$s = 1$	$s = 2$
1	4	2.271971	2.196385	2.168986	2.317916	2.196385	2.172353
2	8	2.273807	2.195577	2.168642	2.320188	2.195577	2.190910
3	16	2.274363	2.195528	2.168657	2.320924	2.195528	2.199760
4	32	2.274501	2.195525	2.168663	2.321119	2.195525	2.203085
5	64	2.274535	2.195525	2.168664	2.321168	2.195525	2.204084
6	128	2.274544	2.195525	2.168665	2.321180	2.195525	2.204350
7	256	2.274546	2.195525	2.168665	2.321183	2.195525	2.204417

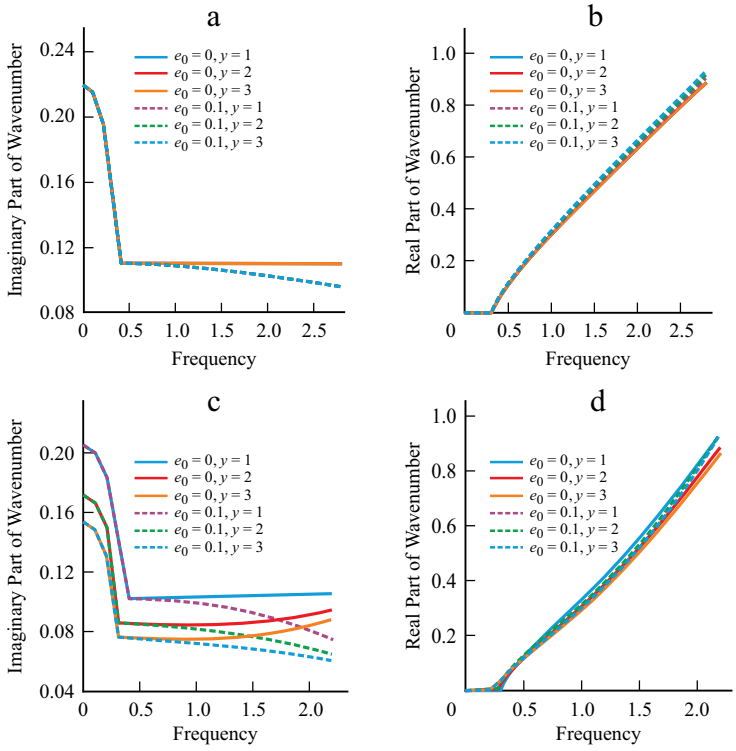

Fig. 5. Nonlocal and gradient index effects on the imaginary (a, c) and real (b, d) parts of wavenumber of aFG Rayleigh(a, b) and aFG Rayleigh-Bishop(c, d) rods at $s = 0.5$.

well-known softening effect. Shear stiffness and rotational inertia effects in the Raylegh–Bishop rod model also decrease the wave frequency in Fig. 3c, d.

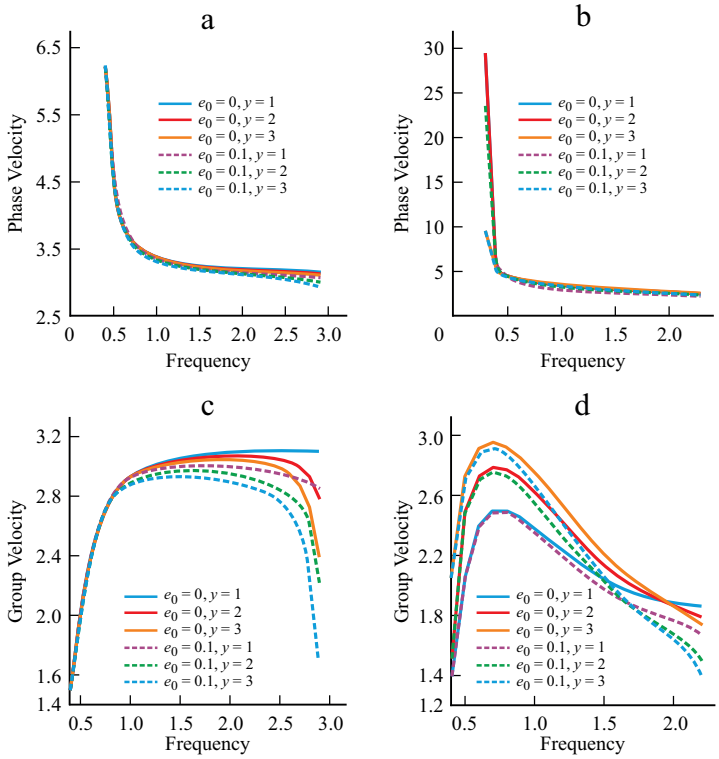

Fig. 6. Nonlocal and gradient index effects on the phase (a, b) and group (c, d) velocities of the aFG Rayleigh (a, c) and aFG Rayleigh-Bishop (b, d) nanorods at $s = 0.5$.

Phase and group velocity variation with wave frequency are shown in Figs. 4. The Rayleigh model presents constant phase and group velocities however, the Raylegh–Bishop, which is a gradient model like nonlocal elasticity, decreases both of them.

In Figs. 5a, b, the results of Rayleigh model for axially graded rod are presented. Material properties are assumed in decreasing variation ($s = 0.5$). In low frequencies, the wavenumber has only an imaginary part and the real part is zero. After a certain value, which is called cut-off frequency, the real part of wave frequency starts to increase and the imaginary part stops decreasing and reaches a constant value. This behavior can be observed only in axially grading structures [63]. No wave can propagate in the structure until the cut-off frequency has passed. Nonlocal effects become obvious at higher frequencies where the real part of the wavenumber increases and the imaginary part decreases.

The effect of the power-law parameter can be observed clearly in the axially graded Raylegh–Bishop model in Fig. 5c, d. If the variation of material properties is considered in Fig. 2, the mean value is the highest when the power-law is assumed to be 3. That indicates, the structure is stiffer than the other cases, and as a result higher wave frequency is obtained.

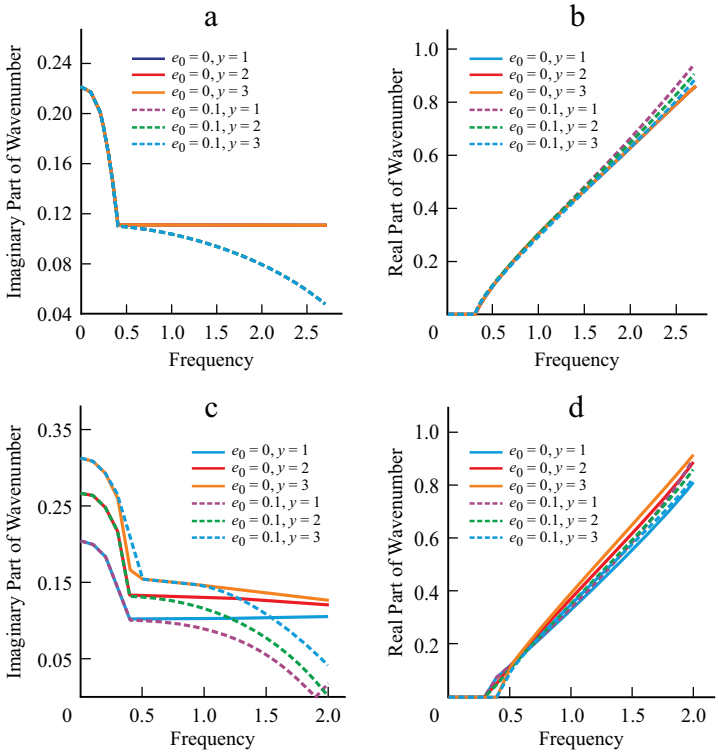

Fig. 7. Nonlocal and gradient index effects on the imaginary (a, c) and real (b, d) parts of the wavenumber of the aFG Rayleigh (a, b) and aFG Rayleigh-Bishop (c, d) rods at $s = 2$.

The power-law parameter decreases the imaginary part of the wave number, in other words, it decreases the cut-off frequency. Increasing the power-law parameter enhances the frequency.

Nonlocal and material grading index effects on phase velocity cannot be detected clearly in Figs. 6a, b. Only at higher frequencies in the Rayleigh model (Fig. 6a), the nonlocal phase velocity separates from local counterpart in decreasing ways. The aforementioned effects are more obvious for group velocity variation in Figs. 6c, d. In the Rayleigh model (Fig. 6c), group velocity decreases with nonlocal, and power-law index parameter effects at high frequencies. Material gradient or power-law index affects differently in the Raylegh–Bishop model (Fig. 6d). The highest power-law index gives the highest group velocity at low frequencies, though this relation is reversed at higher frequencies. Nonlocality shows the decreasing effect on group velocities for both the Rayleigh and the Raylegh–Bishop models.

Wave propagation on axially graded nanorods with enhancing material properties ($s = 2$) can be seen in Fig. 7. Similarly, with the variation characteristic of reducing material properties ($s = 0.5$), imaginary parts of the wave number in the Rayleigh model (Figs. 6a, b) are not affected by nonlocal and grading index parameters. The real part of the wave number

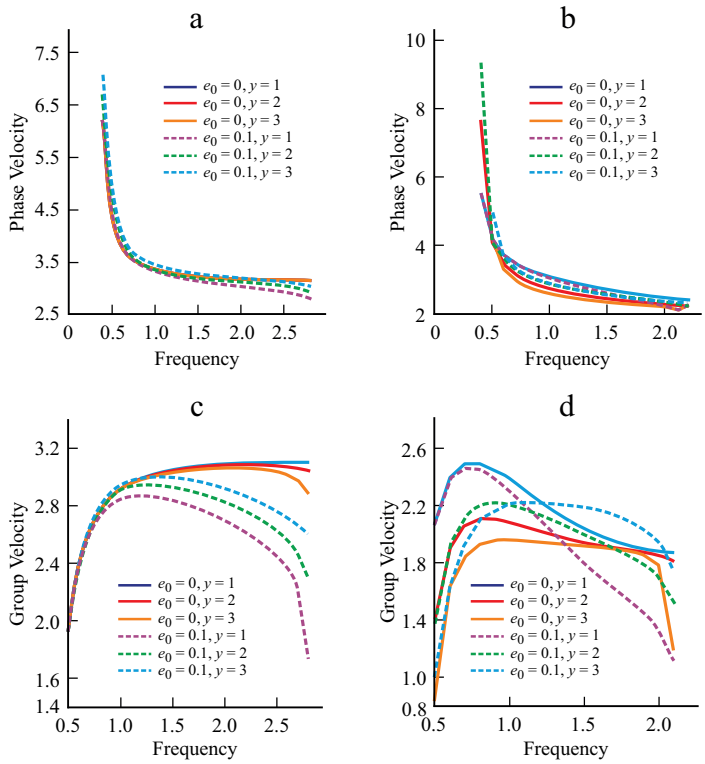

Fig. 8. Nonlocal and gradient index effects on the phase (a, b) and group (c, d) velocities of the aFG Rayleigh (a, c) and aFG Rayleigh-Bishop (b, d) nanorods at $s = 2$.

has little difference only at the high frequencies. In the Rayleigh–Bishop model (Figs. 6c, d), nonlocality shows the same decreasing effect on real and imaginary parts of the wave number, while the material grading index has an increasing effect on the wave number contrary to the reducing material properties case. The reason for this behavior can be interpreted from the mean values of material properties in Fig. 2. Higher material grading index reduces the material properties and increases the frequency. Cut-off frequencies also increase with the power-law index.

Nonlocal and material grading index effects on phase velocities are more obvious in enhancing material properties cases than reducing ones. The power-law parameter decreases the phase velocities, which can be seen clearly in the Raylegh–Bishop model, however, the nonlocal effect increases them (Fig. 8a, b). In the enhancing material properties case, there is a conflict between material grading and nonlocal effects. Nonlocality reduces the effects of enhancing material properties. This conflict can be seen in Figs. 8c, d as well in the group velocity results obtained by Raylegh–Bishop model. For the linear material variation ($y = 1$), the nonlocal group velocity is lower than the local counterpart. On quadratic and cubic variations,

nonlocal frequencies are higher than local counterparts. The material grading effect becomes subtler with increasing the power-law parameter.

4. Conclusion

The longitudinal wave response of axially functionally graded nanorods was investigated. To include the effect of size, shear, and rotational inertia in nanostructures, Eringen's nonlocal elasticity and Raylegh–Bishop theories were employed in the formulation of the problem. Governing equation of the motion for the axially graded nanorod was obtained with Hamilton's minimum energy potential principle. Governing differential equation of motion with variable coefficients was solved by utilizing the higher order Haar wavelet method. The results were compared and validated with continuum mechanics approaches. Effects of material grading index and nonlocal parameters on the wave dynamics of the aFG nanorod were investigated.

Nonlocality is considered in a graded formulation, which is assumed constant in most of the literature. The Grading nonlocal parameter increases the wave frequency according to the constant nonlocal parameter case.

Axially grading material properties bring out cut-off frequencies for the nanorod at low frequencies. Wave numbers consist of both real and imaginary parts. Gradient effects on axial displacement function like shear stiffness, rotational inertia, and nonlocality become apparent at high frequencies. Nonlocality shows softening effect on enhancing and reducing material properties. The material grading index affects differently the wave response of the nanorod depending on the enhancing or reducing material properties variation. In reducing cases, the material grading index works with nonlocality and softens the structure. Although, in enhancing cases, material grading works against nonlocality and the nonlocal effect decreases the stiffening effect of material grading. Axially grading material properties affect the low-frequency behavior and higher order theories affect the high frequency behavior of the nanorod, respectively. Present results could be beneficial in the modeling of semiconductor alloy composite nanowires.

Acknowledgment. This research was supported by the Estonian Research Council Mobilitas Pluss Postdoctoral Researcher Grant "MOBJD704: Development of numerical methods for analysis of advanced composite and nanostructures."

REFERENCES

1. X. Zhuang, C. Z. Ning, and A. Pan, "Composition and bandgap-graded semiconductor alloy nanowires," Adv. Mater., **24**, 13-33 (2012). https://doi.org/10.1002/adma.201103191
2. A. C. Eringen, "Nonlocal polar elastic continua," Int. J. Eng. Sci., **10**, No. 1 (1972). https://doi.org/10.1016/0020-7225(72)90070-5
3. A. C. Eringen, "On differential equations of nonlocal elasticity and solutions of screw dislocation and surface waves," J. Appl. Phys., **54**, 4703-4710 (1983). https://doi.org/10.1063/1.332803
4. M. Arda and M. Aydogdu, "Torsional statics and dynamics of nanotubes embedded in an elastic medium," Compos. Struct., **114**, 80-91 (2014). https://doi.org/10.1016/j.compstruct.2014.03.053
5. M. Arda and M. Aydogdu, "Torsional wave propagation in multiwalled carbon nanotubes using nonlocal elasticity," Appl. Physics, A, **122**, 219 (2016). https://doi.org/10.1007/s00339-016-9751-1
6. M. Aydogdu and M. Arda, "Torsional vibration analysis of double walled carbon nanotubes using nonlocal elasticity," Int. J. Mech. and Mater. in Design. **12**, 71-84 (2016). https://doi.org/10.1007/s10999-014-9292-8

7. M. Aydogdu and M. Arda, “Forced vibration of nanorods using nonlocal elasticity,” Adv. Nano Res. **4**, 265-279 (2016). https://doi.org/10.12989/anr.2016.4.4.265
8. M. Arda and M. Aydogdu, “Torsional dynamics of coaxial nanotubes with different lengths in viscoelastic medium,” Microsystem Technol., **25**, 3943-3957 (2019). https://doi.org/10.1007/s00542-019-04446-8
9. M. Arda and M. Aydogdu, “Dynamic stability of harmonically excited nanobeams including axial inertia,” J. Vibration and Control. **25**, 820-833 (2019). https://doi.org/10.1177/1077546318802430
10. M. Arda and M. Aydogdu, “Nonlocal effect on boundary conditions of cantilever nanobeam,” AIP Conf. Proc. **2293**, (2020). https://doi.org/10.1063/5.0026430
11. M. Arda and M. Aydogdu, “Longitudinal vibration of variable cross-sectional nanorods,” J. Nano Research, **64**, 49-60 (2020). https://doi.org/10.4028/www.scientific.net/JNanoR.64.49
12. M. Arda and M. Aydogdu, “Dynamics of nonlocal strain gradient nanobeams with longitudinal magnetic field,” Math. Methods Appl. Sci. mma.7268 (2021). https://doi.org/10.1002/mma.7268
13. B. Akgöz and Ö. Civalek, “Longitudinal vibration analysis for microbars based on strain gradient elasticity theory,” J. Vibration and Control, **20**, 606-616 (2014). https://doi.org/10.1177/1077546312463752
14. B. Akgöz and Ö. Civalek, “Bending analysis of embedded carbon nanotubes resting on an elastic foundation using strain gradient theory,” Acta Astronaut., **119**, 1-12 (2016). https://doi.org/10.1016/j.actaastro.2015.10.021
15. K. Mercan, H. M. Numanoglu, B. Akgöz, C. Demir, and Civalek, “Higher-order continuum theories for buckling response of silicon carbide nanowires (SiCNWs) on elastic matrix,” Archive of Appl. Mech., 87, 1797-1814 (2017). https://doi.org/10.1007/S00419-017-1288-Z/FIGURES/11
16. B. Akgöz and Ö. Civalek, “A novel microstructure-dependent shear deformable beam model,” Int. J. Mech. Sci., 99, 10-20 (2015). https://doi.org/10.1016/J.IJMECSCI.2015.05.003
17. R. E. D. Bishop, “Longitudinal waves in beams,” Aeronautical Quarterly. **3**, 280-293 (1952).
18. M. Krawczuk, J. Grabowska, and M. Palacz, “Longitudinal wave propagation. Part I. Comparison of rod theories,” J Sound Vib., **295**, 461-478 (2006). https://doi.org/10.1016/j.jsv.2005.12.048
19. M. Shatalov, I. Fedotov, H. M. Tenkam, and J. Marais, “Comparison of classical and modern theories of longitudinal wave propagation in elastic rods,” Proc. 7th South African Conf. on Computational and Appl. Mech., SACAM 2010. pp. 231-23, Kraków (2010).
20. M. Aydogdu, “Longitudinal wave propagation in nanorods using a general nonlocal unimodal rod theory and calibration of nonlocal parameter with lattice dynamics,” Int. J. Eng. Sci., **56**, 17-28 (2012). https://doi.org/10.1016/j.ijengsci.2012.02.004
21. X. F. Li, Z. Shen, K. Y. Lee, “Axial wave propagation and vibration of nonlocal nanorods with radial deformation and inertia,” ZAMM Zeitschrift fur Angewandte Mathematik und Mechanik. **97**, 602-616 (2017). https://doi.org/10.1002/zamm.201500186
22. S.M. Hosseini and F. Li, “Effects of strain gradient on Moore-Gibson-Thompson generalized coupled non-fickian diffusion-thermoelasticity analysis in a Love-Bishop nanorod resonator: A size dependent meshless implementation,” Eng. Anal. Bound. Elem., 152, 383-396 (2023). https://doi.org/10.1016/J.ENGANABOUND.2023.04.026
23. M. Mohammadian and S.M. Hosseini, “A size-dependent differential quadrature element model for vibration analysis of FG CNT reinforced composite microrods based on the higher order Love-Bishop rod model and the nonlocal strain gradient theory,” Eng. Anal. Bound. Elem., 138, 235-252 (2022). https://doi.org/10.1016/J.ENGANABOUND.2022.02.017
24. D. Z. Karličić, S. Ayed, and E. Flaieh, “Nonlocal axial vibration of the multiple Bishop nanorod system”, Math. and Mech. Solids, 24, 1668-1691 (2019). https://doi.org/10.1177/1081286518766577/ASSET/IMAGES/LARGE/10.1177_1081286518766577-FIG3.JPEG
25. J. K. Lee and B. K. Lee, “Coupled flexural-torsional free vibration of an axially functionally graded circular curved beam,” Mech. Compos. Mater., **57**, 833-846 (2022). https://doi.org/10.1007/S11029-022-10003-8/FIGURES/8

26. L. Jaanuska and H. Hein, “Delamination quantification by Haar wavelets and machine learning,” Mech. Compos. Mater., **58**, 249-260 (2022). https://doi.org/10.1007/S11029-022-10025-2/FIGURES/8
27. A. Muc, “Optimizing the thickness/stiffness distribution of infinitely wide porous FGM plates subjected to supersonic flutter constraints,” Mech. Compos. Mater., **56**, 713-720 (2021). https://doi.org/10.1007/S11029-021-09917-6/TABLES/1
28. Y. Xiao, Z. Li, Z. Liu, M. Zang, and Y. Zhu, Effect of material design and weak link setting on the energy absorption of composite thin-walled beams under transverse loading,” Mech. Compos. Mater., **57**, 401-414 (2021). https://doi.org/10.1007/S11029-021-09963-0/TABLES/6
29. K. Kiani, “Free dynamic analysis of functionally graded tapered nanorods via a newly developed nonlocal surface energy-based integro-differential model,” Compos Struct., **139**, 151-166 (2016). https://doi.org/10.1016/j.compstruct.2015.11.059
30. K. Kiani, “Thermo-elasto-dynamic analysis of axially functionally graded non-uniform nanobeams with surface energy,” Int. J. Eng. Sci. **106**, 57-76 (2016). https://doi.org/10.1016/j.ijengsci.2016.05.004
31. F. Ebrahimi and A. Dabbagh, “NSGT-based acoustical wave dispersion characteristics of thermo-magnetically actuated double-nanobeam systems,” Structural Eng. and Mech., **68**, 701-711 (2018). https://doi.org/10.12989/sem.2018.68.6.701
32. L. Q. Yao, C. J. Ji, J. P. Shen, and C. Li, “Free vibration and wave propagation of axially moving functionally graded Timoshenko microbeams,” J. Brazilian Society Mech. Sci. and Eng., **42**, 137 (2020). https://doi.org/10.1007/s40430-020-2206-9
33. H. Zeighampour, Y. Tadi Beni, and M. Botshekanan Dehkordi, “Wave propagation in viscoelastic thin cylindrical nanoshell resting on a visco-Pasternak foundation based on nonlocal strain gradient theory,” Thin-Walled Struct., **122**, 378-386 (2018). https://doi.org/10.1016/j.tws.2017.10.037
34. F. Ebrahimi, M. Dehghan, and A. Seyfi, “Eringen’s nonlocal elasticity theory for wave propagation analysis of magneto-electro-elastic nanotubes,” Adv. Nano Res., **7**, 1-11 (2019). https://doi.org/10.12989/ANR.2019.7.1.001
35. B. UZUN and M. Ö. YAYLI, “A solution method for longitudinal vibrations of functionally graded nanorods,” Int. J. Eng. and Appl. Sci., 12, 78-87 (2020). https://doi.org/10.24107/ijeas.782419
36. Ö. Civalek, B. Uzun, and M. Ö. Yayli, “Torsional and longitudinal vibration analysis of a porous nanorod with arbitrary boundaries,” Physica B, Condens. Matter., 633, 413761 (2022). https://doi.org/10.1016/J.PHYSB.2022.413761
37. Ö. Civalek, B. Uzun, M.Ö. Yayli, Ö. Civalek, B. Uzun, and M.Ö. Yayli, “A Fourier sine series solution of static and dynamic response of nano/micro-scaled FG rod under torsional effect,” Adv. Nano Res., 12, 467 (2022). https://doi.org/10.12989/ANR.2022.12.5.467
38. B. Uzun and M.Ö. Yaylı, “Porosity dependent torsional vibrations of restrained FG nanotubes using modified couple stress theory,” Mater. Today Commun., 32, 103969 (2022). https://doi.org/10.1016/J.MTCOMM.2022.103969
39. B. Uzun, U. Kafkas, B. Deliktaş, and M.Ö. Yaylı, “Size-dependent vibration of porous bishop nanorod with arbitrary boundary conditions and nonlocal elasticity effects,” J. Vibration Eng. and Technol., 11, 809-826 (2023). https://doi.org/10.1007/S42417-022-00610-Z/FIGURES/7
40. Ö. Civalek, Ş.D. Akbaş, B. Akgöz, and S. Dastjerdi, “Forced vibration analysis of composite beams reinforced by carbon nanotubes”, Nanomaterials (Basel), 11, 1-17 (2021). https://doi.org/10.3390/NANO11030571
41. D. Wu, Y. Lei, Z. Wang, B. Yu, and D. Zhang, “Free vibration analysis of carbon-nanotube-reinforced beams resting on a viscoelastic Pasternak foundation by the nonlocal Eshelby–Mori–Tanaka method,” Mech. Compos. Mater., 59, 479-494 (2023). https://doi.org/10.1007/S11029-023-10110-0/FIGURES/7
42. M. Arda, “Axial dynamics of functionally graded Rayleigh–Bishop nanorods,” Microsystem Technologies, 27, 269-282 (2021). https://doi.org/10.1007/s00542-020-04950-2

43. Siraj-ul-Islam, I. Aziz, and B. Šarler, "The numerical solution of second-order boundary-value problems by collocation method with the Haar wavelets," Math. Comput. Model., 52, 1577-1590 (2010). https://doi.org/10.1016/J.MCM.2010.06.023
44. I. Aziz and R. Amin, "Numerical solution of a class of delay differential and delay partial differential equations via Haar wavelet," Appl. Math. Model., 40, 10286-10299 (2016). https://doi.org/10.1016/J.APM.2016.07.018
45. J. Majak, M. Pohlak, K. Karjust, M. Eerme, J. Kurnitski, and B. S. Shvartsman, "New higher order Haar wavelet method: Application to FGM structures," Compos. Struct., **201**, 72-78 (2018). https://doi.org/10.1016/j.compstruct.2018.06.013
46. J. Majak, M. Pohlak, M. Eerme, and B. Shvartsman, "Solving ordinary differential equations with higher order Haar wavelet method," AIP Conf. Proc., **2116**, 1-6 (2019). https://doi.org/10.1063/1.5114340
47. J. Majak, B. Shvartsman, M. Ratas, D. Bassir, M. Pohlak, K. Karjust, and M. Eerme, "Higher-order Haar wavelet method for vibration analysis of nanobeams," Mater. Today Commun., **25**, 101290 (2020). https://doi.org/10.1016/j.mtcomm.2020.101290
48. S. K. Jena, S. Chakraverty, V. Mahesh, and D. Harursampath, "Application of Haar wavelet discretization and differential quadrature methods for free vibration of functionally graded micro-beam with porosity using modified couple stress theory," Eng. Anal. Bound. Elem. **140**, 167-185 (2022). https://doi.org/10.1016/J.ENGANABOUND.2022.04.009
49. S. K. Jena, S. Chakraverty, M. Ratas, and M. Kirs, "Application of HoHWM in the stability analysis of nonlocal Euler-Bernoulli beam," AIP Conf. Proc., **2293**, (2020). https://doi.org/10.1063/5.0026439/726243
50. F. Bulut, Ö. Oruç, and A. Esen, "Higher order Haar wavelet method integrated with strang splitting for solving regularized long wave equation," Math. Comput. Simul., **197**, 277-290 (2022). https://doi.org/10.1016/J.MATCOM.2022.02.006
51. M. Sorrenti, M. Di Sciuva, J. Majak, and F. Auriemma, Static response and buckling loads of multilayered composite beams using the refined zigzag theory and higher-order Haar wavelet method," Mech. Compos. Mater., **57**, 1-18 (2021). https://doi.org/10.1007/S11029-021-09929-2/TABLES/4
52. M. Ratas, A. Salupere, and A. Majak, "Solving nonlinear PDEs using the higher order Haar wavelet method on nonuniform and adaptive grids," Math. Modelling and Analysis. **26**, 147-169 (2021). https://doi.org/10.3846/MMA.2021.12920
53. M. Ratas and A. Salupere, "Application of higher order haar wavelet method for solving nonlinear evolution equations," Mathematical Modelling and Analysis. **25**, 271-288 (2020). https://doi.org/10.3846/mma.2020.11112
54. Swati, M. Singh, and K. Singh, "An efficient technique based on higher order Haar wavelet method for Lane-Emden equations," Math. Comput. Simul., **206**, 21-39 (2023). https://doi.org/10.1016/J.MATCOM.2022.10.031
55. A. C. Eringen, Nonlocal Continuum Field Theories, Springer, New York, (2004). https://doi.org/10.1007/b97697
56. M. Arda, "Evaluation of optimum length scale parameters in longitudinal wave propagation on nonlocal strain gradient carbon nanotubes by lattice dynamics," Mech. Based Design Struct. and Machines, **50**, 4363-4386 (2022). https://doi.org/10.1080/15397734.2020.1835488
57. S. Adali, "Variational principles for multi-walled carbon nanotubes undergoing buckling based on nonlocal elasticity theory," Phys. Lett., A., **372**, 5701-5705 (2008). https://doi.org/10.1016/j.physleta.2008.07.003
58. M. Arda, Axial dynamics of functionally graded Raylegh–Bishop nanorods," Microsystem Technologies, **27**, 269-282 (2021). https://doi.org/10.1007/s00542-020-04950-2
59. Ü. Lepik, and Hein, Haar Wavelets. (2014). https://doi.org/10.1007/978-3-319-04295-4_2
60. J. Majak, B. Shvartsman, K. Karjust, M. Mikola, A. Haavajõe, and M. Pohlak, "On the accuracy of the Haar wavelet discretization method," Compos., Part B, **80**, 321-327 (2015). https://doi.org/10.1016/j.compositesb.2015.06.008
61. A. A. Cottey, "Floquet's theorem and band theory in one dimension," Am. J. Phys., **39**, 1235-1244 (1971). https://doi.org/10.1119/1.197661

62. Y. G. Hu, K. M. Liew, Q. Wang, X.Q. He, and B. I. Yakobson, “Nonlocal shell model for elastic wave propagation in single- and double-walled carbon nanotubes,” J. Mech. Phys. Solids, **56**, 3475-3485 (2008). https://doi.org/10.1016/j.jmps.2008.08.010
63. S. Narendar, “Wave dispersion in functionally graded magneto-electro-elastic nonlocal rod,” Aerosp. Sci. Technol., **51**, 42-51 (2016). https://doi.org/10.1016/j.ast.2016.01.012

Publication IV

L. Kivistik, M. Mehrparvar, M. Eerme, and J. Majak, “Dynamics of flight of the fragments with higher order Haar wavelet method,” *Proceedings of the Estonian Academy of Sciences*, vol. 73, no. 2, pp. 108–115, Mar. 2024, doi: https://doi.org/10.3176/proc.2024.2.02.

Proceedings of the Estonian Academy of Sciences,
2024, **73**, 2, 108–115
https://doi.org/10.3176/proc.2024.2.02
Available online at www.eap.ee/proceedings

SOLID
MECHANICS

Dynamics of flight of the fragments with higher order Haar wavelet method

Lenart Kivistik*, Marmar Mehrparvar, Martin Eerme and Jüri Majak

Department of Mechanical and Industrial Engineering, Tallinn University of Technology, Ehitajate tee 5, 19086 Tallinn, Estonia

Received 2 January 2024, accepted 6 February 2024, available online 11 March 2024

Abstract. Fragments that have an irregular shape and move at high speeds are difficult to assess since experiments require high-tech solutions, and the differential equations that describe the motion cannot be solved analytically. Different numerical and function approximation methods are used to find the trajectory model. This work uses a state-of-the-art, higher order Haar wavelet method to approximate the trajectory model with empirically determined drag force. The initial conditions of the flight of the fragments are determined by the finite element method. The results obtained by utilizing the Haar wavelet method and the higher order Haar wavelet method are compared. The higher order Haar wavelet method outperforms the Haar wavelet method but allows for keeping the implementation complexity of the method in the same range. Utilizing the higher order Haar wavelet method leads to a reduction in the computational cost since the same accuracy with the Haar wavelet method can be achieved with the use of several order lower mesh.

Keywords: higher order Haar wavelet method, Runge–Kutta method, finite element method, trajectory, fragmentation.

1. INTRODUCTION

The study of the flight of fragments provides an opportunity to assess the risk of fast-moving fragments thrown into the environment. The risk of fragments depends on the density of fragments per volume unit and the kinetic energy of the investigated fragment at the location under consideration [1]. The initial parameters of fragmentation are determined by the fragmenting object and the nature of the formation. The fragmenting objects can be fuel tanks, explosive devices, vehicle body parts, etc., and the nature of the formation is mostly explosion, collision, or fracture. Simulations, experiments, and statistical models are used to study the fragments produced by the explosion. Conducting experiments and collecting the information necessary for the flight of fragments, such as fragment mass, dimensions, velocities, accelerations, and direction vectors, are resource- and labor-intensive [2–4]. Statistical models can be used in limited situations based on specific experiments and may not be appropriate for a specific case [5]. Djelosevic and Tepic introduced the probabilistic mass method [6], Ahmed et al. utilized the arbitrary Lagrangian–Eulerian approach [3], and Ugrčić adapted the stochastic failure theory [7] fragmentation analysis of metallic objects. The simulation results can be utilized as initial data for the point mass trajectory model, described by a nonlinear system of ordinary differential equations (ODE). Kljuno and Catovic [8], Szmelter and Lee [9] used the Runge–Kutta

* Corresponding author, lenart.kivistik@taltech.ee

numerical method, and Djelosevic and Tepic [6] used the Taylor series numerical method to solve the ODE system.

For the purpose of solving the trajectory system of equations, herein two recent numerical methods, the Haar wavelet method (HWM) and the higher order Haar wavelet method (HOHWM), are implemented. The HWM, introduced in 1997 by Chen and Hsiao, has been applied with success for solving a wide class of differential and integro-differential equations [10–14]. Pioneering work in the development and application of the HWM was done by Lepik, who considered integer and fractional differential equations as well as integro-differential equations, covering a wide class of problems from mathematics, physics, and evolution equations [10,15–20]. The HWM is known as a method with simple implementation since it is based on the simplest wavelet [10]. Recently, the HWM was applied with success for solving Bratu-type equations [21] – singularly perturbed differential equations with integral boundary conditions [22]. In [23–26], the HWM is combined with AI methods and tools. However, the rate of convergence of the HWM is two, i.e., rather humble. In 2018, the HOHWM was introduced as the principal improvement of the HWM [27]. The rate of convergence of the HOHWM depends on the method parameter and, in simpler cases, is equal to four. The HOHWM has been utilized with success by a number of authors in [28–39] for solving a wide class of ODE [28–33], partial differential equations [34], and fractional Fredholm integro-differential equations [35], but needs still further validation with more complex problems. Herein, the HWM and HOHWM are adapted for solving nonlinear systems of trajectory equations of the fragments.

2. FORMULATION

In this section, the formulation of the flight dynamics of fragments is developed. Beforehand, initial coordinate values, velocity values with regard to coordinates, air density, fragment mass, drag coefficient, and exposed area are all necessary. Next, the trajectory model is simplified, which is then solved by employing the higher order Haar wavelet method.

2.1. Flight dynamics of the fragments

The natural fragmentation simulation of an explosive projectile shell is based on the finite element method and stochastic failure theory and is simulated in the ANSYS AUTODYN software.

The arbitrary Lagrangian–Eulerian approach with the Johnson–Cook strength and fracture method is used to simulate fragmentation and the propagation of fragments into the surrounding air. Numerical analyses determine the fragment's initial position, velocity, mass, and volume. The coordinate system of the simulation is based on the CAD model and is transformed into the coordinate system of the situation. On the rear surface of the unfragmented projectile, the z-axis intersects with the axis of symmetry of the projectile and is at an angle of 60 degrees from the ground. The xy-plane represents the ground surface. Figure 1 visualizes the geometry used in the simulation, the coordinate system, and the scattering of fragments caused by the explosion.

2.2. Trajectory model of the fragments

The path of a fragment moving while being affected by drag and gravitational force can be predicted using the point mass trajectory model based on the Lord Rayleigh's drag equation [5,9,40]:

$$\begin{aligned} x'' &= -\frac{A\rho C_D}{2m}\sqrt{x'^2+y'^2+z'^2}\cdot x', \\ y'' &= -\frac{A\rho C_D}{2m}\sqrt{x'^2+y'^2+z'^2}\cdot y', \\ z'' &= -\frac{A\rho C_D}{2m}\sqrt{x'^2+y'^2+z'^2}\cdot z' - g, \end{aligned} \tag{1}$$

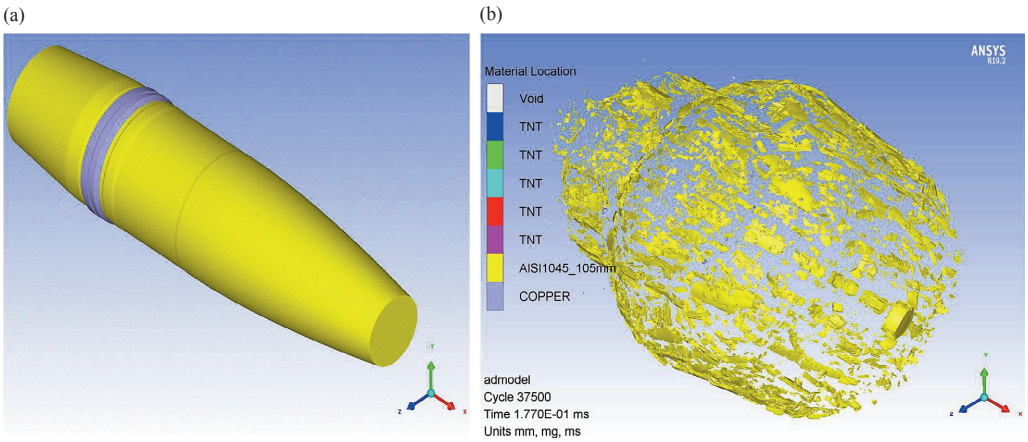

Fig. 1. Unfragmented projectile (a) and fragmentation and propagation of fragments (b).

where x', y' and z' are velocities in each direction, $\rho = 1.20\,\frac{kg}{m^3}$ is the air density, and $g = 9.81\ m/s^2$ is the gravitational acceleration. Also, C_D is the drag coefficient, which as a rule is affected by the Mach number. Still, $C_D = 0.6$ is the result of the most common simplification applied in this study, which assumes a constant drag coefficient [5]. A few mathematical operations are carried out in order to build a solution for the system of differential equations; in Eq. (1) the value of y can be found in terms of x:

$$\frac{x''}{x'} = \frac{y''}{y'} \quad \longrightarrow \quad y = cx + d\ ,\ c = \frac{y_0'}{x_0'}\ , d = y_0 - \frac{y_0'}{x_0'} \cdot x_0. \tag{2}$$

Quasilinearization is a numerical method that solves a series of linearized problems iteratively in order to estimate the solution of the nonlinear differential system of equations. Essentially, quasilinearization involves linearizing the nonlinear problem around the current estimate of the solution at each iteration, solving the resulting linearized problem and using the solution to update the estimate of the solution to the original nonlinear problem. Until convergence is reached, this process is continued iteratively. Then, by substituting $\frac{A\rho C_D}{2m} = k$, the system of three equations can be reduced to two equations:

$$\begin{aligned} x'' &= -k\sqrt{(1+c^2)x'^2 + z'^2}\,x' = f_1(x', z'), \\ z'' &= -k\sqrt{(1+c^2)x'^2 + z'^2}\,z' - g = f_2(x', z'). \end{aligned} \tag{3}$$

In order to linearize the nonlinear systems, the Taylor series expansion has been utilized in Eq. (4):

$$\begin{aligned} x''_{n+1} &= f_1(x'_n, z'_n) + (x'_{n+1} - x'_n)\frac{\partial f_1}{\partial x'_n} + (z'_{n+1} - z'_n)\frac{\partial f_1}{\partial z'_n}, \\ z''_{n+1} &= f_2(x'_n, z'_n) + (z'_{n+1} - z'_n)\frac{\partial f_2}{\partial z'_n} + (x'_{n+1} - x'_n)\frac{\partial f_2}{\partial x'_n}, \end{aligned} \tag{4}$$

where

$$\begin{aligned}
\frac{\partial f_1}{\partial x'} &= -k\left[\frac{(1+c^2)x'\cdot x'}{\sqrt{(1+c^2)x'^2+z'^2}}+\sqrt{(1+c^2)x'^2+z'^2}\right],\\
\frac{\partial f_1}{\partial z'} &= -k\left[\frac{x'\cdot z'}{\sqrt{(1+c^2)x'^2+z'^2}}\right],\\
\frac{\partial f_2}{\partial x'} &= -k\left[\frac{(1+c^2)x'\cdot z'}{\sqrt{(1+c^2)x'^2+z'^2}}\right],\\
\frac{\partial f_2}{\partial z'} &= -k\left[\frac{z'\cdot z'}{\sqrt{(1+c^2)x'^2+z'^2}}+\sqrt{(1+c^2)x'^2+z'^2}\right].
\end{aligned} \tag{5}$$

2.3. Higher order Haar wavelet method

The discontinuous Haar wavelet, a specific family of discrete orthonormal wavelets with a step function-like appearance, is one of the most basic wavelets. A basis, whose components are orthonormal to each other and normalized to the unit length, is made up of the additional wavelets that are derived from the same basic wavelet. This property allows wavelet coefficients to be computed independently of each other. The functions for Haar are given as:

$$h_i(x) = \begin{cases} 1 & \text{for} \quad x \in [\alpha(i), \beta(i)) \\ -1 & \text{for} \quad x \in [\beta(i), \gamma(i)) \\ 0 & \text{elsewhere,} \end{cases} \tag{6}$$

where

$$\begin{aligned}
&\alpha(i) = A + 2k\mu\Delta x,\\
&\beta(i) = A + (2k+1)\mu\Delta x,\\
&\gamma(i) = A + 2(k+1)\mu\Delta x,\\
&i = m + k + 1,\ \mu = \tfrac{M}{m},\ \Delta x = \tfrac{B-A}{2M},
\end{aligned} \tag{7}$$

where integer k = 0,1, ... , $m-1$ specifies the location of the particular square wave, and $m = 2^j$ is the maximum number of square waves arranged in the interval [A,B]. Hence, the integrals of the Haar functions of order n can be presented as in [14]:

$$p_{n,i}(x) = \begin{cases} 0 & x \in [A, \alpha(i)) \\ \dfrac{(x-\alpha(i))^n}{n!} & x \in [\alpha(i), \beta(i)) \\ \dfrac{(x-\alpha(i))^n - 2(x-\beta(i))^n}{n!} & \text{for} \quad x \in [\beta(i), \gamma(i)) \\ \dfrac{(x-\alpha(i))^n - 2(x-\beta(i))^n + (x-\gamma(i))^n}{n!} & x \in [\gamma(i), B) \\ 0 & \text{elsewhere.} \end{cases} \tag{8}$$

As mentioned before, the higher order Haar wavelet techniques make it easier to analyze complicated data patterns more precisely, capturing minute details and subtle fluctuations. This improved resolution is especially helpful in situations where a greater degree of information is essential for correctly interpreting and comprehending the underlying dynamics. The higher order wavelet expansion is introduced in [27]:

$$\frac{d^{n+2s}f(x)}{dx^{n+2s}} = \sum_{i=1}^{\infty} a_i h_i(x),\ \ s = 1,2,.... \tag{9}$$

In Eq. (9), a_i is a component of the unknown coefficient vector. Finally, the method's numerical order of convergence can then be calculated based on [14]:

$$\text{Convergence rate} = \log\left(\frac{F_{i-1}-F_e}{F_i-F_e}\right)/\log(2), \tag{10}$$

where F_e is the existing solution in the literature.

3. NUMERICAL RESULTS

A projectile with a mass of 12 kg and a diameter of 105 mm was used in the simulation as a case study. The 0.17 ms simulation produced about 3950 fragments. Of these fragments, one was selected based on its initial location and velocity. The fragment's location and velocity with respect to the x-axis were then determined using the formulation given in the previous section, and were compared to the results from the HWM (Table 1). The convergence rate in both cases was calculated by Eq. (10), in which F_e was obtained by utilizing the well-known Runge–Kutta method as a reference at t = 2.5 s.

In Table 1, N is the number of collocation points, $N = 2 \cdot m$. As can be observed, in the case of the HOHWM, the absolute error decreases and converges much faster compared to the HWM, allowing for fewer collection points to achieve an accurate result. In Table 2, the results of the location and velocities in each direction are gathered for the same fragment mentioned before at various time steps.

It should be mentioned that since the initial values of coordinates and velocities are in a wide range, an accurate method, such as the utilized HOHWM, and a precise programming process are needed to achieve an accurate result.

Table 1. Comparison of HWM and HOHWM for selected fragment at t = 2.5 s

s	N	x	Error	Convergence rate	x'	Error	Convergence rate
HWM (s = 0)	4	–17.29994925	1.28E–01		–2.78958350	9.85E–02	
	8	–17.39615158	3.18E–02	2.0103933	–2.86413772	2.40E–02	2.0383492
	16	–17.42001639	7.93E–03	2.0030078	–2.88213661	5.99E–03	2.0015815
	32	–17.42596710	1.98E–03	2.0007748	–2.88663071	1.50E–03	2.0009089
	64	–17.42745378	4.95E–04	2.0001951	–2.88775339	3.74E–04	2.0003872
	128	–17.42782539	1.24E–04	2.0000489	–2.88803396	9.35E–05	2.0000500
	256	–17.42791828	3.10E–05	2.0000122	–2.88810410	2.34E–05	2.0000246
HOHWM (s = 1)	4	–17.42072359	7.23E–03		–2.88349768	4.63E–03	
	8	–17.42751557	4.34E–04	4.0576692	–2.88784956	2.78E–04	4.0581877
	16	–17.42792242	2.68E–05	4.0146075	–2.88811028	1.72E–05	4.0142098
	32	–17.42794758	1.67E–06	4.0036622	–2.88812641	1.07E–06	4.0046429
	64	–17.42794915	1.04E–07	4.0009162	–2.88812741	6.69E–08	4.0008970
	128	–17.42794924	6.53E–09	4.0002289	–2.88812748	4.18E–09	4.0002293
	256	–17.42794925	4.08E–10	4.0000549	–2.88812748	2.61E–10	4.0000268
	Runge–Kutta method: –17.42794925				Runge–Kutta method: –2.88812748		

Table 2. Position and velocities of selected fragment at various time steps

t	x	y	z	x'	y'	z'
initial	0.1143	–0.1703	0.8062	–24.2968	–1121.0214	69.5044
0.5 s	–7.3394	–344.8664	21.2146	–9.8396	–455.8405	24.7261
1 s	–11.2112	–524.3401	29.8954	–6.14743	–285.0912	11.4625
1.5 s	–13.8546	–646.9589	33.7039	–4.4587	–206.8792	4.0389
2 s	–15.8341	–738.8114	34.3712	–3.5065	–162.7054	–1.2054
2.5 s	–17.4279	–812.8022	32.6808	–2.8881	–134.0709	–5.4658

4. CONCLUSION

Using finite element analysis, the mass and shape of the fragments, their initial positions, and velocities have been determined. The numerical solution of the fragment trajectory model was performed using the higher order Haar wavelet method with a simplified approach for modeling drag coefficient behavior. The HWM solution has been developed as a reference solution. The rates of convergence obtained by applying HWM and HOHWM were equal to two and four, respectively. The HOHWM provides possibilities for further increase of accuracy (by changing method parameters), but in the latter case, a remarkable increase of the implementation complexity can be observed. Higher accuracy with the same mesh used or equal accuracy with a lower mesh achieved by HOHWM leads to saving computing time, i.e., energy resources, etc.

ACKNOWLEDGMENTS

The study was supported by the following grants: fire support software development project of the Defense Forces (project No. MNKA22074); AI & Robotics Estonia – EDIH (project No. 101083677); Master of Science in Smart, Secure and Interconnected Systems (MERIT) – development of a new pan-European educational ecosystem for training of digital specialists (project No. VEU22048, DIGITAL-2021-SKILLS-01); the European Union's Horizon 2020 Research and Innovation Program, under the grant agreement No. 856602; the European Regional Development Fund, co-funded by the Estonian Ministry of Education and Research, under grant agreement No. 2014-2020.4.01.20-0289; and the Smart Industry Centre (SmartIC) core facility, funded by the Estonian Research Council grant No. TT2. The publication costs of this article were partially covered by the Estonian Academy of Sciences.

REFERENCES

1. Kokinakis, W. and Sperrazza, J. Criteria for incapacitating soldiers with fragments and flechettes. *Ballist. Res. Lab.*, 1965.
2. Angel, J. *Methodology for Dynamic Characterization of Fragmenting Warheads*. Army Research Laboratory, Aberdeen, 2009.
3. Ahmed, K., Malik, A. Q., Hussain, A., Ahmad, I. R. and Ahmad, I. Blast and fragmentation studies of a scaled down artillery shell-simulation and experimental approaches. *Int. J. Multiphys.*, 2021, **15**(1), 49–71. https://doi.org/10.21152/1750-9548.15.1.49
4. Arnold, W. and Rottenkolber, E. Fragment mass distribution of metal cased explosive charges. *Int. J. Impact Eng.*, 2008, **35**(12), 1393–1398. https://doi.org/10.1016/j.ijimpeng.2008.07.049
5. Zecevic, B., Terzic, J., Catovic, A. and Serdarevic-Kadic, S. Characterization of distribution parameters of fragment mass and number for conventional projectiles. In *Proceedings of the New Trends in Research of Energetic Materials, Czech Republic, 13 April 2011*. 1026–1039.
6. Djelosevic, M. and Tepic, G. Probabilistic simulation model of fragmentation risk. *J. Loss Prev. Process Ind.*, 2019, **60**, 53–75. https://doi.org/10.1016/j.jlp.2019.04.003

7. Ugrčić, M. and Ivanišević, M. Characterization of the natural fragmentation of explosive ordnance using the numerical techniques based on the FEM. *Sci. Tech. Rev.*, 2015, **65**(4), 16–27. https://doi.org/10.5937/str1504016u
8. Kljuno, E. and Catovic, A. Trajectory estimation model for a solid body with an irregular shape undergoing extremely high aerodynamic forces. *Period. Eng. Nat. Sci.*, 2021, **9**(2). https://doi.org/10.21533/pen.v9i2.1694
9. Szmelter, J. and Kiat Lee, C. Prediction of fragment distribution and trajectories of exploding shells. *J. Battlef. Technol.*, 2007, **10**(3), 1–6.
10. Lepik, Ü. and Hein, H. Applying Haar wavelets in the optimal control theory. In *Haar Wavelets. Mathematical Engineering*. Springer, Cham, 2014, 123–135. https://doi.org/10.1007/978-3-319-04295-4_9
11. Pervaiz, N. and Aziz, I. Haar wavelet approximation for the solution of cubic nonlinear Schrodinger equations. *Phys. A: Stat. Mech. Appl.*, 2020, **545**, 123738. https://doi.org/10.1016/j.physa.2019.123738
12. Aziz, I. and Khan, I. Numerical solution of diffusion and reaction-diffusion partial integro-differential equations. *Int. J. Comput. Methods*, 2018, **15**(6). https://doi.org/10.1142/S0219876218500470
13. Siraj-ul-Islam, Aziz, I. and Al-Fhaid, A. S. An improved method based on Haar wavelets for numerical solution of nonlinear integral and integro-differential equations of first and higher orders. *J. Comput. Appl. Math.*, 2014, **260**, 449–469. https://doi.org/10.1016/j.cam.2013.10.024
14. Majak, J., Shvartsman, B., Karjust, K., Mikola, M., Haavajõe, A. and Pohlak, M. On the accuracy of the Haar wavelet discretization method. *Compos. B Eng.*, 2015, **80**, 321–327. https://doi.org/10.1016/j.compositesb.2015.06.008
15. Lepik, Ü. Solving PDEs with the aid of two-dimensional Haar wavelets. *Comput. Math. with Appl.*, 2011, **61**(7), 1873–1879. https://doi.org/10.1016/j.camwa.2011.02.016
16. Lepik, Ü. Numerical solution of differential equations using Haar wavelets. *Math. Comput. Simul.*, 2005, **68**(2), 127–143. https://doi.org/10.1016/j.matcom.2004.10.005
17. Lepik, Ü. Haar wavelet method for nonlinear integro-differential equations. *Appl. Math. Comput.*, 2006, **176**(1), 324–333. https://doi.org/10.1016/j.amc.2005.09.021
18. Lepik, Ü. Application of the Haar wavelet transform to solving integral and differential equations. *Proc. Estonian Acad. Sci.*, 2007, **56**(1), 28–46. https://doi.org/10.3176/phys.math.2007.1.03
19. Lepik, Ü. Numerical solution of evolution equations by the Haar wavelet method. *Appl. Math. Comput.*, 2007, **185**(1), 695–704. https://doi.org/10.1016/j.amc.2006.07.077
20. Lepik, Ü. Solving fractional integral equations by the Haar wavelet method. *Appl. Math. Comput.*, 2009, **214**(2), 468–478. https://doi.org/10.1016/j.amc.2009.04.015
21. Swati, Singh, M. and Singh, K. An advancement approach of Haar wavelet method and Bratu-type equations. *Appl. Numer. Math.*, 2021, **170**, 74–82. https://doi.org/10.1016/j.apnum.2021.07.014
22. Ahsan, M., Bohner, M., Ullah, A., Khan, A. A. and Ahmad, S. A Haar wavelet multi-resolution collocation method for singularly perturbed differential equations with integral boundary conditions. *Math. Comput. Simul.*, 2023, **204**, 166–180. https://doi.org/10.1016/j.matcom.2022.08.004
23. Hein, H. and Jaanuska, L. Quantification of cracks in beams on the Pasternak foundation using Haar wavelets and machine learning. *Proc. Estonian Acad. Sci.*, 2022, **71**(1), 16–29. https://doi.org/10.3176/proc.2022.1.02
24. Jaanuska, L. and Hein, H. Delamination quantification by Haar wavelets and machine learning. *Mech. Compos. Mater.*, 2022, **58**, 249–260. https://doi.org/10.1007/s11029-022-10025-2
25. Hein, H. and Jaanuska, L. Comparison of machine learning methods for crack localization. *Acta Comment. Univ. Tartu. Math.*, 2019, **23**(1). https://doi.org/10.12697/ACUTM.2019.23.13
26. Hein, H. and Jaanuska, L. Detection and classification of cracking in nonlocal nanobeams using modal data and Haar wavelets. *AIP Conf. Proc*., 2023, **2849**(1), 250004. https://doi.org/10.1063/5.0162292
27. Majak, J., Pohlak, M., Karjust, K., Eerme, M., Kurnitski, J. and Shvartsman, B. S. New higher order Haar wavelet method: application to FGM structures. *Compos. Struct.*, 2018, **201**, 72–78. https://doi.org/10.1016/j.compstruct.2018.06.013
28. Arda, M., Majak, J. and Mehrparvar, M. Longitudinal wave propagation in axially graded Raylegh–Bishop nanorods. *Mech. Compos. Mater.*, 2024, **59**, 1109–1128. https://doi.org/10.1007/s11029-023-10160-4
29. Sorrenti, M., Di Sciuva, M., Majak, J. and Auriemma, F. Static response and buckling loads of multilayered composite beams using the refined zigzag theory and higher-order Haar wavelet method. *Mech. Compos. Mater.*, 2021, **57**, 1–18. https://doi.org/10.1007/s11029-021-09929-2
30. Majak, J., Shvartsman, B., Ratas, M., Bassir, D., Pohlak, M., Karjust, K. et al. Higher-order Haar wavelet method for vibration analysis of nanobeams. *Mater. Today Commun.*, 2020, **25**, 101290. https://doi.org/10.1016/j.mtcomm.2020.101290
31. Mehrparvar, M., Majak, J., Karjust, K. and Arda, M. Free vibration analysis of tapered Timoshenko beam with higher order Haar wavelet method. *Proc. Estonian Acad. Sci.*, 2022, **71**(1), 77–83. https://doi.org/10.3176/proc.2022.1.07
32. Mehrparvar, M., Majak, J. and Karjust, K. Free vibration analysis of Timoshenko beam by higher-order Haar wavelet method. *AIP Conf. Proc.*, 2023, **2849**(1), 250007. https://doi.org/10.1063/5.0162269
33. Arda, M., Karjust, K. and Mehrparvar, M. Wave propagation in axially graded carbon nanotubes. *AIP Conf. Proc.*, 2023, **2849**(1), 250006. https://doi.org/10.1063/5.0162668
34. Ratas, M., Salupere, A. and Majak, J. Solving nonlinear PDEs using the higher order Haar wavelet method on nonuniform and adaptive grids. *Math. Model. Anal.*, 2021, **26**(1). https://doi.org/10.3846/mma.2021.12920

35. Darweesh, A., Al-Khaled, K. and Al-Yaqeen, O. A. Haar wavelets method for solving class of coupled systems of linear fractional Fredholm integro-differential equations. *Heliyon*, 2023, **9**(9), e19717. https://doi.org/10.1016/j.heliyon.2023.e19717
36. Ahsan, M., Lei, W., Khan, A. A., Ahmed, M., Alwuthaynani, M. and Amjad, A. A higher-order collocation technique based on Haar wavelets for fourth-order nonlinear differential equations having nonlocal integral boundary conditions. *Alex. Eng. J.*, 2024, **86**, 230–242. https://doi.org/10.1016/j.aej.2023.11.066
37. Swati, Singh, M. and Singh, K. An efficient technique based on higher order Haar wavelet method for Lane–Emden equations. *Math. Comput. Simul.*, 2023, **206**, 21–39. https://doi.org/10.1016/j.matcom.2022.10.031
38. Bulut, F., Oruç, Ö. and Esen, A. Higher order Haar wavelet method integrated with strang splitting for solving regularized long wave equation. *Math. Comput. Simul.*, 2022, **197**, 277–290. https://doi.org/10.1016/j.matcom.2022.02.006
39. Ahsan, M., Lei, W., Khan, A. A., Ullah, A., Ahmad, S., Arifeen, S. U. et al. A high-order reliable and efficient Haar wavelet collocation method for nonlinear problems with two point-integral boundary conditions. *Alex. Eng. J.*, 2023, **71**, 185–200. https://doi.org/10.1016/j.aej.2023.03.011
40. Moxnes, J. F., Frøyland, Ø., Øye, I. J., Brate, T. I., Friis, E., Ødegårdstuen, G. et al. Projected area and drag coefficient of high velocity irregular fragments that rotate or tumble. *Def. Technol.*, 2017, **13**(4), 269–280. https://doi.org/10.1016/j.dt.2017.03.008

Fragmendi lennudünaamika analüüs kõrgemat järku Haari lainikute meetodi abil

Lenart Kivistik, Marmar Mehrparvar, Martin Eerme ja Jüri Majak

Ebakorrapärase kujuga ja suurel kiirusel liikuvate fragmentide lennudünaamika on komplitseeritud, mistõttu seda on raske hinnata, kuna katsed eeldavad kõrgtehnoloogilisi lahendusi ning liikumist kirjeldavad diferentsiaalvõrrandid pole analüütiliselt lahendatavad. Trajektoori mudeli koostamiseks leiab kirjandusest erinevaid numbrilisi algoritme. Artiklis on kasutatud empiiriliselt määratud õhutakistusega trajektoori mudeli lähendamiseks kõrgemat järku Haari lainikute meetodit. Fragmentide lennu algtingimused on määratud lõplike elementide meetodi abil. Võrreldud on Haari lainikute ja kõrgemat järku Haari lainikute meetodite tulemusi. Selgub, et sama keerukuse korral tagab kõrgemat järku Haari lainikute meetod suurema täpsuse kui Haari lainikute meetod. Kõrgemat järku Haari lainikute meetodi kasutamine võimaldab vähendada arvutusmahtu, kuna võrdlusmeetodiga sama täpsus saavutati mitu järku madalamat arvutusvõrku kasutades.

Publication V

M. Mehrparvar, L. Kivistik, M. Eerme, and K. Karjust, “Haar wavelet based analysis of dynamics of flight of the fragments,” *AIP conference proceedings*, vol. 3315, no. 1, pp. 240001–240001, Jan. 2025, doi: https://doi.org/10.1063/5.0287481.

Haar Wavelet Based Analysis of Dynamics of Flight of the Fragments

Marmar Mehrparvar[1, a)], Lenart Kivistik[1, b)], Martin Eerme[1, c)] and Kristo Karjust[1, d)]

[1] *Department of Mechanical and Industrial Engineering, Tallinn University of Technology, Tallinn, Estonia*

[a)] *Corresponding author: marmar.mehrparvar@taltech.ee*
[b)] *lenart.kivistik@taltech.ee*
[c)] *martin.eerme@taltech.ee*
[d)] *kristo.karjust@ttu.ee*

Abstract. The current study aims to develop a numerical formulation based on the Haar wavelet method (HWM) to analyze the flight dynamics of fragments. The fragments' differential equations are simplified and then the solution based on the Haar wavelet method is developed where the value of the initial position and velocities of fragments are obtained based on the finite element method. The results of coordinates and velocities of a chosen fragment at various time stamps are presented and the formulation performance is studied.

INTRODUCTION

Developing robust mathematical methods is a necessity to deal with an ever more complex problem in the constantly changing landscape of science research. The Haar wavelet method (HWM), which was first introduced by Chen and Hsiao [1], due to its advantages is an important asset in this endeavor. In order to solve complex problems across disciplines, it is a perfect choice because of its flexibility and computational efficiency. Over the years many works implemented this method to solve various problems [2-10]. Many investigations have been done on the method, for instance, in [11] is studied the accuracy and order of convergence of the Haar wavelet method. However, in 2018 Majak et al. [12] introduced the higher-order Haar wavelet method as a more accurate version of HWM, which could be the subject of further investigation of the current problem. The HOHWM has been employed with success in a number of studies by different authors [13-18]. The potential future study in the workgroup is implementing HOHWM for numerical solutions of design optimization problems [19-28].

The dynamics of fragment flight, which gives insight into the impact characteristics, structural properties, and safety measures, are essential for aviation, materials science, forensics, or meteoritics. It is essential to understand these dynamics in order to conduct scientific research and practical applications, making it a vital cross-disciplinary area of study [29,30].

In this paper, the main focus is on the Haar wavelet method. First, the initial coordinates and velocities are obtained based on the finite element method. At that point, the trajectory model has been discussed and simplified in order to maintain a system of differential equations which is then expanded by the HWM so that the system could be solved numerically. The results for the location and velocity of a chosen fragment in different time stamps are presented and the accuracy of the developed formulation is examined.

FORMULATION

In this section, at first, the flight dynamics of fragments are studied. The differential equations are simplified and then by implementing the Haar wavelet method these equations are obtained.
However, before starting to develop the numerical formulation, The values of the initial coordinates and the velocities concerning the fragments' coordinates (as well as the air density, exposed area, drag coefficient, and mass of the fragment) are needed. The ANSYS AUTODYN solver simulates the natural fragmentation of projectiles and bases its prediction on the finite element approach and stochastic failure theory.
When estimating the fragments' flight, a fixed coordinate system is employed, with the z-axis and the unfragmented projectile's axis of symmetry intersecting on the projectile's rear surface at a height of one meter. Fragmentation of the projectile occurs at a 60-degree angle with respect to the ground. The xy plane represents the earth's surface. The beginning of the fragments' flight occurs at $t = 0.14\ ms$ following the explosion.

Trajectory model of the fragments

The point mass trajectory model can be used to predict the trajectory of a fragment moving under the impact of drag and gravitational force [29]:

$$x'' = -\frac{A\rho C_D}{2m}\sqrt{V_x^2+V_y^2+V_z^2}\cdot x';\ \ y'' = -\frac{A\rho C_D}{2m}\sqrt{V_x^2+V_y^2+V_z^2}\cdot y';\ z'' = -\underbrace{\frac{A\rho C_D}{2m}}_{k}\underbrace{\sqrt{V_x^2+V_y^2+V_z^2}}_{V}\cdot z' - g. \quad (1)$$

where $\rho = 1.20\ kg/m^3$ is the air density, $g = 9.81\ m/s^2$ is the gravitational acceleration, and C_D is the drag coefficient. The value of the Mach number generally affects the drag coefficient. However, in this investigation, the most often used simplification is used and the drag coefficient is assumed to be constant, hence $C_D = 0.6$ [29].

In order to develop a solution for the system of differential equations, Eq. 1, some mathematical procedures are done, and the value of y can be determined in terms of the x:

$$\frac{x''}{x'} = \frac{y''}{y'} \quad \longrightarrow \quad y = cx + d\ ;\ c = \frac{V_{y_0}}{V_{x_0}}\ , d = y_0 - \frac{V_{y_0}}{V_{x_0}}\cdot x_0 \quad (2)$$

The integration constants c and d can be determined using the initial values of the coordinates and velocities. Consequently, the system of 3 equations can be reduced to 2 equations.

$$x'' = -k\sqrt{(1+c^2)x'^2+z'^2}\,x' = f_1(x',z');\quad z'' = -k\sqrt{(1+c^2)x'^2+z'^2}\,z' - g = f_2(x',z') \quad (3)$$

Haar Wavelet method

One of the most fundamental wavelets is the discontinuous Haar wavelet, which is a particular family of discrete orthonormal wavelets that resembles a step function. The additional wavelets created from the same primary wavelet constitute a basis, the elements of which are orthonormal to one another and normalized to the unit length. Because of this characteristic, wavelet coefficients can be computed separately from one another. The Haar functions are provided as

$$h_i(x) = \begin{cases} 1 & \text{for} \quad x \in \left[\xi_1(i), \xi_2(i)\right) \\ -1 & \text{for} \quad x \in \left[\xi_2(i), \xi_3(i)\right) \\ 0 & \text{elsewhere} \end{cases}, \quad \text{where} \quad \begin{aligned} \xi_1(i) &= A + 2k\mu\Delta x \\ \xi_2(i) &= A + (2k+1)\mu\Delta x \\ \xi_3(i) &= A + 2(k+1)\mu\Delta x \end{aligned} \quad (4)$$

where $i = m + k + 1, \mu = \frac{M}{m},\ \Delta x = \frac{B-A}{2M}, m = 2^j$ is a maximum number of square waves arranged in the interval $[A, B]$, and the parameter k indicates the location of the particular square wave. The integrals of the Haar functions of order n can be stated as [11]

$$p_{n,i}(x)=\begin{cases}0 & x\in[A,\xi_1(i))\\ \dfrac{(x-\xi_1(i))^n}{n!} & x\in[\xi_1(i),\xi_2(i))\\ \dfrac{(x-\xi_1(i))^n-2(x-\xi_2(i))^n}{n!} & x\in[\xi_2(i),\xi_3(i))\\ \dfrac{(x-\xi_1(i))^n-2(x-\xi_2(i))^n+(x-\xi_3(i))^n}{n!} & x\in[\xi_3(i),B)\\ 0 & else\ where\end{cases}\quad for \tag{5}$$

NUMERICAL RESULTS

As a case study, in the simulation, a projectile with a mass of $12\ kg$ and diameter of $105\ mm$ was employed. Approximately 3950 fragments were generated during the $0.14\ ms$ simulation, out of these fragments, the initial location and velocity of one of them are chosen, and based on the formulation provided in the previous section, location, and velocity in all directions are calculated in various time stamps, table 1.

TABLE 1. Position and velocities based on the Haar wavelet method for the chosen fragment

t	x	y	z	V_x	V_y	V_z
initial	0.1143	-0.1703	0.8062	-24.2968	-1121.0214	69.5044
1.0	-11.2112	-524.3401	29.8954	-6.14743	-285.0912	11.4625
2.0	-15.8341	-738.8114	34.3712	-3.5065	-162.7054	-1.2054
3.0	-18.7624	-874.7501	29.0023	-2.4553	-113.9810	-9.1834
4.0	-20.9146	-974.7061	16.4569	-1.8853	-87.5647	-15.7229

In order to verify the obtained results, the location of the fragment regarding the x-axis is also calculated with the Runge-Kutta method [29,30], and the results are compared with the results from the Haar wavelet method.

TABLE 2. Validation of Haar wavelet method for chosen fragment at $t=4$

N	x	Error	Convergence rate
4	-19.29378311	1.62E+00	
8	-20.46399640	4.51E-01	1.8455754
16	-20.79527850	1.20E-01	1.9123443
32	-20.88400206	3.11E-02	1.9451119
64	-20.90722492	7.90E-03	1.9779377
128	-20.91314451	1.98E-03	1.9956008
256	-20.91463048	4.95E-04	2.0001319
Runge – Kutta method: -20.91512575			

where N is the number of collocation points, $N=2m$, and the method's numerical order of convergence can then be calculated by

$$\text{Convergence rate} = \log\left(\frac{F_{i-1} - F_R}{F_i - F_R}\right)/\log(2) \tag{6}$$

where F_R is the result calculated by the Runge-Kutta method.

CONCLUSION

In the current work, the HWM has been adapted for the trajectory model of the fragments. In order to predict the initial locations and velocities of fragments finite element approach has been utilized. The trajectory model as a system of differential equations is simplified mathematically and then expanded by the Haar wavelet method, however, the drag coefficient is chosen to be constant. The result exhibits the ability of this method to solve this sort of problem and the results of the fragment's location and velocity are different times after explosion is provided. The developed method can be used as an accurate numerical solution for the analysis of fragments flight dynamics.

ACKNOWLEDGMENTS

VEU22048 "Master of Science in Smart, Secure and Interconnected Systems" (1.10.2022−30.09.2026); Tallinn University of Technology (partner); Financier: European Commission.

REFERENCES

1. C.F. Chen, C.H. Hsiao, IEE Proc Contr Theor Appl, **144**(1), 87-94 (1997)
2. Ü.Lepik, Math. Comput. Simulat. **68**(2), 127-143 (2005)
3. Ü.Lepik, Proc. Estonian Acad. Sci. **56**(1), 28-46 (2007)
4. H.Hein, L. Feklistova, Mech Syst Signal Pr **25** (6), 2257-70 (2011)
5. L. Jaanuska, H. Hein, Int. J. of Mechanics, **10**, 281-287 (2016)
6. Ü. Lepik, H. Hein, Haar wavelets: with applications (Springer, New York, 2014)
7. S.U. Islam, I. Aziz, M. Fayyaz, International Journal of Computer Mathematics, **90** (9), 1971–1989 (2013)
8. N. Pervaiz, I. Aziz, Physica A: Statistical Mechanics and its Applications **545**,123738 (2020)
9. I Aziz, I., Khan, International Journal of Computational Methods **15**(6),1850047 (2018)
10. S.U. Islam, I. Aziz, A.S. Al-Fhaid. Journal of Comp. and Appl. Math. **260**, 449–469 (2014)
11. J. Majak, B. Shvartsman, K. Karjust, M. Mikola, A. Haavajõe and M. Pohlak, Comp. Part B: Eng. **80**, 321-327 (2015)
12. J. Majak, M. Pohlak, K. Karjust, M. Eerme, J. Kurnitski, B.S. Shvartsman, Composite Struct., **201**, 72-78, (2018)
13. J. Majak, M. Pohlak, M. Eerme, and B. Shvartsman, AIP Conf. Proc., **2116**, 330002 (2019). https://doi.org/10.1063/1.5114340
14. M. Ratas, A. Salupere, J. Majak, Mathematical Modelling and Analysis **26** (1), 147–169 (2021)
15. M. Sorrenti, M. Di Sciuva, J. Majak, F. Auriemma, Mechanics of Composite Materials, **57** (1), 1−18 (2021)
16. J.Majak, B.Shvartsman, M.Ratas, D.Bassir, M.Pohlak, K.Karjust, M.Eerme, Mater. Today Commun.,**25**,101290 (2020)
17. F. Bulut, Ö. Oruç, A. Esen, Mathematics and Computers in Simulation, **197**, 277-290 (2022)
18. S.K. Jena, S. Chakraverty, V. Mahesh, D. Harursampath, Eng. Analysis with Bound. Elem., **140**, 167– 185 (2022)
19. S. Guessasma, D. Bassir, Mechanics of Materials, **42**(3), 344-353 (2010)
20. J.K. Lee, B.K. Lee, Mechanics of Composite Materials. **57**, 833–846 (2022)
21. A. Muc, Mechanics of Composite Materials. **56**, 713–720 (2021)
22. J. Lellep, J. Majak, Structural Optimization, **14** (2-3), 116−120 (1997)
23. K. Abouzaid, S. Guessasma, S. Belhabib, D. Bassir, A. Chouaf, European Polymer Journal, **108**, 262-273 (2018)
24. Y. Xiao, Z. Li, Z. Liu, M. Zang, Y., Zhu, Mechanics of Composite Materials. **57**, 401–414 (2021)
25. D. Wu, Y. Lei, Z. Wang, B. Yu, D. Zhang, Mechanics of Composite Materials, **59**, 479–494 (2023)
26. K. Abouzaid, D. Bassir, S. Guessasma and H. Yue, Mechanics of Composite Materials **56**, 805–816 (2021)
27. S. Guessasma, D. Bassir, L. Hedjazi, Materials & Design, **65**, 1053-1063 (2015)
28. J. Lellep, J. Majak, Mechanics of Composite Materials, **36** (4), 261−266 (2000)

29. B. Zecevic and J. Terzic, Characterization of distribution parameters of fragment mass and number for conventional projectiles, 14Th Semin. New Trends Res. Energ. Mater., APRIL, 1026–1039, (2011)
30. S. Stojadinović, R. Pantović, and M. Žikić, Int. J. Rock Mech. Min. Sci., **48**(7), 1086-1094 (2011).

Publication VI

M. Mehrparvar, J. Majak, and K. Karjust, “Enhanced Crack Detection in Composite Plates: Integrating Haar Wavelet Transform with Convolutional Neural Networks,” *E3S Web of Conferences*, vol. 631, p. 01008, 2025, doi: https://doi.org/10.1051/e3sconf/202563101008.

Enhanced Crack Detection in Composite Plates: Integrating Haar Wavelet Transform with Convolutional Neural Networks

Marmar Mehrparvar[1, a)], Jüri Majak[1, b)] and Kristo Karjust[1, c)]

[1] *Department of Mechanical and Industrial Engineering. Tallinn University of Technology. Ehitajate tee 5, 19086, Tallinn, Estonia*

[a)] *Corresponding author: marmar.mehrparvar@taltech.ee*
[b)] *juri.majak@taltech.ee*
[c)] *kristo.karjust@taltech.ee*

Abstract. In order to ensure structural integrity, detecting cracks, as a common structural flaw, is crucial. The current study presents a method for crack detection and prediction in plates under free vibration using the Convolutional Neural Network (CNN) and the Haar wavelet transformation. The Haar wavelet method is employed to preprocess vibration data, extracting key features that improve CNN's ability to identify and localize cracks. The proposed approach establishes high accuracy in detecting crack locations and intensities, showcasing its potential for real-time structural health monitoring.

INTRODUCTION

Composite materials, due to their superior strength-to-weight ratios and their customizability are extensively used in aerospace, civil, and mechanical engineering. However, there are many defects that can occur in them, such as cracks, delamination, etc., that can impose significant challenges to the integrity of the structure. Cracks can compromise the performance and safety of composite structures, thus making early detection and accurate prediction is vital.

There are many crack detection methods already in use, for instance, visual inspection, ultrasonic testing, and other non-destructive evaluation techniques [1-6]. Although, these traditional methods could fall short in terms of accuracy, and efficiency and also could become time-consuming and expensive. However, with the advancement of computational techniques, and machine learning a powerful tool emerged that can be trained in order to recognize patterns, and classify and identify systems. Over the past few years, many studies have been conducted by employing machine learning techniques, for instance, the Artificial Neural network (ANN) has been used to investigate the structural health monitoring and presence of cracks and their severity [7-11]. Furthermore, the Convolutional Neural Network (CNN) is a powerful tool that can be developed in order to automate crack detection, due to its power to process data, recognize patterns, and even its ability to analyze visual data [12].

This paper explores the integration of the Haar wavelet transform with CNN for detecting and predicting cracks in plates under free vibration. The Haar wavelet transform aids in feature extraction from vibration signals, and fed data to enhance the CNN capability to identify crack location and severity accurately.

METHODOLOGY

In this section, a road map is provided to form a methodology for predicting crack location and intensity in a plate. The process starts with the data collection as one of the most critical steps in machine learning. Afterward, the design of the CNN algorithm and the training and validation steps are explained.

Data Collection

Accurate data collection is the first step for effective crack detection in structures using machine learning. In this study, data was sourced from literature and finite element method (FEM) simulations. To increase the dataset, FEM simulations were conducted. A detailed model of the plate was created using FEM software, modeling several crack scenarios with different orientations, lengths, and positions. The FEM-generated data was validated against data from the literature to confirm accuracy.

Data normalization was performed to ensure consistency, with crack positions scaled between -1 and 1 and intensities normalized to a range of 0 to 1.

Convolutional Neural Network

Convolutional Neural Networks (CNNs) are gaining popularity for detecting cracks in structures due to their powerful pattern recognition capabilities. The general form of the architecture is that it consists of layers for convolution, pooling, and fully connected. Convolutional layers detect cracks' essential features such as presence, edges, and texture. Spatial dimensions can be reduced by using pooling layers to improve computational efficiency and reduce overfitting. The presence of cracks in these entire regions can be effectively classified by connecting all the detected features to fully connected layers at the end of the network. When Haar wavelet is integrated into CNN, localized frequency information can be extracted which improves crack detection accuracy through highlighting discontinuity signs associated with the crack initiation stage. This hybrid approach takes advantage of both spatial and frequency domain features for robustly spotting cracks.

Training and Validation

The CNN is trained by using a labeled dataset of vibration signals, in which the crack locations and severities are known. The dataset is divided into training, validation, and test sets. During training, backpropagation is applied to optimize the network weights, and an appropriate loss function such as mean absolute error and mean squared error are used. Performance metrics for this model include accuracy, precision recall, and F1- score. Cross-validation helps to make sure that the model will be robust therefore preventing overfitting.

RESULTS

The integration of the Haar wavelet transform with CNNs significantly improves the accuracy of crack detection in structure. As a case study in this section, an isotropic plate is modeled in various states, i.e. various crack sizes, locations, and severities in FEM software, here ABAQUS is used. The data was fed to CNN, with the integration of wavelet transformation as an enhancement to make the algorithm more robust.

Figure 1 presents the results for 20 predictions of the modeled CNN, the crack's actual location and intensity are shown as well as the predicted results. As mentioned before, all the results are normalized to eliminate any inconsistency in the data set and make it a more coherent dataset. Heatmaps showing the predicted crack locations and severities are overlaid on images of the plates. These visualizations provide a clear representation of the model's ability to predict.

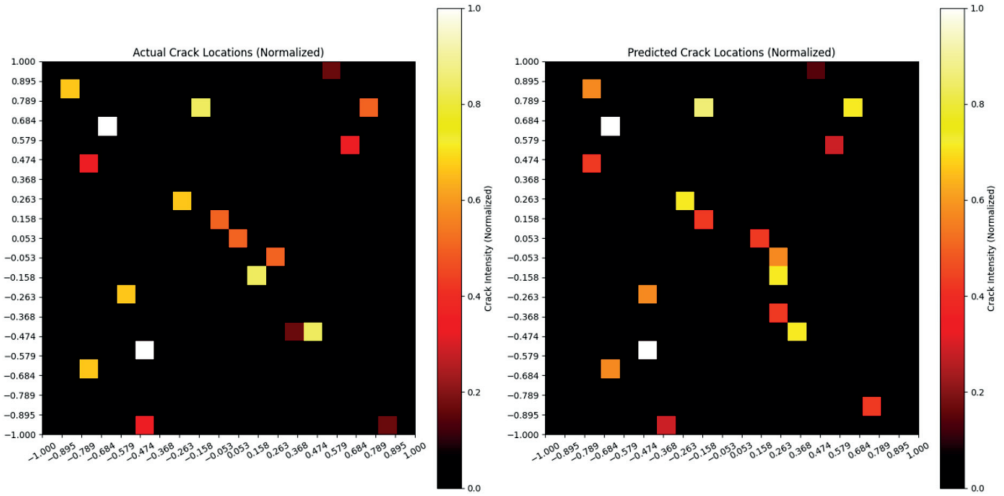

(a) (b)

FIGURE 1. Crack location and intensity in an isotropic plate.

In order to have a visual of the prediction accuracy, the crack position and its corresponding mean absolute error are shown in Figure 2. As it can be seen, for this case study the developed CNN model achieved an acceptable accuracy.

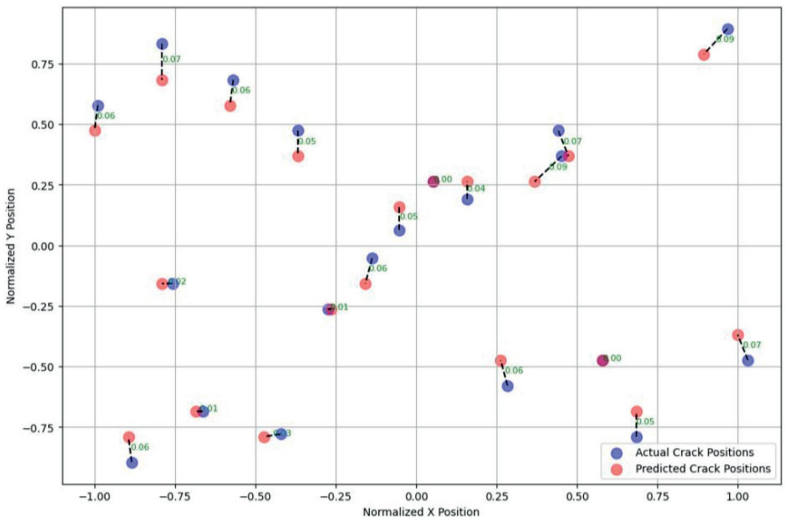

FIGURE 2. Comparison of actual crack position and predicted crack position, and the corresponding mean absolute error.

The key performance metrics are as follows:

- **Accuracy:** The CNN model achieves an accuracy of 96%, significantly higher than traditional methods and standalone CNN models.
- **Precision:** The model's precision, defined as the ratio of true positive crack detections to the total predicted positives, is 94%.

- **Recall:** The recall, or the ratio of true positive crack detections to the total actual positives, is 97%.
- **F1-Score:** The F1-score, which is the harmonic mean of precision and recall, stands at 95.5%.

Traditional methods often fail to detect sub-surface or fine cracks, whereas the proposed method successfully identifies these defects with high reliability.

CONCLUSION

For the detection of cracks in structures under free vibrations, a formulation based on the combination of the Haar wavelet transform and Convolutional Neural Networks (CNNs) is developed. This model combines the strengths of both the CNN's pattern recognition abilities and the Haar wavelet transform's ability to capture local signal variations. According to the findings, this fusion approach is proven to be a reliable and accurate model to detect cracks in a structure. High precision and recall rates achieved by this model can be used for real-world applications such as structural health monitoring and maintenance. In different engineering fields, this technique will enable automated, accurate, and efficient crack detection method thereby improving safety.

Future studies will also investigate its applicability to various structures and materials. Optimal network architecture design as well as the training process can further improve its performance for employing the model for various structural flaws, and improve the prediction power.

ACKNOWLEDGMENTS

This work was partially supported by the "PHC PARROT" program (project number: 48992SA), funded by the French Ministry for Europe and Foreign Affairs, the French Ministry for Higher Education and Research, and the Estonian Research Council.

REFERENCES

1. Gupta, R., Mitchell, D., Blanche, J., Harper, S., Tang, W., Pancholi, K., ... & Flynn, D. (2021). A review of sensing technologies for non-destructive evaluation of structural composite materials. Journal of Composites Science, 5(12), 319.
2. Hu, K., Chen, Z., Kang, H., & Tang, Y. (2024). 3D vision technologies for a self-developed structural external crack damage recognition robot. Automation in Construction, 159, 105262.
3. Yao, Y., Tung, S. T. E., & Glisic, B. (2014). Crack detection and characterization techniques—An overview. Structural Control and Health Monitoring, 21(12), 1387-1413.
4. Hassani, S., Mousavi, M., & Gandomi, A. H. (2021). Structural health monitoring in composite structures: A comprehensive review. Sensors, 22(1), 153.
5. do Cabo, C. T., Valente, N. A., & Mao, Z. (2022). A Comparative Analysis of Imaging Processing Techniques for Non-Invasive Structural Health Monitoring. IFAC-PapersOnLine, 55(27), 150-154.
6. Guo, P., Meng, X., Meng, W., & Bao, Y. (2022). Monitoring and automatic characterization of cracks in strain-hardening cementitious composite (SHCC) through intelligent interpretation of photos. Composites Part B: Engineering, 242, 110096.
7. Saadatmorad, M., Jafari-Talookolaei, R. A., Pashaei, M. H., & Khatir, S. (2022). Damage detection in rectangular laminated composite plate structures using a combination of wavelet transforms and artificial neural networks. Journal of Vibration Engineering & Technologies, 10(5), 1647-1664.
8. Jaanuska, L., & Hein, H. (2022). Delamination quantification by Haar wavelets and machine learning. Mechanics of Composite Materials, 58(2), 249-260.
9. Hein, H., & Jaanuska, L. (2019). Comparison of machine learning methods for crack localization. Acta Et Commentationes Universitatis Tartuensis De Mathematica, 23(1), 125-142.
10. Hein, H., & Jaanuska, L. (2022). Quantification of cracks in beams on the Pasternak foundation using Haar wavelets and machine learning. Proceedings of the Estonian Academy of Sciences, 71(1), 16-29.
11. Yam, L. H., Yan, Y. J., & Jiang, J. S. (2003). Vibration-based damage detection for composite structures using wavelet transform and neural network identification. Composite Structures, 60(4), 403-412.

12. Padsumbiya, M., Brahmbhatt, V., & Thakkar, S. P. (2022). Automatic crack detection using convolutional neural network. Journal of Soft Computing in Civil Engineering, 6(3), 1-17.

List of Publications not Included in This Thesis

VII Karjust, K., Mehrparvar, M., Kaganski, S., & Raamets, T. (2025). Development of a Sustainability-Oriented KPI Selection Model for Manufacturing Processes. Sustainability (2071-1050), 17(14). doi: https://doi.org/10.3390/su17146374.

VIII Kivistik, L., Mehrparvar, M., Eerme, M., Dieves, V., & Majak, J. (2025). Numerical modeling of fragment flight dynamics. Proceedings of the Estonian Academy of Sciences, 74(2), 120-125. doi: https://doi.org/10.3176/proc.2025.2.06.

IX Mehrparvar, M., Majak, J., & Karjust, K. (2024). A comparative analysis of Fuzzy AHP and Fuzzy VIKOR methods for prioritization of the risk criteria of an autonomous vehicle system. Proceedings of the Estonian Academy of Sciences, 73(2), 116-123. doi: https://doi.org/10.3176/proc.2024.2.04.

X Mehrparvar, M., Majak, J., & Karjust, K. (2024). Effect of aggregation methods in fuzzy technique for prioritization of criteria of automated vehicle system. In AIP Conference Proceedings (Vol. 2989, No. 1). AIP Publishing

XI Arda, M., Mehrparvar, M., & Karjust, K. (2024). Dynamics of axially graded nanobeams with follower force effect. In AIP Conference Proceedings (Vol. 3094, No. 1). AIP Publishing.

XII Arda, M., Karjust, K., & Mehrparvar, M. (2023). Wave propagation in axially graded carbon nanotubes. In AIP Conference Proceedings (Vol. 2849, No. 1). AIP Publishing.

Curriculum vitae

Personal data

Name:	Marmar Mehrparvar
Date of birth:	14.10.1993
Place of birth:	Kerman, Iran
Citizenship:	Iran

Contact data

E-mail:	marmar.mehrparvar@taltech.ee, mrmr.mehrparvar@gmail.com

Education

2021–2026	Tallinn University of Technology, Tallinn, Estonia – PhD
2015–2018	Shahid Beheshti University, Tehran, Iran – MSC
2011–2015	Islamic Azad University Science and Research Branch, Tehran, Iran – BSC

Language competence

Persian	Native
English	Fluent
French	Intermediate
German	Basic

Professional employment

2024–	Junior Research Fellow, Tallinn University of Technology, School of Engineering, Department of Mechanical and Industrial Engineering

Awards

2020	Obtaining the title of the best national master's thesis of the Iranian Aerospace Association
2019	Obtaining the title of the best research student at Shahid Beheshti University

Technical skills

- Proficient in Fortran, MATLAB and Python programming
- Proficient in ABAQUS and ANSYS software
- Experienced in AutoCAD, Catia and Tecplot software

Journal publications

1. Karjust, K., Mehrparvar, M., Kaganski, S., & Raamets, T. (2025). Development of a Sustainability-Oriented KPI Selection Model for Manufacturing Processes. Sustainability (2071–1050), 17(14). doi: https://doi.org/10.3390/su17146374.
2. Kivistik, L., Mehrparvar, M., Eerme, M., Dieves, V., & Majak, J. (2025). Numerical modeling of fragment flight dynamics. Proceedings of the Estonian Academy of Sciences, 74(2), 120–125. doi: https://doi.org/10.3176/proc.2025.2.06.
3. Mehrparvar, M., Majaka, J., & Karjusta, K. (2024). A comparative analysis of Fuzzy AHP and Fuzzy VIKOR methods for prioritization of the risk criteria of an autonomous vehicle system. Proceedings of the Estonian Academy of Sciences, 73(2), 116–123. doi: https://doi.org/10.3176/proc.2024.2.04.

4. Kivistik, L., Mehrparvar, M., Eerme, M., & Majak, J. (2024). Dynamics of flight of the fragments with higher order Haar wavelet method. Proceedings of the Estonian Academy of Sciences, 73(2), 108–115. doi: https://doi.org/10.3176/proc.2024.2.02.
5. Arda, M., Majak, J., & Mehrparvar, M. (2024). Longitudinal wave propagation in axially graded Rayleigh-Bishop nanorods. Mechanics of Composite Materials, 59(6), 1109–1128. doi: https://doi.org/10.1007/s11029-023-10160-4.
6. Mehrparvar, M., Majak, J., Karjust, K., & Arda, M. (2022). Free vibration analysis of tapered Timoshenko beam with higher order Haar wavelet method. Proceedings of the Estonian Academy of Sciences, 71(1), 77–83. doi: https://doi.org/10.3176/proc.2022.1.07.
7. Ghannadpour, S. A. M., Haghgoo, M. R., & Mehrparvar, M. (2021). Experimental, semi-analytical and numerical nonlinear analysis of compression-loaded laminates with different boundary conditions. Engineering Structures, 234, 111972. doi: https://doi.org/10.1016/j.engstruct.2021.111972.
8. Ghannadpour, S. A. M., & Mehrparvar, M. (2020). Nonlinear and post-buckling responses of FGM plates with oblique elliptical cutouts using plate assembly technique. Steel and Composite Structures, An International Journal, 34(2), 227–239. doi: https://doi.org/10.12989/scs.2020.34.2.227.
9. Ghannadpour, S. A. M., & Mehrparvar, M. (2020). Modeling and evaluation of rectangular hole effect on nonlinear behavior of imperfect composite plates by an effective simulation technique. Compos. Mater. Eng, 2(1), 25–41.
10. Mehrparvar, M., & Ghannadpour, S. A. M. (2018). Plate assembly technique for nonlinear analysis of relatively thick functionally graded plates containing rectangular holes subjected to in-plane compressive load. Composite Structures, 202, 867–880. doi: https://doi.org/10.1016/j.compstruct.2018.04.053.
11. Ghannadpour, S. A. M., & Mehrparvar, M. (2018). Energy effect removal technique to model circular/elliptical holes in relatively thick composite plates under in-plane compressive load. Composite Structures, 202, 1032–1041. doi: https://doi.org/10.1016/j.compstruct.2018.05.026.

Conference presentations

1. Mehrparvar, M., Majak, J., & Karjust, K. (2025). Enhanced Crack Detection in Composite Plates: Integrating Haar Wavelet Transform with Convolutional Neural Networks. In E3S Web of Conferences (Vol. 631, Pages 01008). EDP Sciences.
2. Mehrparvar, M., Kivistik, L., Eerme, M., & Karjust, K. (2025). Haar wavelet based analysis of dynamics of flight of the fragments. In AIP Conference Proceedings (Vol. 3315, No. 1, p. 240001). AIP Publishing LLC.
3. Mehrparvar, M., Majak, J., & Karjust, K. (2024). Effect of aggregation methods in fuzzy technique for prioritization of criteria of automated vehicle system. In AIP Conference Proceedings (Vol. 2989, No. 1). AIP Publishing.
4. Arda, M., Mehrparvar, M., & Karjust, K. (2024). Dynamics of axially graded nanobeams with follower force effect. In AIP Conference Proceedings (Vol. 3094, No. 1). AIP Publishing.
5. Mehrparvar, M., Majak, J., & Karjust, K. (2023). Free vibration analysis of Timoshenko beam by higher-order Haar wavelet method. In AIP Conference Proceedings (Vol. 2849, No. 1). AIP Publishing.

6. Arda, M., Karjust, K., & Mehrparvar, M. (2023). Wave propagation in axially graded carbon nanotubes. In AIP Conference Proceedings (Vol. 2849, No. 1). AIP Publishing.
7. Mehrparvar, M., Majak, J., Arda, M., & Karjust, K. (2022). HOHWM for solving fractional differential equations. Applications to composite structures. In 25th International Conference on Composite of Structures (ICCS25).
8. Ghannadpour, S. A. M., & Mehrparvar, M. (2018). Post-buckling analysis of relatively thick functionally graded plates containing circular/elliptical holes using plate decomposition technique. Paper presented at Mechcomp 4, Madrid, Spain.
9. Ghannadpour, S. A. M., & Mehrparvar, M. (2017). Post-buckling analysis of functionally graded plates with square/rectangular cutouts. Paper presented at ICCS 20, Paris, France.
10. Ghannadpour, S. A. M., & Mehrparvar, M. (2017). Geometric nonlinear analysis of relatively thick composite plates containing circular/elliptical holes using Ritz method. Paper presented at Mechcomp 3, Bologna, Italy.
11. Ghannadpour, S. A. M., Karimi, M., & Mehrparvar, M. (2017). Nonlinear and post-buckling behaviors of cracked cross-ply composite plates with or without initial imperfection using Rayleigh-Ritz approach. Paper presented at Mechcomp 3, Bologna, Italy.

Elulookirjeldus

Isikuandmed

Nimi:	Marmar Mehrparvar
Sünniaeg:	14.10.1993
Sünnikoht:	Kerman, Iraan
Kodakondsus:	Iraani

Kontaktandmed

E-post:	marmar.mehrparvar@taltech.ee, mrmr.mehrparvar@gmail.com

Hariduskäik

2021–2026	Tallinna Tehnikaülikool, Tallinn, Eesti – PhD
2015–2018	Shahid Beheshti Ülikool, Teheran, Iraan – MSC
2011–2015	Islami Azad Ülikool, Teaduse ja Uurimise Haru, Teheran, Iraan – BSC

Keelteoskus

Pärsia keel	Emakeel
Inglise keel	Kõrgtase
Prantsuse keel	kesktase
Saksa keel	Algtase

Teenistuskäik

2024–	Doktorant-nooremteadur, Tallinna Tehnikaülikool, Inseneriteaduskond, Mehaanika ja tööstustehnika instituut

Auhinnad

2020	Iraani Aerokosmoseühingu parima riikliku magistritöö tiitli omandamine
2019	Parima teadusüliõpilase tiitli omandamine Shahid Beheshti Ülikoolis

Tehnilised oskused

- Programmeerimiskeeled: Fortran, MATLAB, Python
- Teadustarkvarad: ABAQUS, ANSYS, AutoCAD, Catia, Tecplot

Publikatsioonid

1. Karjust, K., Mehrparvar, M., Kaganski, S., & Raamets, T. (2025). Development of a Sustainability-Oriented KPI Selection Model for Manufacturing Processes. Sustainability (2071–1050), 17(14). doi: https://doi.org/10.3390/su17146374.
2. Kivistik, L., Mehrparvar, M., Eerme, M., Dieves, V., & Majak, J. (2025). Numerical modeling of fragment flight dynamics. Proceedings of the Estonian Academy of Sciences, 74(2), 120–125. doi: https://doi.org/10.3176/proc.2025.2.06.
3. Mehrparvar, M., Majaka, J., & Karjusta, K. (2024). A comparative analysis of Fuzzy AHP and Fuzzy VIKOR methods for prioritization of the risk criteria of an autonomous vehicle system. Proceedings of the Estonian Academy of Sciences, 73(2), 116–123. doi: https://doi.org/10.3176/proc.2024.2.04.

4. Kivistik, L., Mehrparvar, M., Eerme, M., & Majak, J. (2024). Dynamics of flight of the fragments with higher order Haar wavelet method. Proceedings of the Estonian Academy of Sciences, 73(2), 108–115. doi: https://doi.org/10.3176/proc.2024.2.02.
5. Arda, M., Majak, J., & Mehrparvar, M. (2024). Longitudinal wave propagation in axially graded Rayleigh-Bishop nanorods. Mechanics of Composite Materials, 59(6), 1109–1128. doi: https://doi.org/10.1007/s11029-023-10160-4.
6. Mehrparvar, M., Majak, J., Karjust, K., & Arda, M. (2022). Free vibration analysis of tapered Timoshenko beam with higher order Haar wavelet method. Proceedings of the Estonian Academy of Sciences, 71(1), 77–83. doi: https://doi.org/10.3176/proc.2022.1.07.
7. Ghannadpour, S. A. M., Haghgoo, M. R., & Mehrparvar, M. (2021). Experimental, semi-analytical and numerical nonlinear analysis of compression-loaded laminates with different boundary conditions. Engineering Structures, 234, 111972. doi: https://doi.org/10.1016/j.engstruct.2021.111972.
8. Ghannadpour, S. A. M., & Mehrparvar, M. (2020). Nonlinear and post-buckling responses of FGM plates with oblique elliptical cutouts using plate assembly technique. Steel and Composite Structures, An International Journal, 34(2), 227–239. doi: https://doi.org/10.12989/scs.2020.34.2.227.
9. Ghannadpour, S. A. M., & Mehrparvar, M. (2020). Modeling and evaluation of rectangular hole effect on nonlinear behavior of imperfect composite plates by an effective simulation technique. Compos. Mater. Eng, 2(1), 25–41.
10. Mehrparvar, M., & Ghannadpour, S. A. M. (2018). Plate assembly technique for nonlinear analysis of relatively thick functionally graded plates containing rectangular holes subjected to in-plane compressive load. Composite Structures, 202, 867–880. doi: https://doi.org/10.1016/j.compstruct.2018.04.053.
11. Ghannadpour, S. A. M., & Mehrparvar, M. (2018). Energy effect removal technique to model circular/elliptical holes in relatively thick composite plates under in-plane compressive load. Composite Structures, 202, 1032–1041. doi: https://doi.org/10.1016/j.compstruct.2018.05.026.

Konverentsid

1. Mehrparvar, M., Majak, J., & Karjust, K. (2025). Enhanced Crack Detection in Composite Plates: Integrating Haar Wavelet Transform with Convolutional Neural Networks. In E3S Web of Conferences (Vol. 631, Pages 01008). EDP Sciences.
2. Mehrparvar, M., Kivistik, L., Eerme, M., & Karjust, K. (2025). Haar wavelet based analysis of dynamics of flight of the fragments. In AIP Conference Proceedings (Vol. 3315, No. 1, p. 240001). AIP Publishing LLC.
3. Mehrparvar, M., Majak, J., & Karjust, K. (2024). Effect of aggregation methods in fuzzy technique for prioritization of criteria of automated vehicle system. In AIP Conference Proceedings (Vol. 2989, No. 1). AIP Publishing.
4. Arda, M., Mehrparvar, M., & Karjust, K. (2024). Dynamics of axially graded nanobeams with follower force effect. In AIP Conference Proceedings (Vol. 3094, No. 1). AIP Publishing.
5. Mehrparvar, M., Majak, J., & Karjust, K. (2023). Free vibration analysis of Timoshenko beam by higher-order Haar wavelet method. In AIP Conference Proceedings (Vol. 2849, No. 1). AIP Publishing.

6. Arda, M., Karjust, K., & Mehrparvar, M. (2023). Wave propagation in axially graded carbon nanotubes. In AIP Conference Proceedings (Vol. 2849, No. 1). AIP Publishing.
7. Mehrparvar, M., Majak, J., Arda, M., & Karjust, K. (2022). HOHWM for solving fractional differential equations. Applications to composite structures. In 25th International Conference on Composite of Structures (ICCS25).
8. Ghannadpour, S. A. M., & Mehrparvar, M. (2018). Post-buckling analysis of relatively thick functionally graded plates containing circular/elliptical holes using plate decomposition technique. Paper presented at Mechcomp 4, Madrid, Spain.
9. Ghannadpour, S. A. M., & Mehrparvar, M. (2017). Post-buckling analysis of functionally graded plates with square/rectangular cutouts. Paper presented at ICCS 20, Paris, France.
10. Ghannadpour, S. A. M., & Mehrparvar, M. (2017). Geometric nonlinear analysis of relatively thick composite plates containing circular/elliptical holes using Ritz method. Paper presented at Mechcomp 3, Bologna, Italy.
11. Ghannadpour, S. A. M., Karimi, M., & Mehrparvar, M. (2017). Nonlinear and post-buckling behaviors of cracked cross-ply composite plates with or without initial imperfection using Rayleigh-Ritz approach. Paper presented at Mechcomp 3, Bologna, Italy.

ISSN 2585-6901 (PDF)
ISBN 978-9916-80-442-1 (PDF)